

**SINGLE-EVENT EFFECT STUDY ON A DC/DC PWM USING  
MULTIPLE TESTING METHODOLOGIES**

A Thesis Submitted to the College of  
Graduate Studies and Research  
In Partial Fulfillment of the Requirements  
For the Degree of Doctor of Philosophy  
In the Department of Leisure Activity  
University of Saskatchewan  
Saskatoon

By

YI REN

© Copyright Yi Ren, February, 2015. All rights reserved.

## **PERMISSION TO USE**

In presenting this thesis in partial fulfilment of the requirements for a Postgraduate degree from the University of Saskatchewan, I agree that the Libraries of this University may make it freely available for inspection. I further agree that permission for copying of this thesis in any manner, in whole or in part, for scholarly purposes may be granted by the professor or professors who supervised my thesis work or, in their absence, by the Head of the Department or the Dean of the College in which my thesis work was done. It is understood that any copying or publication or use of this thesis or parts thereof for financial gain shall not be allowed without my written permission. It is also understood that due recognition shall be given to me and to the University of Saskatchewan in any scholarly use which may be made of any material in my thesis.

Requests for permission to copy or to make other use of material in this thesis in whole or part should be addressed to:

Head of the Department of Electrical and Computer Engineering  
University of Saskatchewan  
Saskatoon, Saskatchewan  
Canada  
S7N 5A9

## ABSTRACT

As the technology advances, the feature size of the modern integrated circuits (ICs) has decreased dramatically to nanometer amplitude. On one hand, the shrink brings benefits, such as high speed and low power consumption per transistor. On the other hand, it poses a threat to the reliable operation of the ICs by the increased radiation sensitivity, such as single event effects (SEEs). For example, in 2010, a commercial-off-the-shelf (COTS) BiCMOS DC/DC pulse width modulator (PWM) IC was observed to be sensitive to neutrons on terrestrial real-time applications, where negative 6- $\mu$ s glitches were induced by the single event transient (SET) effects. As a result, a project was set up to comprehensively study the failure mechanisms with various test methodologies and to develop SET-tolerant circuits to mitigate the SET sensitivity.

First, the pulsed laser technique is adopted to perform the investigation on the SET response of the DC/DC PWM chip. A Ti:Sapphire single photon absorption (SPA) laser with different wavelengths and repetition rates is used as an irradiation source in this study. The sensitive devices in the chip are found to be the bandgap voltage reference circuit thanks to the well-controlled location information of the pulsed laser. The result is verified by comparing with the previous alpha particle and neutron testing data as well as circuit simulation using EDA tools. The root cause for the sensitivity is also acquired by analyzing the circuit. The temperature is also varied to study the effect of the temperature-induced quiescent point shift on the SET sensitivity of the chip. The experimental results show that the quiescent point shifts have different impacts on SET sensitivities due to the different structures and positions of the circuitries. After that, heavy ions, protons, and the pulsed X-ray are used as irradiation sources to further study the SET response of the DC/DC chip. The heavy ion and pulsed laser data are

correlated to each other. And the equivalent LETs for laser with wavelengths of 750 nm, 800 nm, 850 nm and 920 nm are acquired. This conclusion can be used to obtain the equivalent heavy ion cross section of any area in a chip by using the pulsed laser technique, which will facilitate the SET testing procedure dramatically. The proton and heavy ion data are also correlated to each other based on a rectangular parallel piped (RPP) model, which gives convenience in Soft Error Rate (SER) estimation. The potential application of pulsed X-ray technique in SET field is also investigated. It is capable of generating similar results with those of heavy ion and pulsed laser testing. Both the advantages and disadvantages of this technique are explained. This provides an alternative choice for the SET testing in the future. Finally, the bandgap voltage reference circuit in the DC/DC PWM is redesigned and fabricated in bulk CMOS 130nm technology and a SET hardened bandgap circuit is proposed and investigated. The CMOS substrate PNP transistor is much less sensitive to SETs than the BiCMOS NPN transistor according to the pulsed laser test results. The reason is analyzed to be the different fabrication processes of the two technologies. The laser test results also indicate that the SET hardened bandgap circuit can mitigate the SET amplitude dramatically, which is consistent with the SPICE simulation results. These researches provide more understandings on the design of SET hardened bandgap voltage reference circuit.

## **ACKNOWLEDGEMENT**

This research would be impossible to be accomplished without the help and effort from all the professors and specialist. The valuable suggestions and comments can always inspire me on my study. The supports from my friends and families give me strength to persist and to stick to my goal.

First of all, I need to give my gratitude to my supervisor, Dr. Li Chen. His passions and diligence on research impress me so much. During my Ph.D. study, he makes every effort to meet my requirement, such as IC chip fabrication and testing facility access. If ever I could fly higher than the eagle, he is the wind beneath my wings. Also, I need to thank Mr. Rory Gowen, who is the technician in the Department of Electrical Engineering. He is always ready to help with a friendly smile. As a senior systems administrator in College of Engineering, Trevor Zintel deserves all my thanks for his assistance in solving all the issues related to the software tools. His help facilitates my research tremendously. Another person I need to show my appreciation is Dr. Sophie Brunette, who was a science officer at SSSC. She gave me so much support at the beginning of my research in terms of laser operations and principles.

Finally, I would like to say both thank you and sorry to my parents. Most of the time, they do not understand what I am working on. However, they give me all their trust, unselfish love and consistent support. They never complain about my absence from home. I will not acquire all these achievement without their supports and understandings.

# TABLE OF CONTENTS

<b>PERMISSION TO USE</b> .....	<b>i</b>
<b>ABSTRACT</b> .....	<b>ii</b>
<b>ACKNOWLEDGEMENT</b> .....	<b>iv</b>
<b>TABLE OF CONTENTS</b> .....	<b>v</b>
<b>LIST OF FIGURES</b> .....	<b>xiii</b>
<b>LIST OF TABLES</b> .....	<b>xviii</b>
<b>LIST OF ABBREVIATIONS</b> .....	<b>xix</b>
<b>1. Introduction</b> .....	<b>1</b>
1.1 Introduction.....	1
1.2 Motivation and Objective .....	4
1.2.1 Motivation.....	4
1.2.2 Objectives .....	5
1.3 Thesis Organizations.....	5
<b>2. Background</b> .....	<b>10</b>
2.1 Single-Event Effects .....	10
2.1.1 Single-Event Transient (SET).....	12

2.1.2 Single-Event Upset (SEU) .....	13
2.1.3 Single-Event Latch-up (SEL) .....	14
2.1.4 Single-Event Function Interrupt (SEFI).....	14
2.2 SEE Testing Methodology .....	15
2.2.1 Alpha Particle.....	15
2.2.2 Neutron .....	16
2.2.3 Proton.....	16
2.2.4 Heavy Ion.....	17
2.2.5 Pulsed Laser Technique.....	17
2.2.6 Pulsed X-ray Technique .....	20
2.3 Summary .....	21
References.....	21
<b>3. Single-Event Effects Analysis of a Pulse Width Modulator IC in a DC/DC Converter ...</b>	<b>24</b>
3.1 Introduction.....	26
3.2 DC/DC Converter Designs .....	28
3.3 Experimental Details.....	29
3.3.1 Device under Test.....	29
3.3.2 Testing Facilities .....	31
3.4 Experiment Results .....	33
3.5 3D TCAD Modeling .....	36
3.6 Circuit Simulation and Analysis .....	37

3.6.1 Bandgap Circuit Simulation.....	37
3.6.2 Root Cause for 6- $\mu$ s Glitch .....	39
3.7 Hardening Approaches.....	40
3.8 Conclusion .....	41
Acknowledgement .....	42
References.....	42
<b>4. The Effect of Temperature-Induced Quiescent Operating Point Shift on Single-Event Transient Sensitivity in Analog/Mixed-Signal Circuits .....</b>	<b>45</b>
4.1 Introduction.....	48
4.2 Experimental Details.....	50
4.2.1 Device under Test.....	50
4.2.2 Temperature Change and Measurement.....	52
4.2.3 Laser Facility .....	53
4.3 Experimental Results .....	54
4.4 Discussions .....	56
4.4.1 Comparator .....	56
4.4.2 Buffer .....	58
4.4.3 Bandgap Monitor .....	60
4.4 Conclusions.....	60
References.....	61



<b>5. SET Sensitivity Dependency of a DC/DC PWM on Laser Repetiton Rate and Wavelength</b>	<b>65</b>
.....	
5.1 Introduction.....	67
5.2 Experimental Setups and Laser Parameters .....	69
5.2.1. Laser Facility and Device under Test.....	69
5.2.2. Laser Wavelength.....	71
5.2.3. Laser Pulse Duration.....	71
5.2.4. Laser Repetition Rate.....	72
5.2.5. Laser Spot Size .....	73
5.3 Experimental Results .....	73
5.3.1. 800nm Laser Results.....	74
5.3.2. 920nm Laser Results.....	75
5.3.3. 990nm Laser Results.....	75
5.4 Discussions .....	76
5.5 Conclusions.....	78
References.....	78
<b>6. Correlation of Heavy-Ion and Laser Testing on a DC/DC PWM Controller.....</b>	<b>81</b>
6.1 Introduction.....	83
6.2 DC/DC PWM Controller IC .....	86
6.3 Experimental Details.....	86
6.3.1 Device under Test (DUT).....	86

6.3.2 Setups .....	88
6.3.3 Irradiation Facilities .....	89
6.4 Experimental Results .....	92
6.4.1 Heavy-Ion Data .....	92
6.4.2 Laser Data .....	93
6.5 Analyses and Discussions .....	95
6.6 Applications .....	101
6.7 Conclusions.....	103
Acknowledgement .....	104
References.....	104
<b>7. Single-Event Transient Measurements on a DC/DC Pulse Width Modulator Using Heavy Ion, Proton, and Pulsed Laser .....</b>	<b>107</b>
7.1 Introduction.....	109
7.2 Experimental Details.....	111
7.2.1 DUT and Setups .....	111
7.2.2 Irradiation Facilities .....	112
7.3 Experimental Data .....	113
7.4 Analyses and Discussions .....	115
7.4.1 Heavy Ion vs. Proton Data .....	116
7.4.2 Pulsed Laser vs. Proton Data .....	121

7.5 Conclusions.....	122
References.....	122
<b>8. Single-Event Transient Measurement on a DC/DC PWM Controller Using Pulsed X-ray Technique.....</b>	<b>125</b>
8.1 Introduction.....	127
8.2 Experimental Details.....	130
8.2.1 Device under Test (DUT).....	130
8.2.2 Irradiation Facilities.....	131
8.3 Experimental Results.....	133
8.4 Discussions.....	137
8.5 Conclusions.....	139
References.....	140
<b>9. The Single-Event Transient Study of a CMOS BGR Using Pulsed Laser Technique ....</b>	<b>142</b>
9.1 Introduction.....	143
9.2 Device under Test.....	146
9.3 Experimental Details.....	147
9.3.1 Irradiation Facility.....	147
9.3.2 Experimental Results.....	148
9.4 Discussions.....	149
9.5 Applications.....	155

9.6 Conclusions.....	156
Acknowledgements.....	157
References.....	157
<b>10. A RHBD Bandgap Reference Utilizing Single Event Transient Isolation Technique ...</b>	<b>158</b>
10.1 Introduction.....	160
10.2 SET Isolation Structure.....	162
10.3 Radiation Hardened Bandgap Reference .....	165
10.4 Chip Test Results .....	167
10.4.1 Irradiation Facility .....	167
10.4.2 Irradiation Process .....	168
10.4.3 Test Results .....	169
10.5 Discussions .....	173
10.5.1 Positive SET Mitigation.....	173
10.5.2 The SET Sensitivity of the PMOS Switch.....	173
10.5.3 Power Dissipation of the Inverter Chain.....	174
10.5.4 Capacitance .....	175
10.6 Conclusions.....	175
Acknowledgements.....	175
References.....	175
<b>11. Summary and Contributions .....</b>	<b>178</b>

11.1 Summary .....	178
11.2 Contributions.....	180
<b>Appendix A .....</b>	<b>182</b>
<b>LIST OF PUBLICATIONS .....</b>	<b>182</b>

## LIST OF FIGURES

<b>Figure 1.1</b> Single-Event Effect (SEE) schematic.....	2
<b>Figure 1.2</b> Total Ionizing Dose (TID) schematic.....	3
<b>Figure 2.1</b> Single-Event Effect (SEE) current. ....	12
<b>Figure 3.1</b> Block level circuit diagram for a DC/DC converter.....	28
<b>Figure 3.2</b> Test circuit for the complete DC/DC converter.....	30
<b>Figure 3.3</b> (a). The 6- $\mu$ s PGOOD transient observed during pulsed laser testing; (b). The 6- $\mu$ s transient waveforms observed during alpha particle testing. The two waveforms show consistent signatures. ....	34
<b>Figure 3.4</b> The chip micrograph and threshold laser energy for SET of the bandgap sub-circuit. 35	
<b>Figure 3.5</b> SET current pulse simulation waveform. ....	36
<b>Figure 3.6</b> SET propagation path. ....	37
<b>Figure 3.7</b> Schematic simulation for the 6 $\mu$ s glitch on PGOOD. ....	38
<b>Figure 3.8</b> Root cause for 6- $\mu$ s glitch.....	39
<b>Figure 3.9</b> Schematic simulation for hardened bandgap by redesigning the bandgap circuits. 40	
<b>Figure 4.1</b> Waveform for 6- $\mu$ s glitch. ....	49
<b>Figure 4.2</b> Schematic for the DC/DC PWM Controller.....	50
<b>Figure 4.3</b> Symbolic connection of sensitive circuits. ....	51

<b>Figure 4.4</b> Analog circuits under test. ....	53
<b>Figure 4.5</b> Temperature dependence of SET thresholds. ....	56
<b>Figure 4.6</b> Temperature dependence of the current gain for Q0. ....	57
<b>Figure 4.7</b> Temperature dependence of the bias currents for Q0. ....	58
<b>Figure 4.8</b> Temperature dependence of voltages at node B and C. ....	59
<b>Figure 5.1</b> Test circuit for the complete DC/DC PWM converter. ....	68
<b>Figure 5.2</b> Simplified laser path. ....	70
<b>Figure 5.3</b> Micrograph of the DC/DC PWM controller. ....	72
<b>Figure 5.4</b> Threshold power and energy per pulse for 800 nm. ....	73
<b>Figure 5.5</b> Sensitive node schematic for POR and Band Gap. ....	77
<b>Figure 6.1</b> Block level circuit diagram for a DC/DC converter. ....	85
<b>Figure 6.2</b> Test circuit for the complete DC/DC PWM controller. ....	87
<b>Figure 6.3</b> Block diagram for heavy-ion testing. ....	88
<b>Figure 6.4</b> Experimental heavy-ion testing setup in the vacuum chamber. ....	90
<b>Figure 6.5</b> Scanning block units and laser spot size. ....	91
<b>Figure 6.6</b> Cross-section for heavy-ion testing. ....	92
<b>Figure 6.7</b> Cross-sections for 750 nm, 800 nm, 850 nm and 920 nm laser. ....	94
<b>Figure 6.8</b> Cross-section curve fitting for heavy ion and 750 nm wavelength. ....	97
<b>Figure 6.9</b> Cross-section curve fitting for heavy ion and 800 nm wavelength. ....	98
<b>Figure 6.11</b> Cross-section curve fitting for heavy ion and 920 nm wavelength. ....	99

<b>Figure 6.10</b> Cross-section curve fitting for heavy ion and 850 nm wavelength. ....	99
<b>Figure 6.12</b> Laser threshold and equivalent LET in terms of wavelength. ....	100
<b>Figure 6.13</b> Layout of the controller IC and each individual blocks. ....	101
<b>Figure 6.15</b> Calculated heavy-ion cross-sections for individual areas. ....	103
<b>Figure 6.14</b> Cross-sections for individual areas laser testing. ....	103
<b>Figure 7.1</b> Block diagram for the heavy ion test. ....	112
<b>Figure 7.2</b> Calibrated energy vs. cross-section for 920 nm laser. ....	116
<b>Figure 7.3</b> LET vs. cross-section for heavy ion. ....	117
<b>Figure 7.4</b> Proton energy vs. cross-section for proton. ....	118
<b>Figure 7.5</b> Proton LET vs. energy in silicon. ....	119
<b>Figure 7.6</b> Rectangular Parallelepiped (RPP) model for proton. ....	120
<b>Figure 8.1</b> Block level circuit diagram for a DC/DC converter. ....	129
<b>Figure 8.2</b> Test circuit for the complete DC/DC PWM controller. ....	130
<b>Figure 8.3</b> The sample setup in the pulsed X-ray testing. ....	132
<b>Figure 8.4</b> Experimental heavy ion testing setup in the vacuum chamber. ....	133
<b>Figure 8.5</b> SET induced at PGOOD output by X-ray and laser. ....	134
<b>Figure 8.6</b> Sensitive areas in the pulsed X-ray testing. ....	135
<b>Figure 8.7</b> Irregular oscillations at PGOOD pin. ....	136
<b>Figure 8.8</b> The heavy ion and laser experiment results. ....	137
<b>Figure 9.1</b> (a) The schematic of the BGR circuit; (b) The schematic of the AMP circuit. ....	145



<b>Figure 9.2</b> The laser facility setup.....	147
<b>Figure 9.3</b> SETs for transistors Q1 (Q2) at laser energies of 22 nJ, 45 nJ and 91 nJ. ....	149
<b>Figure 9.4</b> SETs for transistors N1 (N2) at laser energies of 0.55 nJ, 1.1 nJ and 1.2 nJ. ....	150
<b>Figure 9.5</b> SETs for transistors P1 (P2) at laser energies of 2.4 nJ, 4 nJ and 4.5 nJ.....	150
<b>Figure 9.6</b> Cross-section for bipolar NPN transistor.....	151
<b>Figure 9.7</b> SET process in the base-emitter region of a bipolar NPN transistor.....	152
<b>Figure 9.8</b> Cross-section for bipolar PNP transistor. ....	154
<b>Figure 9.9</b> TCAD simulation of SET current in a bipolar NPN model. ....	155
<b>Figure 10.1</b> Schematic for the RHBD structure.....	162
<b>Figure 10.2</b> The implementation of the Switch and Sensor.....	163
<b>Figure 10.3</b> Simulation result of the RHBD structure. ....	164
<b>Figure 10.4</b> Schematic of the RHBD BGR circuit.....	165
<b>Figure 10.5</b> Laser Facility Setup.....	167
<b>Figure 10.7</b> Negative SET for laser energy 4.5 nJ.....	169
<b>Figure 10.6</b> Negative SET for laser energy 0.65 nJ.....	169
<b>Figure 10.10</b> Positive SET for laser energy 4.5 nJ.....	170
<b>Figure 10.9</b> Positive SET for laser energy 0.65 nJ.....	170
<b>Figure 10.8</b> Negative SET for laser energy 35 nJ.....	170
<b>Figure 10.11</b> Positive SET for laser energy 35 nJ.....	171
<b>Figure 10.12</b> SET glitches for hitting the PMOS switch. ....	172

**Figure 10.13** Schematic of the improved RHBD BGR circuit. ....174

## LIST OF TABLES

<b>Table 4.1 Experiment Data .....</b>	<b>55</b>
<b>Table 5.1 Laser Results for 800 nm.....</b>	<b>74</b>
<b>Table 5.2 Laser Results for 920 nm.....</b>	<b>75</b>
<b>Table 5.3 Laser Results for 990 nm.....</b>	<b>76</b>
<b>Table 6.1 Heavy ions in use and cross section data.....</b>	<b>89</b>
<b>Table 6.2 Laser Threshold and equivalent LET over wavelength .....</b>	<b>94</b>
<b>Table 6.3 Comparison with previous work.....</b>	<b>100</b>
<b>Table 7.1 Heavy ions in the experiment .....</b>	<b>113</b>
<b>Table 7.2 Heavy ions test data .....</b>	<b>114</b>
<b>Table 7.3 Proton test data .....</b>	<b>115</b>
<b>Table 10.1 Experiment Data .....</b>	<b>172</b>

## LIST OF ABBREVIATIONS

AMS	Analog Mix Signal
ASET	Analog Single Event Transient
COTS	Commercial off the Shelf
DRAM	Dynamic Random-Access Memory
DSET	Digital Single Event Transient
FIT	Failure in Time
FPGA	Field-Programmable Gate Array
GEO	Geosynchronous Equatorial Orbit
HEMT	High-Electron-Mobility Transistor
HI	Heavy Ion
IC	Integrated Circuit
JFET	Junction Field Effect Transistor
LEO	Low Earth Orbit
LET	Linear Energy Transfer
LPF	Low Pass Filter
MBU	Multiple Bit Upset
MCU	Multiple Cell Upset
PLL	Phase Loop Lock
POR	Power on Reset
PSA	Pressure-Sensitive Adhesive
PWM	Pulse Width Modulator
RHBD	Radiation Hardened By Design
RPP	Rectangular Parallel Piped
SBU	Single Bit Upset
SCR	Silicon-Controlled Rectifier
SCU	Single Cell Upset
SE	Soft Error

SEE	Single Event Effect
SER	Soft Error Rate
SET	Single Event Transient
SEU	Single Event Upset
SEL	Single Event Latch-up
SEFI	Single Event Function Interrupt
SEB	Single Event Burnout
SEGR	Single Event Gate Rupture
SPA	Single Photon Absorption
SRAM	Static Random-Access Memory
SRIM	Stopping and Range of Ions in Matter
TCAD	Technology Computer Aided Design
VR	Voltage Reference
TID	Total Ionizing Dose
TPA	Two Photon Absorption

# 1. INTRODUCTION

## 1.1 Introduction

In the last four decades, Integrated Circuit (IC) industry has developed dramatically. The feature size, which is the minimum size of a transistor, of the fabrication process is decreasing from 10 microns in 1971 to 32 nanometer in the early 2010s. In fact, 16 nanometer chips are underway. Since the transistor count per square millimeter of silicon is determined by the surface area of a transistor, the density of transistors increases quadratically with a linear decrease in the feature size. This advance not only decreases the power of the IC, but also minimizes the area of the chip and hence the costs. Furthermore, it accelerates the operation speed of the ICs. However, there are also some downsides along with the shrinking, one of which is the elevating sensitivity to Single-Event Effects (SEEs).

A SEE is the interaction between an energetic particle and the IC materials, such as Silicon and III-V materials. When the particle is penetrating the chip, it ionizes the material along its path and generates extra electron-hole (E-H) pairs as is shown in Fig. 1.1. These excessive carriers will be collected by the electric field between the PN junction of the device, which results in current and voltage variations in the device. In a well-designed IC, soft errors induced by SEEs appear to be the most troublesome both in terrestrial and high altitude or space environment. The error rate caused by SEEs can be as much as 5,000 FIT (Failure in Time: 1 failure per  $10^9$  hours of device operation), while the typical hard failure rates in ICs add up only to 5-200 FIT.

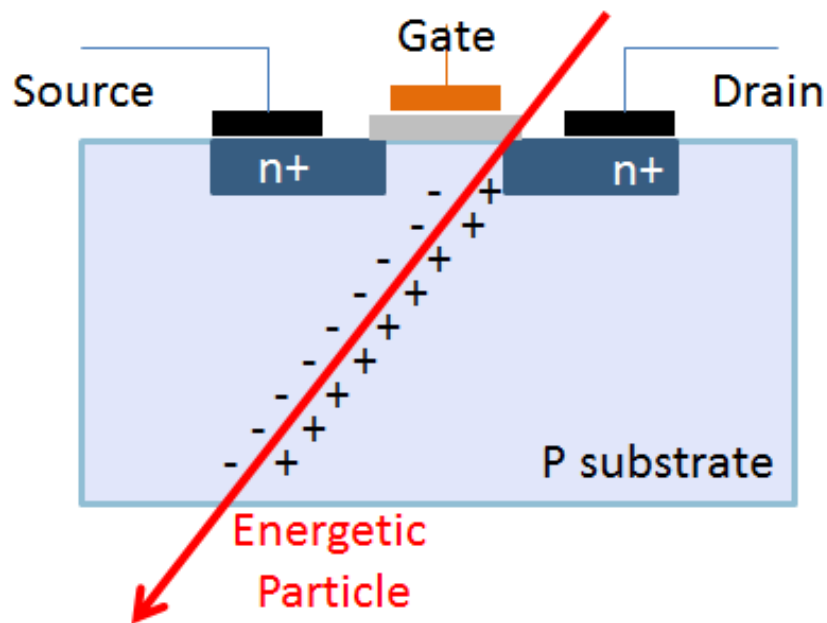


**Figure 1.1** Single-Event Effect (SEE) schematic.

One important SEE phenomenon is the Single-Event Transient (SET). It is a temporary voltage or current transient due to the passage of an energetic particle through sensitive nodes, such as the source and the drain PN junctions. The SET happens in analog ICs, which is known as Analog Single-Event Transient (ASET). There are mainly four types of particles contributing to the SET, namely alpha particles, neutrons, protons, and heavy ions. Their mechanisms of generating SEEs are different from each other. Alpha particles usually derive from the package material  $^{10}\text{B}$  and generate charges through direct ionizations. The mechanisms for high energy neutrons and protons are similar, which have both direct and indirect ionizations while they are different for low energies in that the proton cross-section is smaller due to the existence of the Coulomb Barrier. The mechanism for heavy ions is direct ionization.

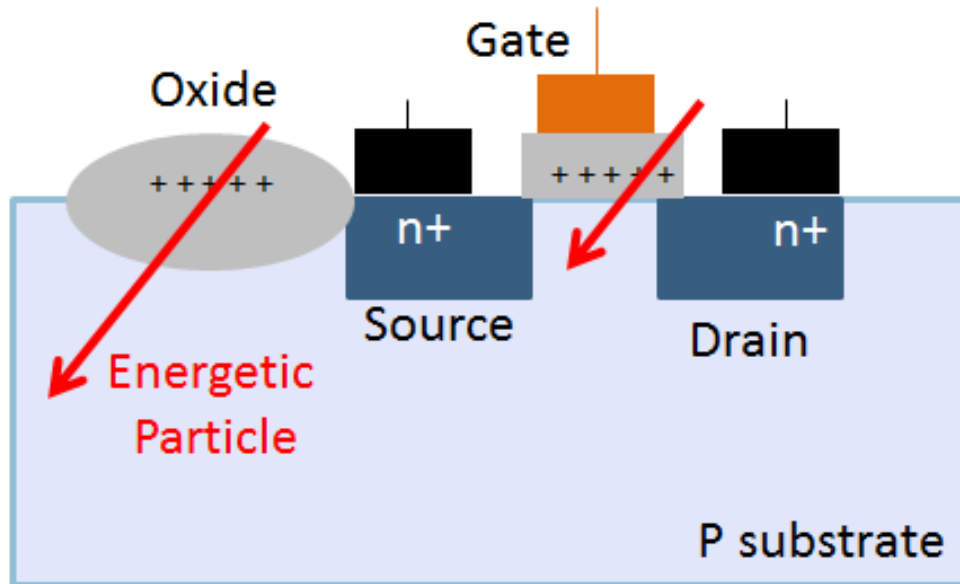


**Figure 1.2** Total Ionizing Dose (TID) schematic.

Another radiation effect similar to SEE is Total Ionizing Dose (TID). Unlike SEE, TID happens at isolation layers, such as poly gate dielectric ( $\text{SiO}_2$  or nitrated  $\text{SiO}_2$ ) and field oxide, which is shown in Fig. 1.2. It is an accumulative long term effect. When the energetic particle hits the oxide, E-H pairs will be generated due to the ionization process. However, the mobility of the electron is fast (for example,  $1350 \text{ cm}^2/\text{vs}$ ) while that of the hole is much slower (for example,  $480 \text{ cm}^2/\text{vs}$ ). As a result, the electrons are collected by the electric field at once while the holes are trapped inside the oxide. The transport of the hole can be as long as many decades. TID can arise along with SEE testing and hence affect the SEE testing.

Generally speaking, there are multiple methodologies to evaluate the SEE, including alpha particles, neutrons, protons, heavy ions, pulsed laser and X-ray. There are several famous facilities capable of performing these testing in the world, such as TSL Uppsala in Sweden,



TRIUMF UBC in Canada, Berkeley Lab in the United States and CIAE in China. These facilities generate moderate radiation environment for SET investigations. However, they are time-consuming and the cost is huge. In addition, it is not easy to locate the sensitive nodes. As a result, researchers began to use pulsed laser to study SEEs. The pulsed X-ray was also proposed as an alternative in recent years. These efficient, economical alternatives can mimic the SET with acceptable accuracy via photon-material interaction. And the well-controlled step size makes it feasible to pinpoint the sensitive nodes to sub-micrometer level. This information helps to verify and improve Radiation Hardened by Design (RHBD) techniques.

## **1.2 Motivation and Objective**

### ***1.2.1 Motivation***

SEE has always been one of major concerns for the reliable applications of DC/DC pulse width modulator (PWM) converter circuits for space applications. As a complex analog/mix signal circuit, each of its sub-circuit can be affected by SEEs. These circuits can have different sensitivities to SEEs and the responses of the DC/DC PWM also vary.

However, the previous SEE studies are all oriented to universe or satellite applications. Four years ago, a commercial network switch was observed to be malfunction during pre-qualification neutron testing. This is an odd phenomenon related to Single Event Transient (SET). After some further investigation, it was decided that the DC/DC PWM chip was sensitive to single-event effects caused by the neutrons on ground level. This is interesting as it is the first report that a DC/DC PWM converter chip is found to be sensitive to SET on ground level applications. As a result, it is both significant and necessary to perform an in depth study on the root cause and its

responses to different irradiation sources. Motivated by this purpose, multiple investigations are carried out.

### ***1.2.2 Objectives***

The objectives of this research are as follows:

1. The comprehensive study on the single-event effect sensitivity of a commercial off the shelf DC/DC PWM chip using multiple methods, including alpha particle, neutron, proton, heavy ion, pulsed laser and X-ray techniques.
2. The comparison of the multiple testing methodologies and the correlations of the data acquired from them.
3. The investigation of SET sensitivity in CMOS bandgap reference circuits and the realization of a SET hardened bandgap reference structure based on the SET isolation technique.

## **1.3 Thesis Organizations**

This thesis is based on the manuscripts published and submitted during the author's Ph. D. program. The main contents of the thesis are composed of the research results acquired in each manuscript. A brief introduction is attached before each chapter to explain its relationship to previous chapters. And the conclusions are summarized at the end of it. The details of the thesis organizations are as follows.

Chapter 1 includes a general introduction to the concepts of single-event effects and DC/DC PWM converter. The TID effect is also described in short. The motivation and objective of this research is presented in this chapter.

Chapter 2 is a detailed explanation to the concepts and knowledge background used in this study. The mechanisms and principles of single-event effects are explained. Different forms of single-event effects are also presented such as SET, SEU, SEL and SEFI. After this, multiple SEE evaluation and testing methodologies are described. For example, the sources of alpha particle, neutron, proton, heavy ion, pulsed laser and X-ray are introduced and the physical principles of these methodologies are explained. The feasibility and limits of each method are analyzed and compared. As an alternative and effective SEE testing method, the pulsed laser technique is described in more details. Both the single photon absorption (SPA) and the two photon absorption (TPA) techniques are presented. The advantages and disadvantages of the pulsed X-ray technique are also presented in this chapter.

The manuscript included in Chapter 3 presents a comprehensive SET sensitivity study on the DC/DC PWM using the pulsed laser technique. The SPA laser with multiple wavelengths is adopted. The DUT is a commercial-off-the-shelf DC/DC PWM chip, which was found to be sensitive to SET on ground level applications. Our study shows that the laser can trigger exactly the same 6- $\mu$ s SET glitches with those of alpha and neutron particle testing. The most sensitive sub-circuit is found to be the bandgap sub-circuit inside the DC/DC PWM chip. It requires least laser energy to have the 6- $\mu$ s SET glitches. The root cause for the 6- $\mu$ s constant is also found out by using model simulations. Radiation hardened methods are also proposed to mitigate the SET effects.

Chapter 4 presents a manuscript that discusses the effects of temperatures on SET sensitivity of Analog/Mix Signal (AMS) circuits. Our study implies that the temperature can change the quiescent point of the circuits dramatically. As a result, some circuits become harder or easier to be affected by SET glitches. However, there are also circuits that see no significant

change in terms of SET sensitivity with respect to temperatures variations. The different responses to temperatures are analyzed from the view of circuit structures and quiescent point shift. The applications of these findings are also discussed.

Chapter 5 presents a manuscript talking about the SET sensitivity dependency of a DC/DC PWM chip on the pulsed laser wavelength and repetition rate. Multiple repetition rates and wavelengths are used to evaluate the SET responses of the DC/DC PWM chip. As expected, different phenomena are observed as the combination of repetition rate and wavelength changes. These phenomena are compared with previous particle testing results, which indicates that the combination of laser repetition rate and wavelength affect not only the SET shape but also the threshold laser energy per pulse. The reasons are discussed in terms of the circuit structures.

Chapter 6 includes a manuscript that discusses the correlation between the pulsed laser and heavy ion testing data. The energy per pulse of the laser is correlated to the LET of heavy ions in terms of threshold energy for the SET. As a result, the equivalent LETs of the pulsed laser for multiple wavelengths are acquired. The results are also compared with the studies of previous research. The applications of the laser equivalent LET are discussed, which shows the capability to plot the cross section for any specific area in the chip.

The manuscript presented in Chapter 7 analyzes the relationship between proton testing data and those from laser and heavy ion tests. The different mechanisms of proton-induced and heavy-ion-induced SET are discussed and verified. The proton testing data is correlated to those of heavy ion by means of a rectangular parallel piped (RPP) model. The data are proven to be reasonable. However, it is not feasible to correlate the proton data to the pulsed laser data. The reason is discussed at the end of the manuscript. The applications of these results are also discussed.

The manuscript included in Chapter 8 investigates the feasibility of pulsed X-ray application in SEE testing on the DC/DC PWM circuit. The advantages of this method, such as enhanced penetration capability, are discussed. On the other hand, its limitations are also discussed. For example, the low energy absorption coefficient of the X-ray hinders its application in SEE testing. Also, the TID effect due to the X-ray irradiation limits the irradiation time. The result indicates that pulsed X-ray can be used to test devices that are particularly sensitive to SEEs.

Chapter 9 discusses the impact of different fabrication processes on the SET sensitivity. A bandgap reference circuit similar to the one in the DC/DC PWM chip was redesigned and fabricated in IBM bulk CMOS 130nm technology. Its SET sensitivity of different devices was studied using the pulsed laser technique. Unlike our previous study in the BiCMOS DC/DC PWM chip, the proportional to absolute temperature (PTAT) current generator transistors (previously mentioned as 3 by 3 areas) are not the most sensitive devices. The reason is determined to be the different bipolar structures in BiCMOS and bulk CMOS technology. Further analysis is performed to explain the difference between the two technologies. This knowledge also gives hints to radiation hardened by design techniques.

In Chapter 10, a novel SET hardened bandgap circuit based on the SET isolation technique is proposed and verified. The sample circuit is fabricated in the IBM bulk CMOS 130nm technology. The structure can dramatically suppress the SET amplitude by temporarily isolating the output within the bandgap core circuit. In this way the majority of the SET glitches will be prevented from propagating to the output. The pulsed laser technique is used to verify the structure. The experimental data show that the proposed structure can effectively reduce the SET effects in the circuits. The SPICE simulation is also performed, and the results are consistent

with those of the pulsed laser test. This structure provides more choices for engineers and researchers in designing RHBD bandgap reference circuits.

Chapter 11 summarizes all the results of this research. The potential applications and contributions of this work are also presented. The future work to improve this research is listed at the end of this chapter, which points out the direction for future study.

## **2. BACKGROUND**

The main purpose of this chapter is to provide a brief review of all the related background knowledge of this research, such as basic concepts and principles. To be specific, it includes the concepts of different types of single-event effects, the principles of different SEEs testing methodologies, and the structure of DC/DC PWM circuit. The main SEE types, such as SET, SEU, SEL and SEFI, are introduced. Also, the theories behind alpha particle, neutron, proton, heavy ion, pulsed laser and X-ray techniques are elaborated and detailed.

### **2.1 Single-Event Effects**

With the fast march of modern IC industry, the feature size of the chip is scaled down from micro meter to nanometer range. On one hand, this shrink brings advantages with respect to chip area, power dissipation, and cost. On the other hand, it makes the chips vulnerable to SEEs, which have become a significant reliability issue.

As presented in Chapter 1, a SEE is the interaction between an energetic particle and the IC materials (such as silicon and III-V materials), or it can be defined as any measurable or observable change in state or performance of a microelectronic device, component, subsystem, or system (digital or analog) resulting from a single energetic particle strike. It normally happens in a PN junction where the depletion region exists. Its essence can be better explained by the field-funneling effect presented in [1, 2].

The SEE is composed of two processes, namely the charge deposition and the charge collection. When the nuclear particle hits the sensitive node, a cylindrical track is formed along with the traverse of the particle. The radius of this track is in submicron level. The material along

the track will be ionized and excess carriers in the form of electron-hole pairs are created with high concentration. This is the course of charge deposition. When these carriers pass the depletion region, they will be collected by the electric field. As a result, a current or voltage perturbation will appear. This is the course of charge collection. This charge collection can distort the potential of the depletion region into a funnel shape, which is called field-funneling effect. This funnel effect can improve the charge collection rate as the electric field is extended into the substrate. The funnel effect is also related to the substrate doping density. This charge collection is caused by the electric field and is the result of the drift of the carriers. As a result, we can call it prompt charge collection. Another type of charge collection dominates when the funnel-shape electric field recovers. It is caused by the carrier density gradient, or in other words, the diffusion of the carriers. Accordingly, it is defined as diffusion charge collection. Both the prompt and diffusion charge collections make up the whole charge diffusion process.

One significant result of the charge collection is the temporary SEE current as is shown in Fig. 2.1. The first half before the peak of the current is in response to the prompt charge collection. It is usually in the order of several picoseconds. On the contrary, the other half is for the diffusion charge collection. And it is usually slow in the order of several hundreds of picosecond depending on the type and energy of the nuclear particle.

The SEE can cause both hard errors and soft errors. The hard error is irreversible and it means the device is damaged or ruined permanently. It includes single-event burnout (SEB) and single-event gate rupture (SEGR), which are often observed in power devices. The soft errors are the ones can be recovered by a power cycle or system reset. It contains single-event transient,



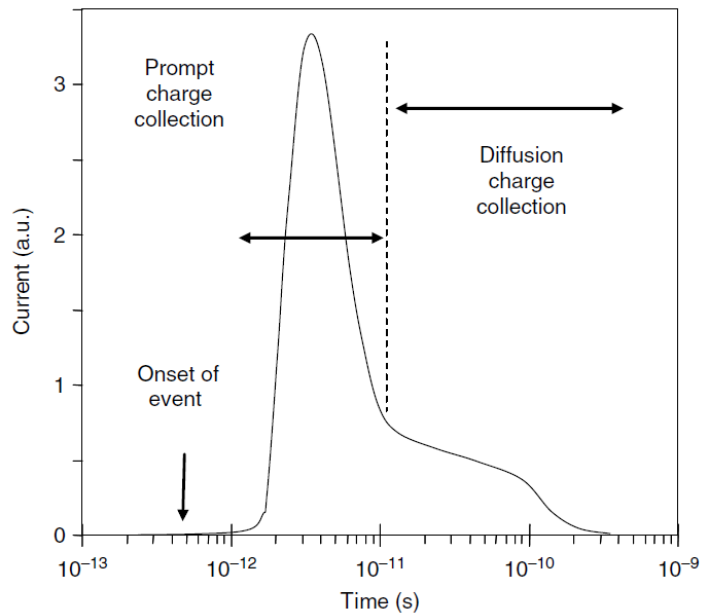


**Figure 2.1** Single-Event Effect (SEE) current.

single-event upset, single-event latch-up, and single-event function interrupt. Note that single-event latch-up can also cause a permanent damage to ICs in some cases. Our research is focused on soft errors, which are presented in details as follows.

### **2.1.1 Single-Event Transient (SET)**

One important type of SEEs is Single-Event Transient (SET). It is the interaction between nuclear particles and the atoms in the materials (usually silicon) when particles penetrate the sensitive nodes of a device, such as the reversed biased p-n junction. This interaction causes temporary voltage and current glitches in the circuits.

SET can be further classified into Digital SET (DSET) and Analog SET (ASET). DSET is often observed in digital circuits, such as combinational and sequential logics. It is also common in registers or memories, which is closely related to Single-Event Upset introduced on the

following section. ASET happens in linear ICs, such as phase loop lock (PLL), operational amplifier (Op-Amp), comparator, voltage references (VR). The effect of SET on the performance or function of the circuit is related to many factors, such as the circuit type, operating configuration, temperature, and striking location. As a result, two parameters are selected to normalize the different SET sensitivities.

Pulse duration and pulse amplitude are normally used as criteria to measure SET glitches. They are two key parameters to evaluate SET phenomenon. The pulse duration is the time from the onset of the SET to the end when the voltage recovers to normal. The SET pulse amplitude is the peak voltage or current variation it reaches. In fact, both parameters reflect the charges collected by the analog circuit from the nuclear strike. For example, the same amount of charge collected can cause different shapes of SET current glitches when hitting on different locations on the circuit. However, the integrations of these current glitches over time are the same, which is the charge collected.

### ***2.1.2 Single-Event Upset (SEU)***

Another popular SEE, especially in SRAM circuits, is the Single-Event Upset (SEU). It can be defined as the state change of memories (SRAM and DRAM) caused by nuclear particle striking on sensitive nodes. This phenomenon was first observed by Timothy C. May and M.H. Woods in 1978 [3]. Ever since then, SEU has been an increasingly critical Soft Error (SE) source.

The energetic particles can cause the state changes of one storage cell, known as Single Cell Upset (SCU), or Single Bit Upset (SBU). However, as the technology scales down, especially when in sub 250 nm nodes, it is more likely that a single strike causes the state changes of

multiple cells and bits, known as Multiple Cell Upsets (MCU) and Multiple Bit Upsets (MBU) [7].

One key concept in SEU evaluation is the critical charge, which is defined as the minimum amount of charge required for the circuit to generate one SEU according to [8]. The concept of critical charge also exists in SET. However, it is not easy to be decided as the values are arbitrary. Note that SET is only considered when it is affecting the function or performance of the circuits. As a result, a specific criterion should be set when talking about critical charge in SET, for example, the SET pulse duration or pulse magnitude.

### ***2.1.3 Single-Event Latch-up (SEL)***

Single-event latch-up (SEL) can drive the transistors in the circuit into an erroneous high-current state, which eventually short the circuit and fail its functionality. In modern CMOS technologies, there are many parasitic bipolar transistors, such as NPN or PNP. One type of parasitic structure is the PNPN. This structure is similar to a thyristor or silicon-controlled rectifier (SCR). In fact, an energetic particle strikes on the sensitive nodes can switch on this SCR, which makes SEL an important SEE phenomenon. However, the SEL can be recovered by applying a power reset.

### ***2.1.4 Single-Event Function Interrupt (SEFI)***

According to JEDEC89a, the definition of SEFI is a soft error that causes the component to reset, lock-up, or otherwise malfunction in a detectable way, but does not require power cycling of the device (off and back on) to restore operability.

## **2.2 SEE Testing Methodology**

Ever since SEE was first observed in 1979 [5], various SEE evaluation methods have been developed to study this phenomenon. Generally speaking, there are two categories of testing methods, namely particle-based testing and optics-based testing. Particle testing uses alpha, neutron, proton, and heavy ion (HI) particles while the optical one contains pulsed laser and X-ray. The mechanisms of these will be elaborated in the following sections.

The evaluation of SEE is usually measured by means of cross section curve. Cross section is defined as the likelihood of the energetic particle interacting with the atoms of material. In other words, it is the number of events per unit fluence. It reflects the area of the device sensitive to SEE. The LET stands for Linear Energy Transfer, which is a commonly used concept in the SEE evaluation. It is the energy transferred by ionizing particle per unit distance.

### ***2.2.1 Alpha Particle***

As mentioned previously, the first observed evident of SEEs is SEUs in a DRAM caused by alpha particles emitted by the nuclear reaction from uranium and thorium in the packaging materials [3]. Alpha particle is composed of two neutrons and two protons. In other words, it is a Helium nucleus with charge. Even though the energy of alpha particle differs a lot, it is usually between 3 MeV to 7 MeV.

Even though packaging materials have been improved in modern IC industry so that the chip is unlikely to be affected by alpha particles, it is still an excellent method to study SEE. The commonly used alpha particle irradiation source is Americium 241 (AM-241). When AM-241 decays to Neptunium 237, it emits alpha particles with energy of 5.4 MeV.

### **2.2.2 Neutron**

Neutron has no net electronic charge. As a result, it is hard to stop. The SEEs in terrestrial applications are almost all caused by neutrons. These neutrons are generated by the nuclear interaction between the oxygen and nitrogen in the atmosphere and cosmic particles with enough energy to penetrate the atmosphere [9]. The flux in terrestrial environment features a spectrum in reverse proportion to the particle energy.

Two famous neutron irradiation facilities all around the world are TRIUMF Neutron Facility (TNF) at TRIUMF lab in Vancouver, Canada and Atmospheric-like Neutrons from thick Target (ANITA) at Svedberg Laboratory (TSL) in Uppsala, Sweden. TNF can provide energy up to 400 MeV while ANITA can generate a neutron beam similar to that of the atmosphere spectrum.

### **2.2.3 Proton**

Proton is a very important subatomic particle. For example, in low and medium earth orbits, 93% of the trapped particles are protons [10].

There are two mechanisms for proton-induced SEE, namely direct and indirect. When the proton energy is high, for example higher than 60 MeV, the LET for proton in silicon is relatively low. As a result, it is likely to trigger SEEs indirectly by collision with material atoms and the generation of secondary particles. On the contrary, when the proton energy is relatively low and the LET in silicon is higher, the proton tends to cause SEEs by directly ionizing the material and depositing extra charges. Obviously, the cross section in the indirect case is much smaller as it is dominated by the nuclear reaction rate of proton collisions. Both types of protons induced SEE plays critical roles of determining soft error rate (SER) in devices.

One commonly used proton facility in the world is Proton Irradiation Facility (PIF) at TRIUMF lab in Vancouver, Canada [11].

#### ***2.2.4 Heavy Ion***

Heavy ion is the nucleus of heavy element. Generally speaking, all the ions heavier than proton can be considered as heavy ions. The LETs of the heavy ions are related to both the ion types and the ion energies. The LET needs to be carefully selected while performing a SEE testing so that a reasonable error count can be triggered and the device will not be ruined.

Even though there are no heavy ions in the terrestrial environment, they are everywhere in the space. As a result, heavy ions are very significant tools to study the SEE. Basically, two types of heavy ion accelerators are widely used, namely the cocktail cyclotron, such as the 88-Inch cyclotron at Lawrence Berkeley national laboratory in the United States and the tandem accelerator, such as the HI-13 tandem electrostatic Van de Graaff accelerator at the Institute of Atomic Energy (CIAE) in Beijing, China [12].

#### ***2.2.5 Pulsed Laser Technique***

Laser is initially an acronym for "light amplification by stimulated emission of radiation". It was first reported in 1960 as ruby laser. Three factors are required to generate laser, which are gain medium, resonator or optical cavity, and pumping mechanisms. When the light from the light source goes into the resonator, it will be amplified by the gain medium in it. In order for the gain medium to amplify the light, it first needs to be pumped by a pumping mechanism such as electric field so that its electrons can be in the stimulated states. There is a pair of mirrors on both ends of the optical cavity and the light inside the cavity will be amplified by bouncing back and forth in between. Only a specific wavelength related to the distance of the cavity will be

amplified. As one of the mirrors is half transparent, the light will go out at some point in the form of laser. The outgoing laser can have different spot sizes based on different configurations of the mirrors [13].

Lasers can be divided into different categories according to different criteria. From the perspective of gain medium types, there are gas laser, liquid laser and solid laser. In terms of pumping methods, there are optical, electrical and chemical lasers. From the time interval point of view, there are continuous laser and pulsed laser.

Pulsed laser technique has been widely used in Nuclear & Plasma Sciences Society (NPSS) as a complementary tool for SEE investigations ever since 1990s [14-15]. One reason for this is that it possesses a lot of advantages in terms of SEE testing. As other types of lasers, the pulsed laser has excellent spatial and temporal coherence. These features provide excellent benefits in SEE testing. The first benefit is the well-controlled irradiation location. As we know, the location of the laser beam size is precisely controlled with a resolution in micrometer level. This makes it much easier to study the different SEE sensitivities inside the devices. The second one is the well-controlled timing. Similar to the well-controlled location, the irradiation time of the laser is also easy to control. In this case, we can control the time interval between each laser pulse. It can also be synced with external frequency generator to acquire a wider range of frequency selection. The third one is the well-controlled energy. The laser energy per pulse can be easily controlled, for example, using optical attenuators. In this way, we can gradually modify the laser energy to reduce the risk of ruining the devices. The fourth one is the better accessibility and affordability. The cost of laser facility is much lower compared with accelerators, which makes it much more affordable. As a result, it is easier to get access to laser facilities. There are also other advantages that make pulsed laser a useful alternative tool for SEE study.

Even through the charge generation mechanism in silicon by a laser is quite different from that of particles, the charge generated can be absorbed by circuit nodes, which is very similar to heavy ions. According to optical absorption mechanisms, if the photon energy is larger than the bandgap of the material, it can be absorbed and material will be ionized. This so-called Single Photon Absorption (SPA) finds a lot of application in SEE field [16-18]. For a generic SPA testing, the laser is applied from the top or front side of the die. It is focused on the region of interest. After that, the energy will be increase until SEE is observed. This SPA front side irradiation facilitates the SEE study significantly. However, as the IC technology advances, the number of metal layers are increasing, which will stop the laser from accessing the devices in the circuits. In this case, SPA front side irradiation meets its bottleneck due to the multiple layers of metal filling on top of the die. SPA back side irradiation comes out under this context. The only different is that it is applied from the back side of the die, namely the substrate. This can be realized in two ways. One is to use a relatively long wavelength laser, such as 1064 nm [19, 20], which has a much smaller absorption coefficient. And hence it can penetrate the thick substrate to hit on the actual transistors on the die. The other way is to use a medium wavelength, such as 800 nm [21], but the substrate is thinned to around 100 nm and below before the testing.

The aforementioned photon mechanism only absorbs one photon at a time. Even though SPA back side irradiation solves the problem in some sense, the dramatic energy loss while traversing the thick substrate degrades its practical value. Also, the cost and time to thin the substrate aggravates its limitation. As a result, researchers begin to seek for better application of pulsed laser technique. In 2002, the Two Photon Absorption (TPA) laser was proposed to be applied in SEE studies [22]. This methodology takes advantage of the second order nonlinear optical absorption of laser in materials. In other words, when the laser intensity is extreme high,



two photons can be absorbed simultaneously at the focusing point. Based on this principle, the long wavelength laser with photon energy lower than the bandgap energy of materials, such as silicon, can be adopted to perform the SEE testing. In other words, when the laser is applied from the back side (substrate) of the die, it will traverse the substrate with little absorption as its photon energy is too low to ionize the silicon. However, at its focusing point, where the laser is focused and its density is high, two photons are absorbed at the same time to generate one pair of electron and hole. The generated charge will be collected by the nodes in the circuits for SEE studies. As time goes by, the increasing metal layers on the chip covers the transistors throughout, which block the laser coming from the front side of the chip. Also, modern IC chips tend to use the flip chip package, which only exposes the substrate to the top. As a result, TPA is becoming more and more popular in SEE testing.

### ***2.2.6 Pulsed X-ray Technique***

As a complementary optical tool to simulate radiation environment, X-ray has always been playing its critical role in TID testing as a radiation source. However, recently, researchers have reported the potential application of pulsed X-ray in SEE testing [23]. X-ray is usually generated from the electromagnetic radiation of electrons transfer from higher energy levels to lower ones. Two obvious benefits of pulsed X-ray compared with its laser counterpart is the smaller resolution and the metal penetration ability. Theoretically, the resolution for X-ray can go to sub-micro level thanks to its much shorter wavelength. This feature is very attractive in the SEE testing of advanced IC technologies. To add to its advantage, the much higher photon energy makes it relatively transparent to metal interconnections on top of the chip. This makes the front side irradiation feasible even when metal layers are on the way, which facilitates the testing.

However, some potential side effects are to be dealt with, such as low absorption coefficient and TID effect on the testing results.

## **2.3 Summary**

In this chapter, the basic principles and concepts about single-event effects, such as single event transient, single event upset, and single event latch-up, are described. Some fundamental concepts, for example linear energy transfer (LET), are also explained. This knowledge is the basics to understand the research in this field.

The theories behind the various SEE testing technologies are also introduced and elaborated in this chapter. Both the particle-based and the optical-based methods are explained. To be specific, alpha particle, neutron, proton, heavy ion, pulsed laser and X-ray are introduced from the perspective of SEE testing. This knowledge will provide basic understandings for the experiment processes presented in this thesis.

## **References**

- [1] C. M. Hsieh, P. C. Murley, and R. R. Obrien, "A Field-funneling Effect on the Collection of Alpha-Particle-Generated Carriers in Silicon Devices," *IEEE Electron Device Letters*, vol. 2, no. 4, pp. 103 - 105, April. 1981.
- [2] R. Baunmann, "Effects of Terrestrial Radiation on Integrated Circuits," in *Handbook of Semiconductor Manufacturing Technology*, 2000, CRC Press.
- [3] T. C. May, and M. H. Woods, "Alpha-particle-induced soft errors in dynamic memories," *IEEE Trans. Electron Devices.*, vol. 26, no. 1, pp. 2 - 9, Jan. 1979.
- [4] T. C. May, and M. H. Woods, "A New Physical Mechanism for Soft Errors in Dynamic Memories," *Reliability Physics Symposium*, pp. 33 - 40, 1978.
- [5] T. C. May, "Soft Errors in VLSI: Present and Future," *IEEE Trans. Components, Hybrids,*

- and Manufacturing Technology, vol. 2, no. 4, pp. 377 - 387, Dec. 1979.
- [6] E. S. Meieran, P. R. Engel, and T. C. May, "Measurement of Alpha Particle Radioactivity in IC Device Packages," Reliability Physics Symposium, pp. 13 – 22, 1979.
- [7] E. Ibe, H. Taniguchi, Y. Yahagi, K. Shimbo, and T. Toba, "Impact of scaling on neutron-induced soft error rate in SRAMs from a 250 nm to a 22 nm design rule," IEEE Trans. Electron Devices., vol. 57, no. 7, pp. 1527 - 1538, Jul. 2010.
- [8] F. W. Sexton, "Measurement of Single-Event Phenomena in Devices and ICs," in 1992 IEEE Nuclear Space Radiation Effects Conf. Short Course, New Orleans, LA, pp. III-1–III-55.
- [9] C. S. Dyer, S. N. Clucas, C. Sanderson, A. D. Frydland, and R. T. Green, "An Experimental Study of Single-Event Effects Induced in Commercial SRAMs by Neutrons and Protons From Thermal Energies to 500 MeV," IEEE Trans. Nucl. Sci., vol. 51, no. 5, pp. 2817–2824, Oct. 2004.
- [10] J. D. Popp, "Developing Radiation Hardened Complex System on Chip ASICs in Commercial Ultra Deep Submicron CMOS Processes," IEEE NSREC short course, 2010.
- [11] E.W. Blackmore, "Operation of the TRIUMF (20-500 MeV) proton irradiation facility," Radiation Effects Data Workshop, 2000, TRIUMF, Vancouver, BC.
- [12] G. Guo, D. Shen, S. Shi, Q. Chen, J. Liu, J. Xu, X. Lu, N. Hui, L. Cai, L. Gao, H. Wang, R. Teng, B. Wu, D. Wang, S. Du, and H. Fan, "Irradiation facility and technique to increase LET for SEE testing on tandem accelerator," Radiation and Its Effects on Components and Systems (RADECS), pp. 724 -728, Sept. 2011.
- [13] D. L. Andrews, "Lasers in Chemistry," Springer Press, 1986.
- [14] S. Buchner, D. McMorrow, C. Poivey, J. Howard, Y. Boulghassoul, L. W. Massengill, R. Pease, and M. Savage, "Comparison of single-event transients induced in an operational amplifier (LM124) by pulsed laser light and a broad beam of heavy ions," IEEE Trans. Nucl. Sci., vol. 51, pp. 2776–2781, Dec. 2004.
- [15] J. S. Melinger, S. Buchner, D. McMorrow, W. J. Stapor, T. R. Weatherford, and A. B. Campbell, "Critical evaluation of the pulsed laser method for single event effects testing and

- fundamental studies,” IEEE Trans. Nucl. Sci., vol. 41, pp. 2574–2584, Dec. 1994.
- [16] S.D. LaLumondiere, R. Koga, P. Yu, M.C. Maher, and S.C. Moss, “Laser-induced and heavy ion-induced single-event transient (SET) sensitivity measurements on 139-type comparators,” IEEE Trans. Nucl. Sci., vol. 49, no.6, pp. 3121 -3128, Dec. 2002.
- [17] S. Buchner, D. McMorrow, A. Sternberg, L. Massengill, R.L. Pease, and M. Maher, “Single-event transient (SET) characterization of an LM119 voltage comparator: an approach to SET model validation using a pulsed laser,” IEEE Trans. Nucl. Sci., vol. 49, no.3, pp. 1502 -1508, Jun. 2002.
- [18] J.A. Mazer, S. Buchner, and K. Kang, “Laser simulation of single-event upset in a p-well CMOS counter,” IEEE Trans. Nucl. Sci., vol. 36, no. 1, pp. 1330 -1332, Feb. 1989.
- [19] F. Darracq, H. Lapuyade, N. Buard, F. Mounsi, B. Foucher, P. Fouillat, M.C. Calvet, and R. Dufayel, “Backside SEU laser testing for commercial off-the-shelf SRAMs,” IEEE Trans. Nucl. Sci., vol. 49, pp. 2977 -2983, Dec. 2002.
- [20] C. Weulersse, F. Bezerra, F. Miller, T. Carriere, N. Buard, and W. Falo, “Probing SET sensitive volumes in linear devices using focused laser beam at different wavelengths,” RADECS Conference, 2007.
- [21] D. Lewis, V. Pouget, F. Beaudoin, P. Perdu, H. Lapuyade, P. Fouillat, and A. Touboul, “Backside laser testing of ICs for SET sensitivity evaluation,” IEEE Trans. Nucl. Sci., vol. 48, no. 6, pp. 2193 -2201, Dec. 2001.
- [22] D. McMorrow, W. T. Lotshaw, J. S. Melinger, S. Buchner, and R. L. Pease, “Subbandgap laser-induced single event effects - carrier generation via two-photon absorption,” IEEE Trans. Nucl. Sci., vol. 49, no. 6, pp. 3002 -3008, Dec. 2002.
- [23] D.M. Cardoza, S.D. LaLumondiere, M.A. Tockstein, S.C. Witczak, Y. Sin, B.J. Foran, W.T. Lotshaw, and S.C. Moss, “Single Event Transients Induced by Picosecond Pulsed X-Ray Absorption in III–V Heterojunction Transistors,” IEEE Trans. Nucl. Sci., vol. 59, pp. 2729–2738, Dec. 2012.

### **3. SINGLE-EVENT EFFECTS ANALYSIS OF A PULSE WIDTH MODULATOR IC IN A DC/DC CONVERTER**

*Published as:*

Y. Ren, L. Fan, L. Chen, S.-J. Wen, R. Wong, N. W. van Vonno, A. F. Witulski, and B. L. Bhuva, “Single-Event Effects Analysis of a Pulse Width Modulator IC in a DC/DC Converter,” *Springer Journal of Electronic Testing: Theory and Applications*, vol. 28, no. 6, pp. 877–883, Dec., 2012.

In the previous chapter, the mechanisms of two main radiation effects in electronic devices, namely the SEE and TID, are introduced. As the IC technology advances, the TID effect is becoming less and less significant due to the even thinner gate oxide (around several nanometers). On the other hand, SEE has become a more significant problem in the field of radiation effect studies due to the reduced feature size of transistors. The different types of SEEs, including SET, SEU, and SEB, are further discussed. The general SEE evaluation methodologies, such as alpha particle, neutron, proton, heavy ion, pulsed laser and X-ray, are also presented and compared in chapter 2. The advantages and disadvantages for each method are analyzed. The fast development of SEE testing technology also accelerates the pace of SEE study, which in return, requires more accurate and convenient testing techniques.

In this manuscript, a commercial-off-the-shelf DC/DC PWM chip sensitive to SEEs is investigated using a pulsed laser. During pre-qualification neutron testing, a 6- $\mu$ s glitch was observed at the PGOOD pin of the DC/DC PWM chip. The laser testing can trigger exactly the

same Single Event Transient (SET). In addition, the most sensitive devices are pinpointed by gradually decreasing the laser energy per pulse. The laser testing result indicates that the most sensitive devices are nine bipolar transistors inside the bandgap circuit of the chip. This is also verified by means of circuit level simulation and 3D-TCAD modeling. The simulation result further reveals the cause of the 6- $\mu$ s glitch, which is a capacitor on the SET propagation path. Finally, two mitigation methods based on system level and chip level are proposed to alleviate the SET sensitivity of the DC/DC chip. To be specific, from system level, a Low Pass Filter (LPF) can be applied to the PGOOD pin of the DC/DC chip so that the 6- $\mu$ s SET glitch is filtered. The chip level solution is to increase the bias currents in the sensitive path, in which way both the amplitude and duration of the SET pulse is decreased. It is also verified by circuit level simulations.

To sum up, a comprehensive study on the SET sensitivity of a COTS DC/DC chip is performed using pulsed laser technique. Both the most sensitive devices and its root cause are pinpointed. In addition, two solutions are proposed to mitigate the SET sensitivity. The results are also verified by circuit level simulations.

# **Single-Event Effects Analysis of a Pulse Width Modulator IC in a DC/DC Converter**

Y. Ren, L. Fan, L. Chen, S.-J. Wen, R. Wong, N. W. van Vonno, A. F. Witulski, B. L. Bhuvu

## **Abstract**

Alpha particles, neutrons and laser-beam test results on an integrated pulse width modulation (PWM) controller operating in a DC/DC converter are presented in this paper. The PWM is fabricated on a 600-nm Bi-CMOS technology. Single-Event Transient (SET) derived from a bandgap circuit was amplified by a filter capacitor in the propagation path. Finally, a constant 6- $\mu$ s SET pulse was observed on PGOOD pin which is a supervisory signal. This glitch caused system resets. Pulsed laser technology was adopted to locate the origin of the SET. The 3D TCAD and circuit simulation tools were used to analyze the root cause. System and circuit level hardening approaches to mitigate the SET are also presented.

## **Index terms**

Single-Event Transient, Pulse Width Modulator, DC/DC Converter, Laser.

## **3.1 Introduction**

Any complex electronic system requires multiple DC voltages to function. These required DC voltages are usually generated by DC/DC switching converters to convert a single DC input source to multiple regulated DC output voltages with high power efficiency. These DC/DC converters use a supervisory circuit block that outputs a signal to indicate normal operation of the converter. The main system controller relies on this signal (usually only on this signal) to

monitor the health of the whole system (or to monitor the DC power supply to various parts of the system). Upon failure detection on this signal (a transition on this signal), the main system controller may determine to shut down or restart the whole system. If false signals are introduced by soft errors causing by Single-Event Effect (SEE), the system malfunctions. As a result, it is very important to understand the effects of single-events on DC/DC converters and develop techniques to harden them against single events.

SEE has always been a main source of soft errors in electronic devices. It is the interaction between particles and atoms in the material (usually silicon) when particles penetrate the devices. To be specific, the energized particle ionizes the material atom and generates electron-hole pairs, which are collected by the electric field in the PN junction. This causes current and voltage variations in electronic devices. These variations propagate in the circuits and lead to system failure. Previously, researchers have reported that each part of the DC/DC converters can exhibit unexpected single-event effects (SEEs) [1]-[4]. Soft-start circuits can greatly affect the controller response, depending on the PWM configuration [5], [6]. Others have reported SEE sensitive areas in the control circuitry using pulsed laser techniques [7]-[9]. Previous studies also reported a long duration pulse in a sole bandgap reference circuit in both heavy-ion and laser testing [11], which shows the bandgap circuit itself is potentially sensitive to SET. As far as the authors know, this is the first paper analyzing comprehensively how the bandgap circuit SET affects a complex commercial DC/DC converter in ground application using pulsed laser technique. This paper also shows that CMOS process with larger feature size, such as 600 nm, is also vulnerable to SET. Capacitors in the SET propagation path are potential threats to the chip function, which designers should be able to predict and take into consideration in the initial design.



### 3.2 DC/DC Converter Designs

Fig. 3.1 shows the major components of a DC/DC converter circuit based on pulse width modulation technique. The circuit contains a Pulse Width Modulation (PWM) block, power devices, and passive components. PWM block further contains a PWM circuit, a bandgap reference circuit, soft-start circuit, and an error amplifier. PWM block generates the signal that controls the duty cycle (designated as  $D$ ) of the power transistor (or percent of time that power transistor is ON). The converter topology determines the relationship between the DC input and output voltages. For the commonly used buck converter, the relationship is described by [12]

$$V_{out} = DV_{in} \quad (3.1)$$

The soft-start circuit limits the load current, shown as  $i_L$  in Fig. 3.1 by means of modulating

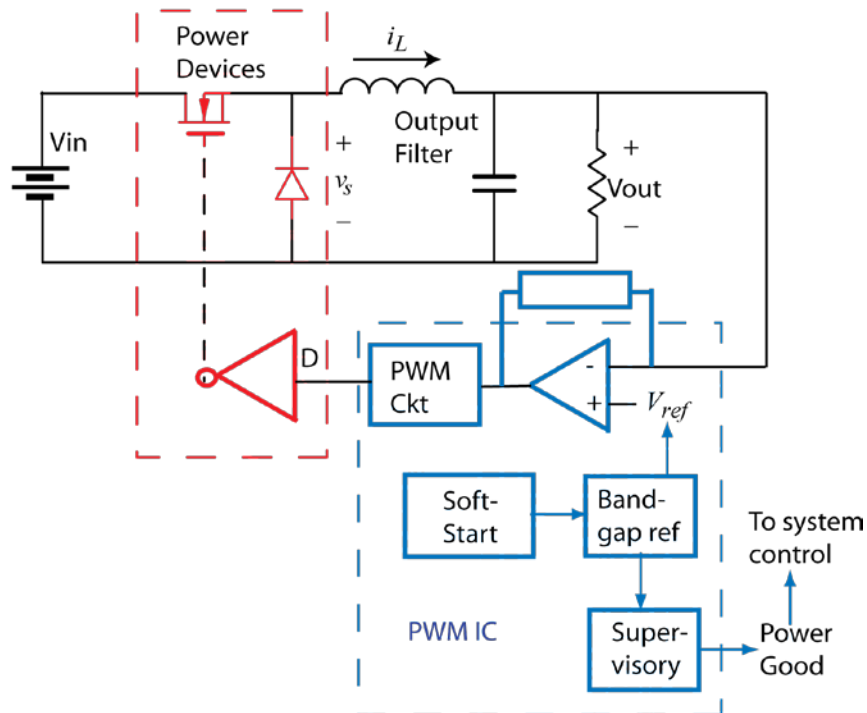


**Figure 3.1** Block level circuit diagram for a DC/DC converter.

the duty cycle at the start up. PWM block also generates a “Power Good” signal through Supervisory circuit (shown in Fig. 3.1) to monitor the health of the DC/DC converter. The supervisory circuit monitors all other blocks to generate “Power Good” signal. System-level controllers monitor this “Power Good” signal with the assumption that any transitions on it represent a faulty operation of DC/DC converter.

Single-events can affect any one of circuits in PWM [1]-[10], but hits to the PWM often do not significantly disturb the output voltage of the converter because perturbations of individual duty cycles are filtered by the LC filter on the output of the converter. The output voltage responds only to the average duty cycle. Any hits on soft-start will also not have a significant impact on overall operation of the circuit. However, a single event strike in the supervisory circuit or the bandgap reference circuit is particularly severe because it may send a false signal to a system controller that shuts down or resets the entire system the DC/DC converter resides in, even though the output voltage of the converter is not affected. The following sections describe an investigation of a DC/DC converter chip that has been causing system resets in a terrestrial environment. An SET induced 6- $\mu$ s glitch was observed in both alpha particle and pulsed laser experiments. The mechanism was probed by means of 3D TCAD modeling and circuit level simulation.

### **3.3 Experimental Details**

#### ***3.3.1 Device under Test***

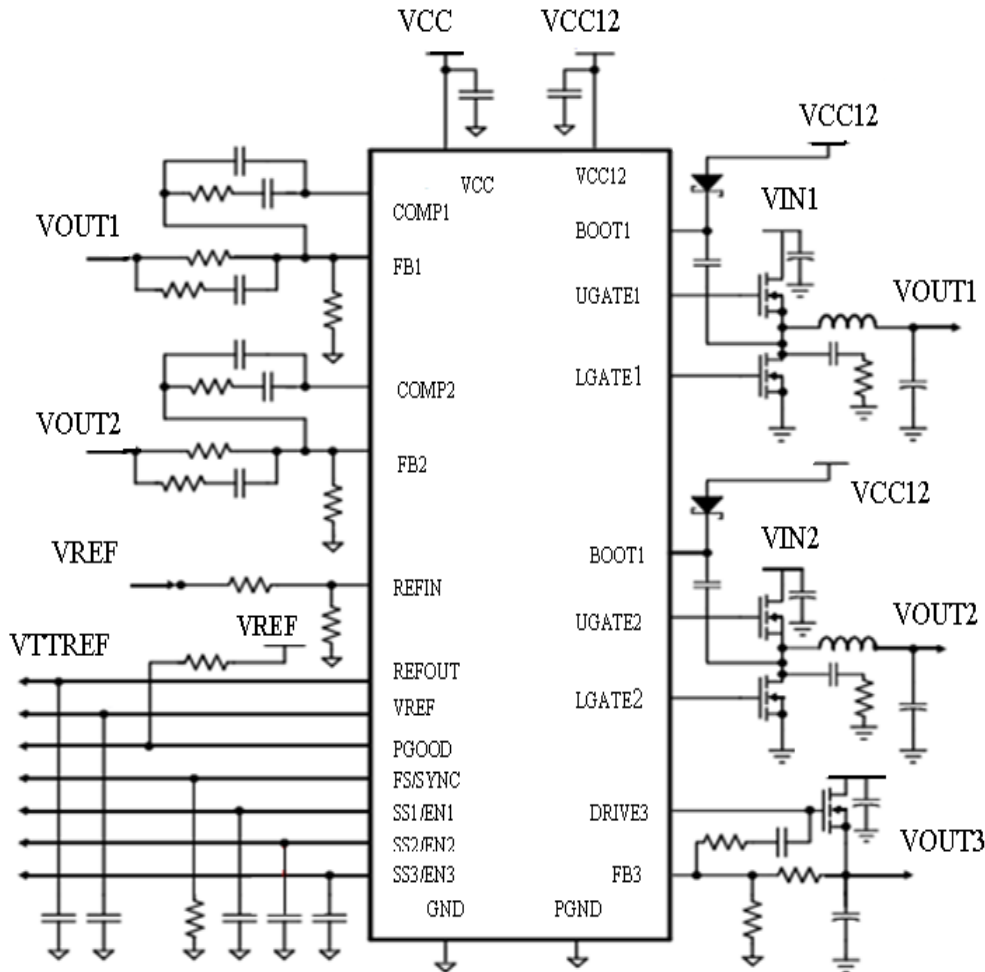


**Figure 3.2** Test circuit for the complete DC/DC converter.

The DC/DC converter under study is a triple regulator that has two independent synchronously-rectified buck controllers (OUT1 and OUT2) and a linear controller (OUT3) to offer precise regulation of up to three voltage rails. The test circuit is shown in Fig. 3.2. The three soft-start pins, namely SS1/EN1, SS2/EN2 and SS3/EN3, are grounded through a capacitor respectively. The PGOOD pin is an open-drain pull-down device output connected to VCC, which is the high level voltage monitoring almost every circuit in the controller IC. When power is first applied to the IC, the PGOOD output is pulled low indicating an initial condition. After all

three soft-start pins complete their ramp-up with no faults (no short detected on switchers), the power is considered “GOOD” as indicated by a high PGOOD pin.

The DC/DC converter IC from a 600-nm Bi-CMOS process was used in the above configuration within a Cisco Layer-2 Switch. Switches and routers are the building blocks for all business communications, from data to voice and video to wireless access. This Switch was introduced in the commercial market in 2007. During normal qualification testing by the manufacturer, the whole Layer-2 Switch was exposed to neutron beams. The neutron exposure resulted in silent reboot without any error symptoms or error recordings in the data transmission. The failure rates observed for neutron exposure were in the 500 FIT range.

### ***3.3.2 Testing Facilities***

To identify the failure mechanism for this Layer-2 Switch, multiple alpha particle exposures were carried out where most I/O signals on the Switch were monitored for failure signature. For alpha particles exposure, an Am-241 disc was placed directly over a decapped and depassivated DC/DC converter within a Switch as well as on evaluation boards. The energy of the alpha particles was 5.48 MeV. The flux and fluence values for the alpha particle exposures were estimated as  $1 \times 10^4 \text{ cm}^{-2} \text{ s}^{-1}$  and  $3.6 \times 10^7 \text{ cm}^{-2}$ , respectively.

The neutron tests were performed at the Svedberg Laboratory (TSL) in Uppsala, Sweden with a neutron energy range of 11-175 MeV. The flux and fluence values for the neutron exposures were  $2 \times 10^5 \text{ cm}^{-2} \text{ s}^{-1}$  and  $7.2 \times 10^8 \text{ cm}^{-2}$ , respectively.

The laser-induced SEE testing facility used in this work is located at Saskatchewan Structural Sciences Centre (SSSC). The basis of the laser scanning system is a Zeiss LSM410 confocal microscope, which is on a floating optical table to reduce mechanical vibration

transferred to the instrument. The Coherent, Inc. Mira laser system is the source of the testing laser. It has a tunable Ti:sapphire laser with wavelengths ranging from 700 nm to 1000 nm. The Mira system is capable of emitting a continuous wave beam, picosecond and femtosecond pulses, with tunable repetition rates from 10 kHz to 75 MHz. The laser beam is focused on the surface of the die (spot diameter is 1.6  $\mu\text{m}$ ) through the microscope. The working distance of the objective lens is 0.61 mm for the 20X type. The translation of the device under test (DUT) was precisely controlled by an XYZ motorized stage with a resolution of 0.1  $\mu\text{m}$ . During laser testing, all necessary outputs of the DC/DC converter were monitored on a digital oscilloscope.

The laser experiments consisted of scanning the entire die on a decapped package with pulsed laser. In general, the laser experiments were carried out in three steps. First, a fast, whole chip, continuous auto-scanning was adopted to locate the relatively sensitive areas. Secondly, a slow, localized auto-scanning was used to pinpoint the most sensitive transistors. Finally, a manual spot scanning was introduced to determine the sensitivity of nodes in these transistors.

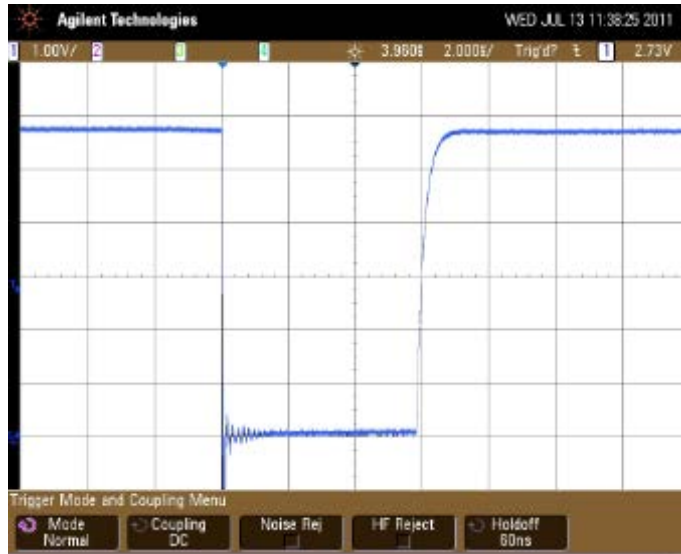
Two types of laser sets were used, one of which was for imaging while the other for SEE generation. HeNe 633 continuous wave laser was selected to image the layout of the chip. As for the SEE laser, considering the correlation between wavelength and absorption coefficient [13], [14], pulsed lasers of three different wavelengths, namely 800 nm, 920 nm and 990 nm, were chosen to perform the experiments in order to guarantee the fidelity and validity. The laser pulse energy was varied continuously through the combination of internal polarizers and external optical densities to establish a threshold level at any location that was found to exhibit SEE sensitivity. In the experiments, the laser pulse width was set at 1 ps and the repetition rate was 10 kHz. The SEE and HeNe 633 laser were aligned accurately to make sure they irradiated concentrically. One photon-absorption front side irradiation technique was employed here, as the

DC/DC converter controller was based on a three-metal-layer process with very little metal layers on top of the active devices targeted for study. The waveforms from the DUT outputs were captured for SEE analysis using digital oscilloscopes triggering on several of the outputs when they transgressed the limits of normal operations. The PGOOD signal was used as the indicator for SET events.

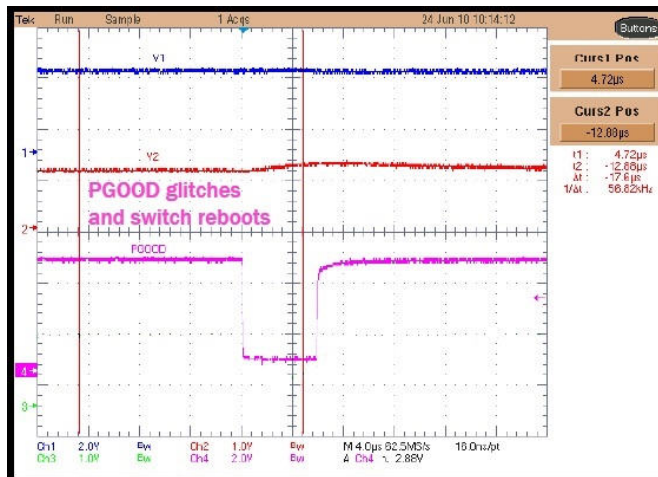
### **3.4 Experiment Results**

During alpha particles and neutron beam exposures, the Switch repeatedly went through the restart process. After checking for all possible scenarios that can cause a restart, it was determined that the main cause of the restart was the PGOOD signal from DC/DC converter IC. This was verified by checking PGOOD signal during testing. SET pulses as long as 6  $\mu$ s were recorded for both neutron and alpha particle exposures. Since these experiments cannot be used to identify the sensitive sub-circuits responsible for generating the 6- $\mu$ s SET pulses, laser-beam experiments were carried out.

For laser experiments, systematical scanning of the whole chip using 800 nm, 920 nm and 990 nm laser pulses with 10 kHz repetition rate were carried out to identify the most sensitive areas. The SET pulses on PGOOD output for these sensitive regions were recorded and shown in Fig. 3.3(a). The 6- $\mu$ s glitch was observed using any of the three wavelengths. Fig. 3.3(b) shows the PGOOD signal (the pink waveform) recorded during alpha particle exposures. Both the exposures show similar pulse width for PGOOD output.



(a)



(b)

**Figure 3.3** (a). The 6- $\mu$ s PGOOD transient observed during pulsed laser testing; (b). The 6- $\mu$ s transient waveforms observed during alpha particle testing. The two waveforms show consistent signatures.

Once the most sensitive areas on the IC were identified, more experiments were carried out to identify the laser-energy threshold for all of the sensitive areas. The most sensitive sub-circuit

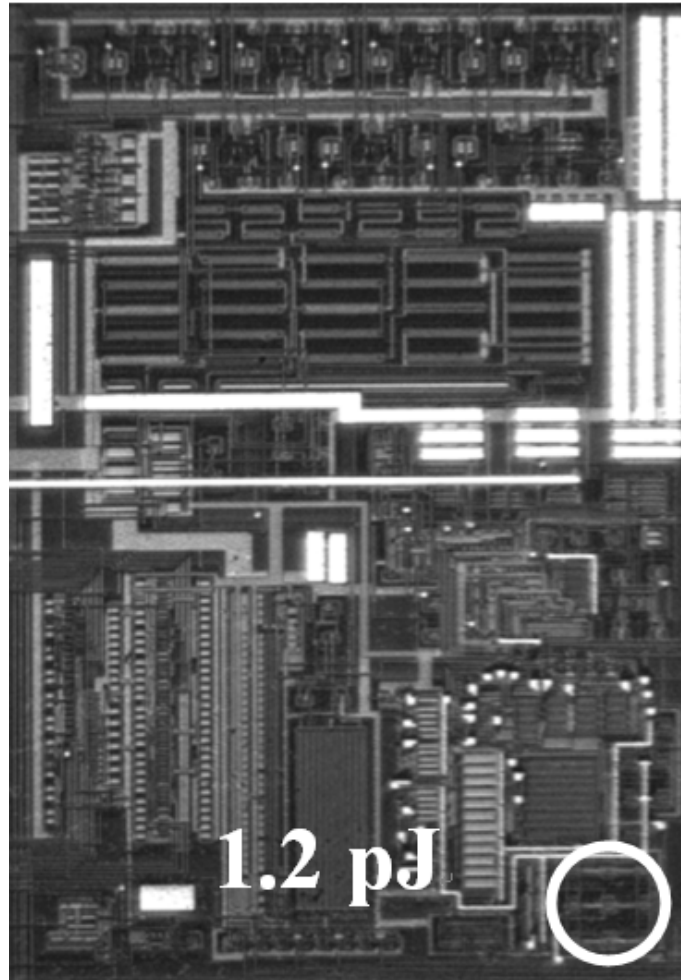


**Figure 3.4** The chip micrograph and threshold laser energy for SET of the bandgap sub-circuit.

on the IC was the bandgap reference circuit. A bipolar transistor pair in it is even more sensitive than other transistors. The reason was found to be the relatively small quiescent current values for the most sensitive nodes. This resulted in low restoring currents, causing long SET pulses. The laser energy threshold for a hit on bandgap circuit to generate an SET pulse on PGOOD output was 1.2 pJ (800 nm). A die photograph showing the location of bandgap sub-circuit along with the threshold laser energy is shown in Fig. 3.4.



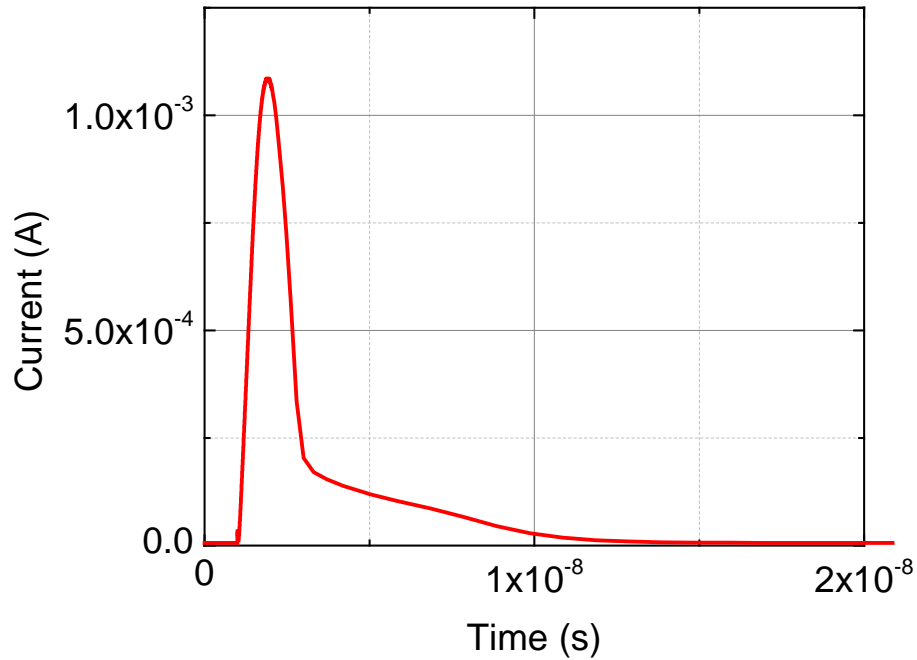


**Figure 3.5** SET current pulse simulation waveform.

### 3.5 3D TCAD Modeling

3D TCAD modeling was carried out by using Sentaurus TCAD to gain information of the current pulse generated by particle striking. As the sensitive transistors in bandgap circuit are bipolar configurations, a NPN transistor model was built. The dimension of the NPN transistor model is  $20\ \mu\text{m} \times 20\ \mu\text{m} \times 20\ \mu\text{m}$  for the technology used in the chip and the model contains about 200,000 elements.

In the 3D TCAD SET simulations, the bias currents were properly set according to the working condition of the circuit. Three nodes, namely the base, the emitter and the collector, were stricken. We found that the collector node exhibited the most pronounced pulse.

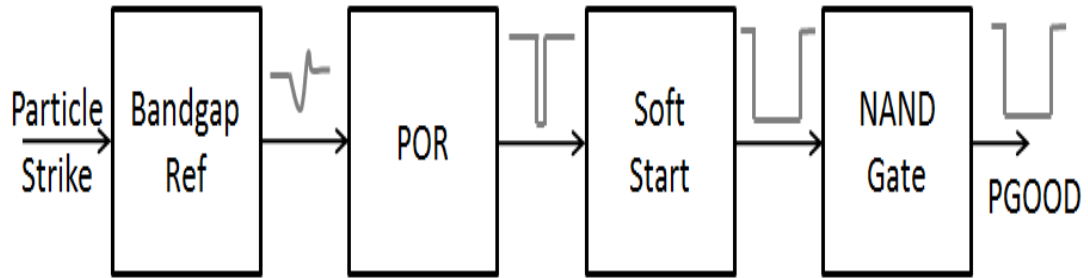


**Figure 3.6** SET propagation path.

3D TCAD simulation results are shown in Fig. 3.5. The pulse duration and amplitude are about 10 ns and 1.2 mA, respectively. The fast incremental part of the current pulse curve contributes to the drift process of the generated carriers while the slow decreasing curve is the result of the diffusion caused by non-equilibrium carrier gradient. This SET current pulse is further used in the following circuit schematic simulation as a stimulus in critical nodes.

## **3.6 Circuit Simulation and Analysis**

### ***3.6.1 Bandgap Circuit Simulation***

Transistor-level circuit simulation was performed to investigate the SET origin and propagation. We employed a double exponential current stimulus [15] to characterize the effect of SET in critical nodes. Simulation results demonstrated that the output variation of the bandgap reference circuit is the origin of the 6- $\mu$ s glitch. The SET pulses on the internal nodes of the bandgap reference circuit propagated to the power-on reset (POR) and soft start circuits sequentially, which eventually triggered the erroneous pulses on the PGOOD output, interrupting

the DC/DC converter operation (Fig. 3.6). The bandgap offers a voltage reference to POR. The POR generates an enable signal to soft-start circuit. Since the bandgap is internally sensitive due to small quiescent current in critical path, it is much easier to trigger voltage variation on bandgap. As a result, other related circuits, such as POR and soft-start, are less sensitive than bandgap. The circuit simulation result (Fig. 3.7.) is consistent with those of particles and laser experiments.

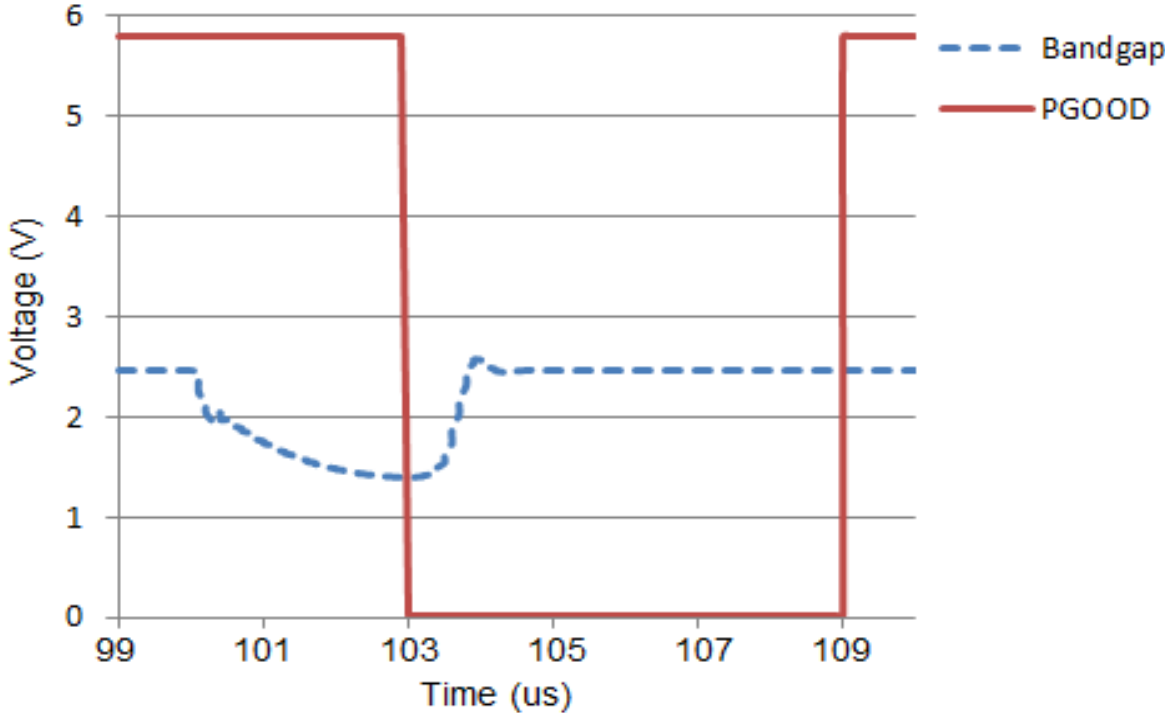


**Figure 3.7** Schematic simulation for the 6  $\mu$ s glitch on PGOOD.

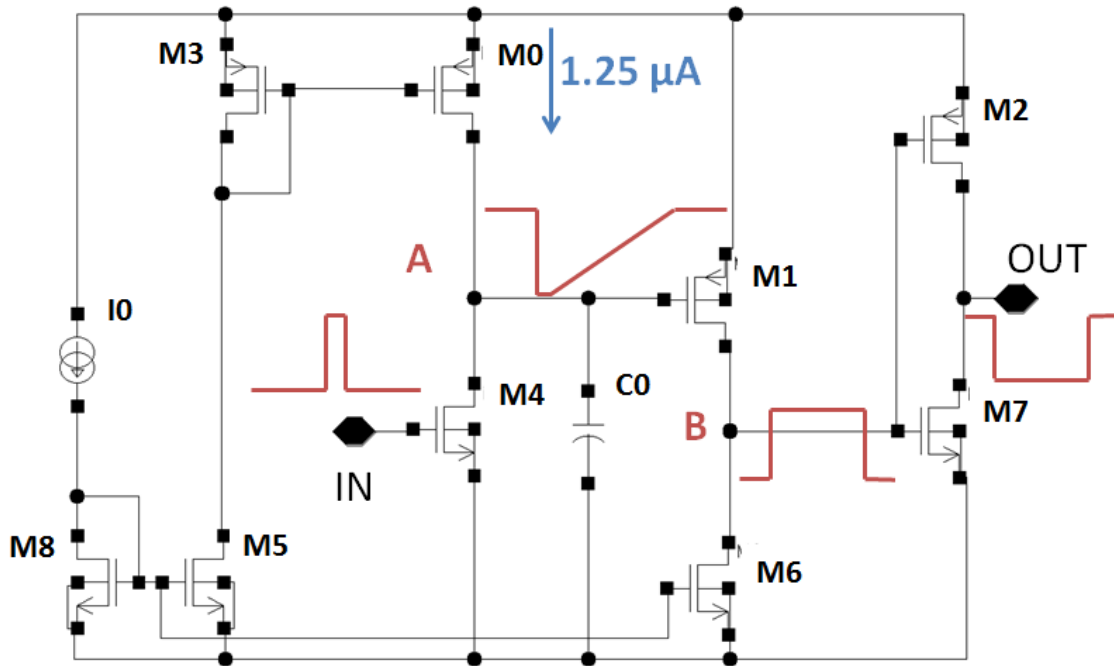


**Figure 3.8** Root cause for 6- $\mu$ s glitch.

### 3.6.2 Root Cause for 6- $\mu$ s Glitch

From the circuit schematic (Fig. 3.8), we can see that the root cause for the constant 6- $\mu$ s glitch is a filter capacitor in the SET propagation path. Normally, M1 is off and node A is high. Node B is low and OUT is high. When SET in bandgap circuit propagates to IN, node A drops low first and then is charged by M0 to its normal potential. Theoretically, the charging current is 1.25  $\mu$ A, the capacitance of C0 is 1.5 pF and the delta voltage of node A is 5 V. As a result, the charging time for the slope of node A is 6  $\mu$ s. The slope is reformed by the subsequent inverters. Finally, a constant 6- $\mu$ s glitch is observed on PGOOD.

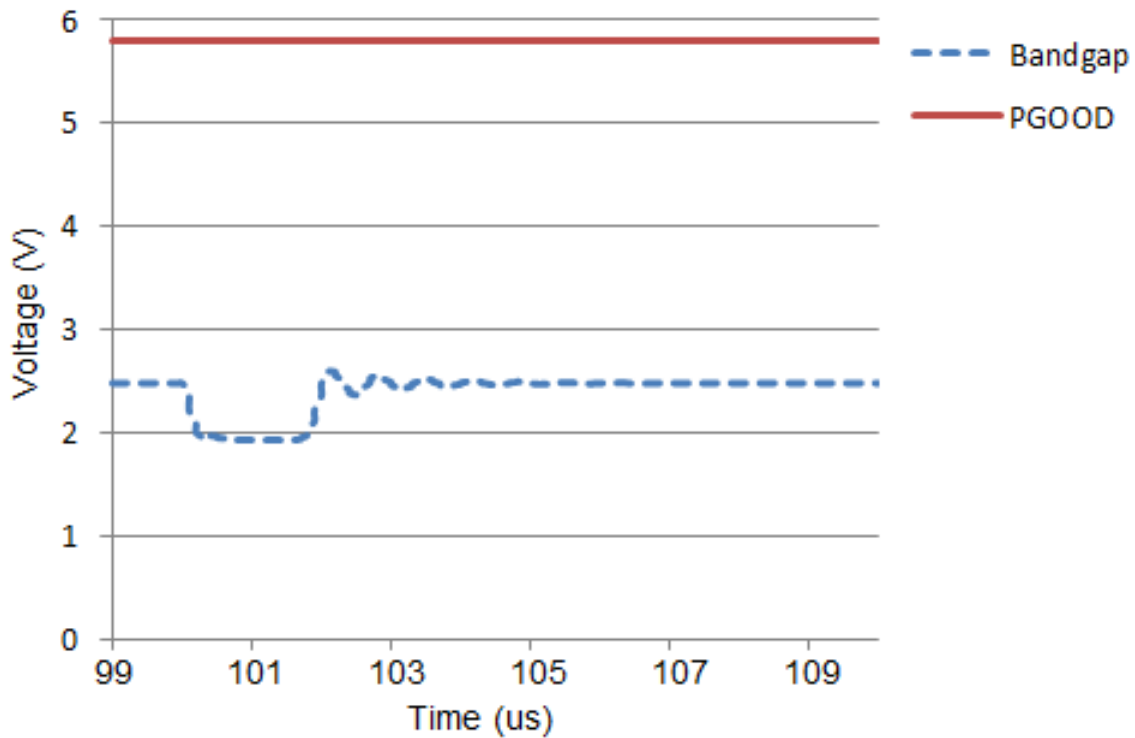


**Figure 3.9** Schematic simulation for hardened bandgap by redesigning the bandgap circuits.

### 3.7 Hardening Approaches

Since the DC/DC converter circuit was already in use in routers and Switches, two separate hardening approaches were developed for the IC. The first approach is an external hardening method, where a simple low-pass filter (LPF) composed of a resistor and a capacitor was added to the board and connected directly to the PGOOD output. The filter eliminated the 6- $\mu$ s transient pulses on the PGOOD. It worked well since the pulse widths on PGOOD induced by real failure modes are much longer than 6  $\mu$ s. This method was verified with the testing boards using the

same neutron and alpha test setups and the 6- $\mu$ s pulses were not observed as before under identical test conditions. Routers and Switches were tested with neutron and alpha particle exposures after the addition of this LPF to verify the effectiveness of this approach. No SET pulses were observed on LPF output during these experiments. This solution has been used in the routers and Switches and passed the qualification tests.

Another approach is to modify the internal circuits of the DC/DC converter IC to improve the SET tolerance of sub-circuits. The quiescent and restoring currents drive for the most sensitive nodes in the bandgap reference circuit were increased. Specifically, the quiescent current mirror for the bandgap reference is increased from 100  $\mu$ A to 1 mA. This current mirror provides bias current to the bandgap circuit. After this increase, the voltage perturbation for the bandgap reference voltage was reduced from 1 V to 0.5 V in magnitude and 3.95  $\mu$ s to 2.05  $\mu$ s in duration. This small change was sufficient to remove the 6- $\mu$ s SET pulse from the PGOOD output as shown in Fig. 3.9. This mitigation technique will increase the power consumption for these sub-circuits. However, the total current for the IC is about 60 mA. The additional current introduced to stabilize the bandgap reference is less than 1 mA, which is less than 2% of the total power consumption of the IC. Since this DC/DC converter IC was not designed for low-power portable applications, the overall increase in the power consumption for the IC is not significant.

### **3.8 Conclusion**

Single-event transient effects on a DC/DC converter by itself and within a Switch were studied with alpha particle, neutron and laser-beam irradiations. The results were analyzed by 3D TCAD modeling and circuit simulation. Test results clearly showed that the SET pulses on the internal reference voltage (bandgap) circuit can interfere with the protection circuits and generate

transients on the PGOOD status signal. Since this is the signal used by all monitoring circuits, an error on this output resulted in severe service disruptions for Switch applications. The results also indicated that SET also poses a potential threat to integrated circuits in process with larger feature size, such as 600-nm technology if the SEE is not properly predicted in the design. The quiescent and bias currents in some critical paths of an analog system should be carefully considered in circuit designing. As DC/DC converters are used in most complex electronics systems today, careful monitoring and testing of these parts are necessary to ensure error-free operation at the system-level. This paper identifies the most sensitive parts that may disrupt system operation. Hardening approaches to address this problem are also developed to mitigate this threat. This will allow designer to understand the SET vulnerability of analog/mix signal system and design it in a more reliable way.

## **Acknowledgement**

The authors would like to thank Sophie Brunet of the Saskatchewan Structural Science Center (SSSC) for her taking part in the laser experiments.

## **References**

- [1] K.A. Label, R.K. Barry, K. Castell, H.S. Kim, and C.M. Seidleck, "Implications of single event effect characterization of hybrid DC-DC converters and a solid state power controller," *IEEE Trans. Nucl. Sci.*, vol. 42, no. 6, pp. 1957-1963, Dec. 1995.
- [2] N.W. van Vonno, L.G. Pearce, J.S. Gill, H.W. Satterfield, E.T. Thomson, T.E. Fobes, A.P. Williams, and P.J. Chesley, "Total Dose and Single Event Testing of a Hardened Point of Load Regulator ," *Proc. Radiation Effects Data Workshop (REDW)*, pp. 80-88, Jul. 2010.
- [3] P.C. Adell, R.D. Schrimpf, W.T. Holman, J.L. Todd, S. Caveriviere, R.R. Cizmarik, and K.F. Galloway, "Total dose effects in a linear Voltage regulator," *IEEE Trans. Nucl. Sci.*, vol. 51,

- no. 6, pp. 3816–3821, Dec. 2006.
- [4] J.W. Howard, Jr., M.A. Carts, K.A. LaBel, J.D. Forney, and T.L. Irwin, “Single event effects testing of the Linfinity SG1525A pulse width modulator controller,” Proc. Radiation Effects Data Workshop (REDW), pp. 133-140, Jul. 2003.
- [5] S.H. Penzin, W.R. Crain, K.B. Crawford, S.J. Hansel, J.F. Kirshman, and R. Koga, “Single event effects in pulse width modulation controllers,” IEEE Trans. Nucl. Sci., vol. 43, no. 6, pp. 2968–2973, Dec. 1996.
- [6] S.H. Penzin, W.R. Crain, K.B. Crawford, S.J. Hansel, and R. Koga, “The SEU in pulse width modulation controllers with soft start and shutdown circuits,” Proc. Radiation Effects Data Workshop (REDW), pp. 73–79, Jul. 1997.
- [7] P.C. Adell, R.D. Schrimpf, B.K. Choi, W.T. Holman, J.P. Attwood, C.R. Cirba, and K.F. Galloway, “Total-dose and single-event effects in switching DC/DC power converters,” IEEE Trans. Nucl. Sci., vol. 49, no. 6, pp. 3217–3221, Dec. 2002.
- [8] P.C. Adell, R.D. Schrimpf, W.T. Holman, J. Boch, J. Stacey, P. Ribero, A. Sternberg, and K.F. Galloway, “Total-dose and single-event effects in DC/DC converter control circuitry,” IEEE Trans. Nucl. Sci., vol. 50, no. 6, pp. 1867–1872, Dec. 2003.
- [9] A.M. Chungg, R. Jones, M.J. Moutrie, P.H. Duncan, R.H. Sorensen, S. Mattsson, S. Larsson, R. Fitzgerald, and T. O’Shea, “Laser Simulation of single event effects in pulse width Modulators,” IEEE Trans. Nucl. Sci., vol. 52, no. 6, pp. 2487-2494, Dec. 2005.
- [10] P.C. Adell, A.F. Witulski, R.D. Schrimpf, F. Baronti, W.T. Holman, and K.F. Galloway, “Digital Control for Radiation-Hardened Switching Converters in Space,” IEEE Transactions on Aerospace and Electronic Systems, vol. 46, no. 2, pp. 761 - 770, Apr. 2010.
- [11] A. Zanchi, S. Buchner, C. Hafer, S. Hisano, and D. B. Kerwin, “Investigation and mitigation of analog SET on a bandgap reference in triple-Well CMOS using pulsed laser techniques,” IEEE Trans. Nucl. Sci., vol. 58, no. 6, pp. 2570-2577, Dec. 2011.
- [12] R.W. Erickson, D. Maksimovic, “Fundamentals of Power Electronics,” Second Edition, 2004.
- [13] C. Weulersse, F. Bezerra, F. Miller, T. Carriere, N. Buard, and W. Falo, “Probing SET



sensitive volumes in linear devices using focused laser beam at different wavelengths,”  
IEEE Trans. Nuc. Sci. vol. 55, no.4, pp. 2007-2012, Aug. 2008.

[14]S.P. Buchner, D. Wilson, K. Kang, D. Gill, J.A. Mazer, W.D. Raburn, A.B. Campbell, and  
A.R. Knudson, “Laser Simulation of Single Event Upsets,” IEEE Trans. Nuc. Sci. vol. 34,  
no. 6, pp. 1227-1233, Dec. 1987.

[15]S. Buchner, and D. McMorrow, “Single-Event Transients in Bipolar Linear Integrated  
Circuits,” IEEE Trans. Nucl. Sci., vol. 53, no. 6, pp. 3079–3102, Dec. 2006.

#### **4. THE EFFECT OF TEMPERATURE-INDUCED QUIESCENT OPERATING POINT SHIFT ON SINGLE-EVENT TRANSIENT SENSITIVITY IN ANALOG/MIXED-SIGNAL CIRCUITS**

*Published as:*

Y. Ren, and L. Chen, “The Effect of Temperature-Induced Quiescent Operating Point Shift on Single-Event Transient Sensitivity in Analog/Mixed-Signal Circuits,” *Springer Journal of Electronic Testing: Theory and Applications*, vol. 30, no. 3, pp. 377 - 382, 2014.

In the previous chapter, a commercial-off-the-shelf (COTS) DC/DC PWM converter chip sensitive to SET are studied using pulsed laser technique. The root cause for this sensitivity is pinpointed. However, all the evaluation and analysis are performed in a fixed temperature, namely the room temperature. As is known, the temperature is a key parameter to affect both the laser absorption in materials and the performance of the electronic devices. As a result, it is both significant and necessary to study the aforementioned DC/DC PWM chip with changed temperatures using the pulsed laser technique.

In this manuscript, the temperature is varied while testing the DC/DC PWM chip with the pulsed laser. The effect of temperature induced quiescent operating point shift on single event transient sensitivity in analog/mix signal circuits is discussed. Some basic analog circuits inside the DC/DC chip are selected to explain the effects. These circuits include comparator, current mirror and bandgap monitor. The wavelength of the laser is properly selected so that the absorption coefficient of laser in the material is relatively constant despite the temperature variations.

Different SET sensitivity trends are observed for different devices. In other words, with changed temperature, the SET sensitivity for some device can stay relatively constant while that for others see an increase. These are decided by the temperature induced quiescent bias point shift. The experiment results also indicate that devices of symmetric position in the circuit, such as the differential transistor pair, have the same SET sensitivity trend. This can be explained by their similar quiescent bias point. Circuit-level simulation is also used to analyze this sensitivity change by changing the temperature. It fits well with the experimental data.

# **The Effect of Temperature-Induced Quiescent Operating Point Shift on Single-Event Transient Sensitivity in Analog/Mixed-Signal Circuits**

Y. Ren, and L. Chen

## **Abstract**

This paper discusses the different sensitivities of laser-induced single-event transients (SET) with changed temperature (from 300 K to 348 K) for an analog/mixed-signal DC/DC PWM controller IC. Basic analog circuits, such as the amplifier, the comparator, and the current mirror, are selected to perform the experiment. The SET energies for some devices decrease while those for others remain constant. The SPICE simulation implies that the temperature-induced quiescent operating point shift can dramatically affect the SET sensitivity, especially in a complex analog/mixed-signal system. This effect also gives insights on radiation hardened design and testing in analog/mixed-signal circuits.

## **Index terms**

Single-event transients (SETs), temperature effects, lasers, quiescent operating point shift, bipolar transistors, bandgap reference, comparator, analog/mixed-signal circuits, radiation hardened by design.

## 4.1 Introduction

Single-event effects (SEEs) have always been a main source of soft errors in electronic devices [1-2]. It is caused by a single energetic particle traversing the sensitive regions of a device. In this case, the particle deposits sufficient charges and ionizes the material. The generated electron-hole pairs will be collected by the electric field in the p-n junction, which causes a voltage or current transient. The transient can propagate through the circuitry and hinder the system function, or even lead to system failures. In a well-designed IC, soft errors induced by SEEs have been the most troublesome issue both in terrestrial and high altitude or space environment. As a result, it is both necessary and significant to study the effects in the ICs.

As one of the most important factors that affect the SEE response of ICs, the temperature has always been a concern for researchers and engineers working in this area. As is widely known, the temperature dramatically affects the parameters of semiconductor devices [3]. For example, the bipolar transistor current gain ( $\beta$ ) is enhanced at an increased temperature. As a result, the performance of the IC changes dramatically with respect to temperature variations, which can give rise to distinct SEE responses. Previously, researchers have investigated the temperature dependence of SEE responses on epi-layer junctions [4-5], inverters [6], SRAMs [7], operational amplifiers and voltage comparators [8], or specific technologies [9-14]. However, these works mainly explained the different SET sensitivity in terms of temperature induced current gain variations of the transistors.

In this paper, the effect of temperature-induced quiescent operating point shift on SET sensitivity is discussed. For a transistor to work properly, it requires to be biased by a DC voltage or current. The steady-state voltage or current at a specified terminal of the transistor is called quiescent operating point. Quiescent operating point shift affects the SET sensitivity. For

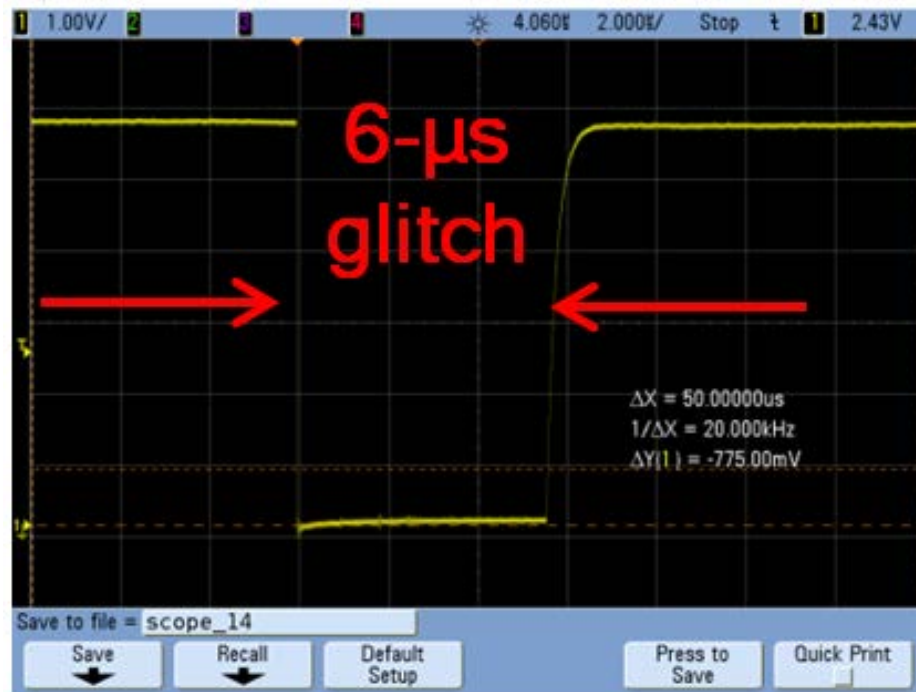


**Figure 4.1** Waveform for 6- $\mu$ s glitch.

example, the transistors can become harder or easier to cutoff. This study is based on an analog/mixed-signal DC/DC PWM controller IC, which was found to be sensitive to SET in our previous investigation [15]. The data for the DC/DC PWM controller presented here are acquired using pulsed-laser beams. The temperatures are ranged from 300 K to 348 K considering the operation temperature limitation (350 K) for the PWM controller. The comprehensive irradiation experiments for this chip in room temperature were previously performed [15-17], which gives us advantages and insights for this temperature effects study. The experiment results and simulations imply that the temperature-induced quiescent-point shift in analog/mixed-signal circuits plays a key role in the SET sensitivity of the IC.

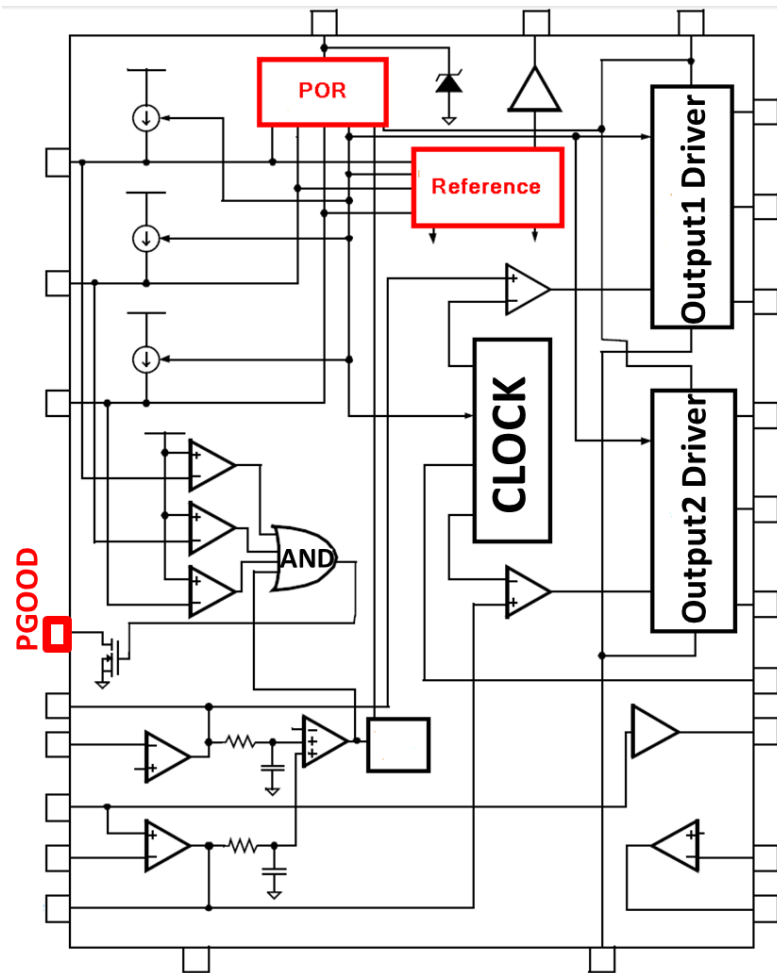
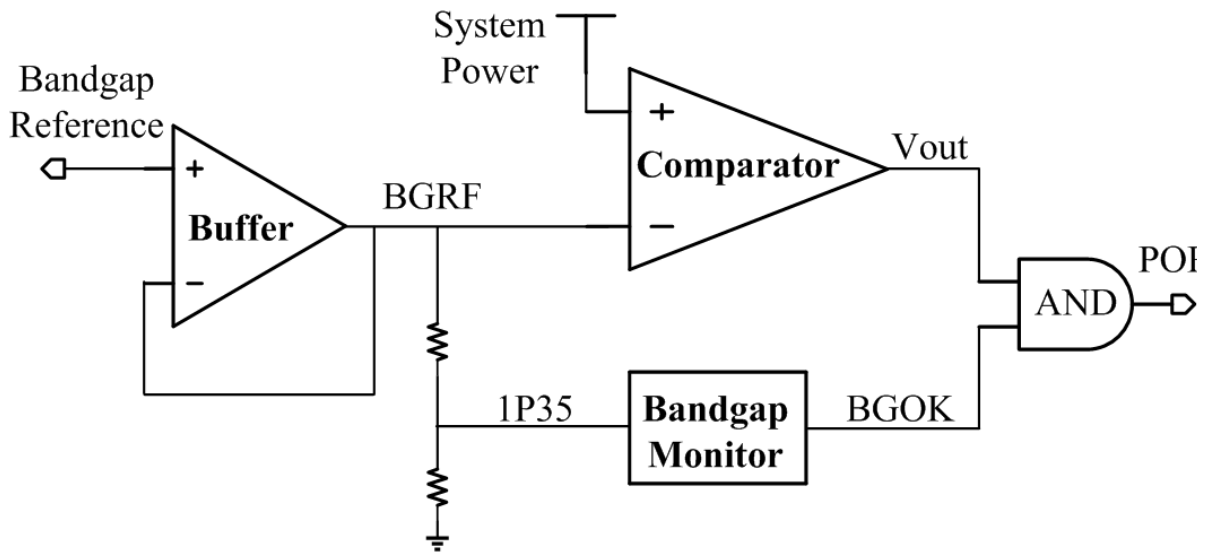


Figure 4.2 Schematic for the DC/DC PWM Controller.

## 4.2 Experimental Details

### 4.2.1 Device under Test

The DC/DC PWM chip under test is within an internet switch which went through silent reset spontaneously. Our study showed that the chip is sensitive to SET and generates 6- $\mu$ s negative glitches at its Power Good pin (PGOOD). The image of the 6- $\mu$ s glitch is shown in Fig.



**Figure 4.3** Symbolic connection of sensitive circuits.

4.1. The switch system reboots once it detects this 6- $\mu$ s glitch. The schematic for the DC/DC PWM IC is shown in Fig. 4.2. Our previous study indicates that the sensitive areas are related to the Reference and the Power-On Reset (POR) circuits, which are highlighted in red in Fig. 4.2 [15]. The symbolic connection of related sensitive circuits in the Reference and POR circuits are shown in Fig. 4.3. When the initial SET amplitude is small, it won't propagate to the PGOOD pin. However, when it is big enough to cut off a specific NMOS transistor on its propagation path, it will propagate to the PGOOD pin and generate a 6- $\mu$ s glitch. The 6- $\mu$ s time constant is decided by a filter capacitor on the propagation path. This phenomenon makes the chip an excellent vehicle to investigate the temperature effect on SET from a circuit level where PGOOD



is monitored for the 6- $\mu$ s glitch as a criterion. The minimum energy to trigger this 6- $\mu$ s glitch is defined as the SET threshold energy. This is different from normal SET testing where the SET threshold energy cannot be specified. However, it proves to be effective and convenient in our case.

The simplified schematics for each block in Fig. 4.3 are shown in Fig. 4.4. The Buffer, which is an amplifier operating in unity gain configuration, regulates the bandgap reference voltage so that it is stabilized. The Comparator is supervising the system power supply voltage by outputting '1' when the initial system power-on is ready. The Bandgap Monitor circuit is a current mirror to supervise the bandgap circuit status by outputting '1' at BGOK when its input (1P35) is 1.35 V. The outputs of the Comparator and Bandgap Monitor generate a POR signal through an AND gate. Those circuits are basic analog modules that are commonly used in analog/mixed-signal circuits. The selected PNP bipolar transistors have the same size. A resistor was also selected to better explain the quiescent operating point shift effect.

#### ***4.2.2 Temperature Change and Measurement***

A flexible heater is used to change the temperature of the chip. It is with pressure sensitive adhesive (PSA). The maximum operating temperature is 393 K and the rating voltage is 28 V. The watt density is 10 W/in<sup>2</sup>. A multimeter with a K type thermocouple, which is capable of probing temperature, is used. The temperature range of the heater is from 73 K to 1623 K with a resolution of 0.1 K.

As the chip is decapped on the top, the heater is adhered to the chip from the backside of PCB. To be specific, it is adhered to the backside of the PCB with thermally conductive grease to guarantee high thermal conductivity. The temperature is controlled by changing the input voltage

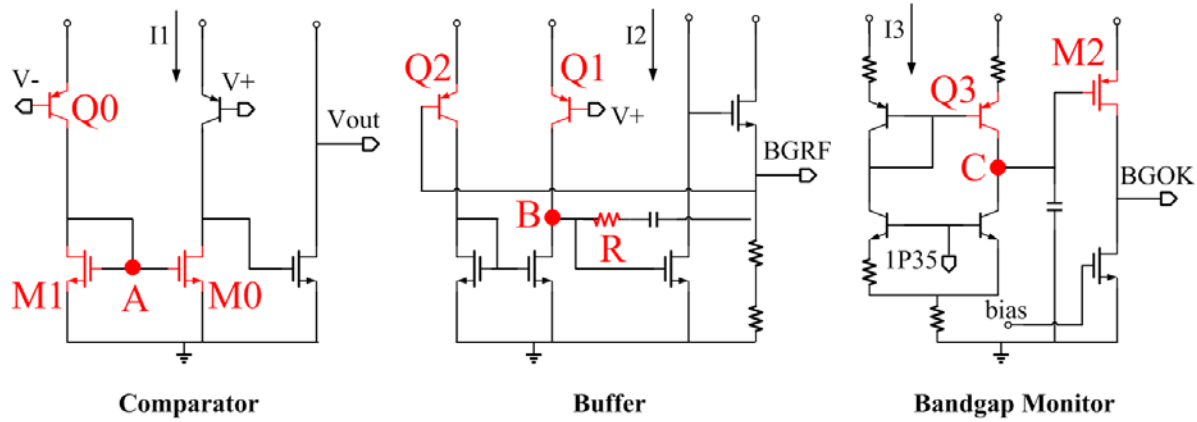


**Figure 4.4** Analog circuits under test.

of the heater. According to the specification, the DC/DC PWM controller has a maximum operating temperature of 75°C. As a result, the temperature should be lower than this to guarantee the functionality of the chip and the fidelity of the experiment results. As the die of the chip is delicate, the temperature from the pins of the package is sampled. Although errors might be introduced in this way, the accuracy is enough as the main purpose is to compare the tendency of the temperature dependence rather than to have an accurate modeling.

#### **4.2.3 Laser Facility**

The laser facility used in this work is located at the Saskatchewan Structural Sciences Centre (SSSC) in University of Saskatchewan. The basis of the laser scanning system is a Zeiss LSM410 confocal microscope which is located on a floating optical table to reduce mechanical vibration transfer to the instrument. The laser system is a Mira 900-D pumped by a Verdi V-10 (made by Coherent). It has a tunable Ti:Sapphire laser with wavelengths ranging from 700 nm to

1000 nm. The laser system is capable of emitting a continuous wave beam or picosecond and femtosecond pulses. It has a Pulse Picker 9200 which is a stand-alone accessory for the laser system to change the pulse repetition rate. In our case, it gives a repetition rate selection from 10 kHz to 75 MHz.

Note that the laser absorption in silicon material has different temperature coefficients with respect to the wavelength. The laser has higher temperature coefficient when its photon energy is near silicon band gap, which means a laser with shorter wavelength has a relatively constant absorption coefficient [18]. On the other hand, the laser with longer wavelength has a bigger penetration depth. As a result, 920 nm laser is adapted in our testing. Its absorption coefficient is around  $150 \text{ cm}^{-1}$  with a change less than 10% from 300 K to 348 K. This variation is acceptable for our testing.

For the experiment, the DUT is fastened on the testing plate using screws with electrical insulating properties. The laser beam is focused on the surface of the die through a microscope objective. The laser spot size diameter and pulse duration are  $1.6 \text{ }\mu\text{m}$  and 130 fs, respectively. Its resolution is good enough for our testing as the process feature size is large. For example, the area of each PNP transistor under test is  $16 \text{ }\mu\text{m}$  by  $20 \text{ }\mu\text{m}$ .

### **4.3 Experimental Results**

Four bipolar transistors with the same size ( $16 \text{ }\mu\text{m}$  by  $20 \text{ }\mu\text{m}$ ) and one resistor were tested and analyzed in the experiment. For each device at a specific temperature, laser energy is increased until 6- $\mu\text{s}$  glitch is captured at PGOOD pin. Since the 6- $\mu\text{s}$  glitch at PGOOD is caused by the internal SET in the DC/DC PWM chip (6- $\mu\text{s}$  is the charging time for a capacitor on the SET propagation path as we mentioned before), it is taken as a criterion of the effective SET for

**Table 4.1 Experiment Data**

Device	SET Threshold Laser Energy (pJ)					
	298K	303K	313K	328K	348K	delta
Q0	42.8	42.8	42.8	42.8	42.8	0
Q1	29.2	28.1	24.5	22.9	22.1	-24%
Q2	21.2	19.4	16.7	15.4	14.7	-30%
Q3	45	42.8	41	36.3	34.6	-23%
R0	34.6	30.7	23.6	22.2	21.2	-39%

the DC/DC PWM IC. Once it is observed, the laser energy will not be further increased. And this energy is recorded as the SET threshold energy for the device under this temperature. In this way, we can record the SET sensitivity of each device. The data for five temperature points are showed in Table 4.1 and plotted in Fig. 4.5. We can see that the temperature dependence of the SET threshold energy is different between these devices in that it remains relatively constant for Q0 while decreases for Q1, Q2, Q3 and R0. However, SET thresholds for Q1 and Q2 show very consistent temperature dependence. The SET threshold energy for R0 sees the biggest variation, which is about -39% between 300 K and 348 K. All the devices except R0 are PNP bipolar transistors with the same size. In this way, the only differences between them are the quiescent operating point and the circuit structure they reside in.

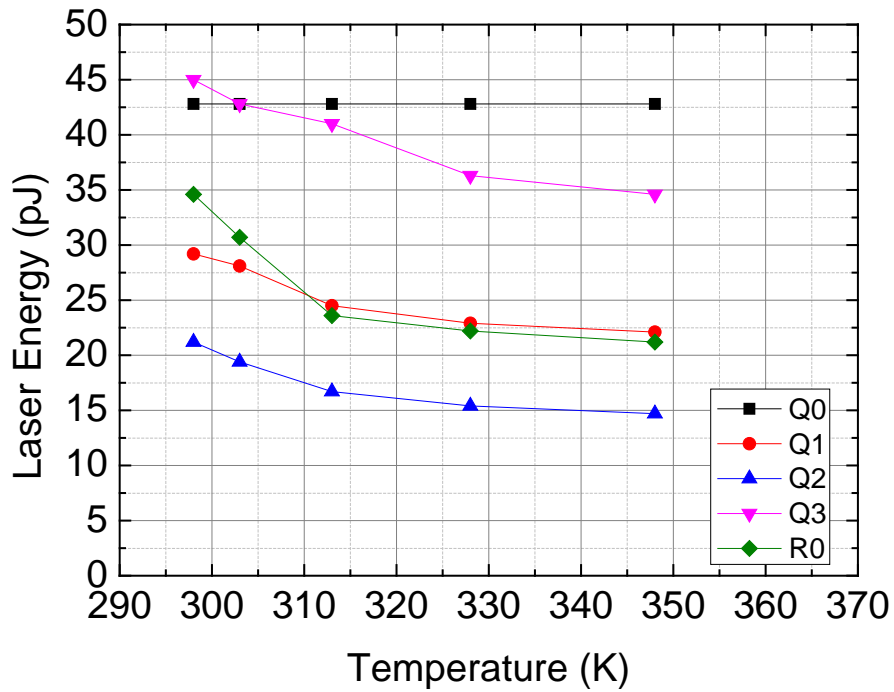


**Figure 4.5** Temperature dependence of SET thresholds.

The Spice simulation is used to verify and explain the experiment results. To mimic the SET, double exponential current pulse is used as the stimulus. In this temperature study, the current gains, the quiescent operating point shifts of the sensitive devices tested above (including base, emitter, collector voltages and quiescent currents) are simulated and compared under different temperatures.

## 4.4 Discussions

### 4.4.1 Comparator

From Table 4.1 we can see that the input stage Q0 of the comparator has relatively constant threshold energy (42.8 pJ) over the whole temperature range. Previously, researchers have reported increased SET threshold energy due to shrinking SET pulse at increased temperature for the input stage of the LM139 voltage comparator [8]. The paper indicated that enhanced current gains of transistors prevented the switching of the comparator. However, it was a testing for an independent bipolar comparator IC while our testing set the BiCMOS-based comparator in an analog/mixed-signal circuit context. In other words, a current gain enhancement of 29% for Q0 was observed from the simulation as is shown in Fig. 4.6, which was consistent with [8]. On the other hand, the quiescent collector current  $I_C$  decreased because the temperature-induced quiescent operating point shift decreased the base current  $I_B$  according to the simulation (Fig. 4.7). As a result, the SET threshold energy of the comparator input stage Q0 in our testing remained relatively constant with increased temperature.

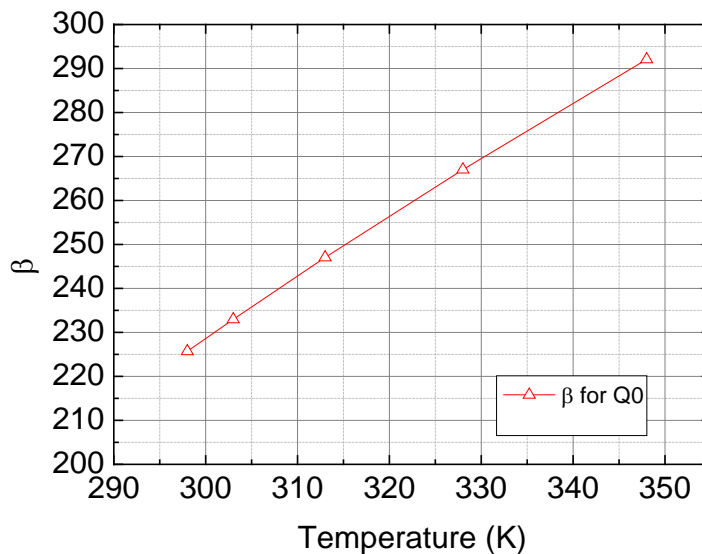


**Figure 4.6** Temperature dependence of the current gain for Q0.

The SET on Q0 propagates through the CMOS current mirror (M0 and M1). The temperature simulation also showed that the quiescent operating voltage on node A decreased with temperature as well as the threshold voltage of M0. This makes the overdrive voltage of M0 a relative constant over the temperature range. In this case, the voltage variation to switch the state remains the same level. This also makes the SET threshold energy relatively constant for Q0.

#### 4.4.2 Buffer

Table 4.1 shows that, for the same temperature, Q2 is more sensitive compared with Q1. This can be explained by the configuration of the Buffer amplifier. It makes the output feedback to the base of Q2. On the other hand, the base of Q1 is always connected to the output of bandgap reference which is stable. From the data, we also see the same trend for Q1 and Q2 (the

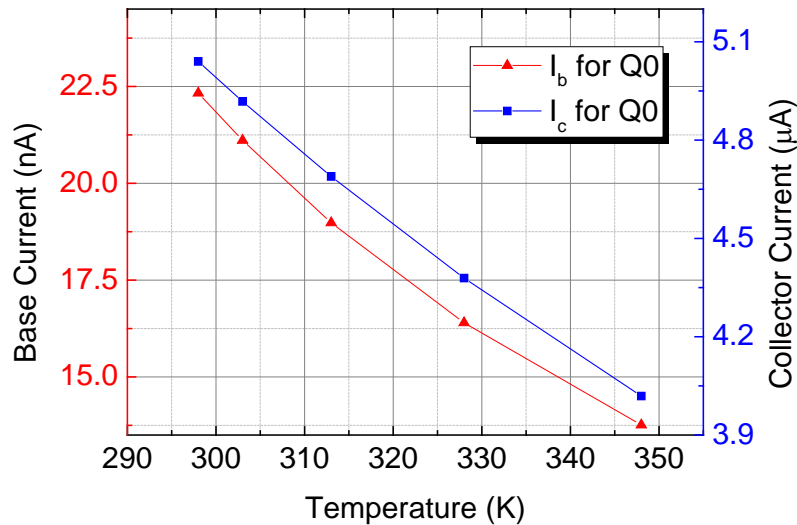


**Figure 4.7** Temperature dependence of the bias currents for Q0.

red and blue curve in Fig. 4.5) with respect to the increasing temperature. This is because they are in the similar positions in the circuit, which give them identical quiescent operating points. The SPICE simulation shows that they have the same bias voltage and current at each temperature.

The temperature response of the resistor R is another example to explain the effect of quiescent operating point variation on SET sensitivity. The only concern related to temperature for R is the resistance variation [19]. In fact, our simulation indicated an increase of 3% (40 Kohm to 41.4 Kohm) from 298K to 348 K. As a result, this effect can be neglected in our analysis. The fast SET pulsed on R can be coupled to the output of the buffer by the Miller compensation capacitor. The simulation shows that the quiescent operating point of R on node B decreased from 854 mV to 788 mV with an increased temperature (red curve in Fig. 4.8). This

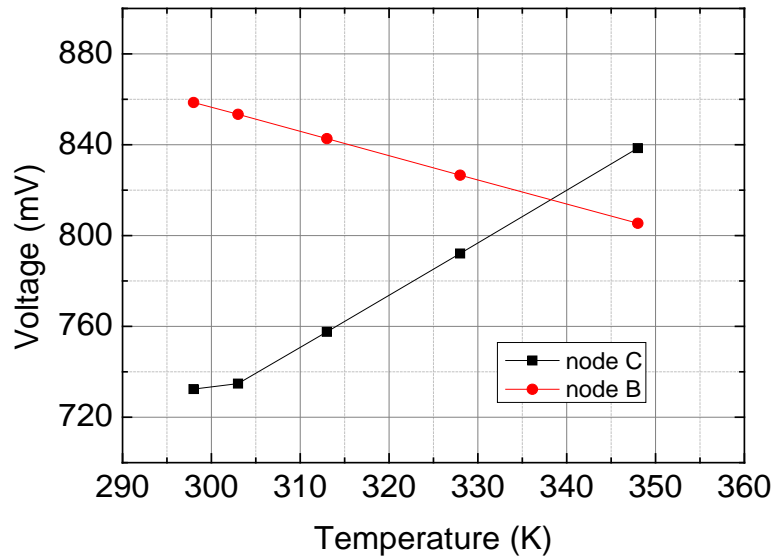


**Figure 4.8** Temperature dependence of voltages at node B and C.



decrease in quiescent operating point makes it easier to pull down the Buffer output. This explains the SET threshold energy decrease for R in Table 4.1.

#### ***4.4.3 Bandgap Monitor***

The SET threshold energy decrease of Q3 at increased temperature can also be explained by the quiescent operating point shift. In normal operation, M2 is on and the output is high. The simulation showed that the DC voltage at node C shifted from 728 mV to 850 mV (17%) with the increased temperature (black curve in Fig. 4.8). As a result, it is easier for a SET pulse on Q3 to pull down the output of this Monitor circuit.

### **4.4 Conclusions**

In this chapter, the effects of temperature on laser-induced SET sensitivities of an analog/mixed-signal DC/DC PWM controller are analyzed. Basic analog circuits, such as comparator, amplifier and current mirror, are selected for the investigation. The results see a maximum decrease of about 39% in the SET threshold laser energy with an increasing temperature from 298 K to 348 K. The simulations imply that the temperature-induced quiescent operating point shift is a critical factor affecting the SET sensitivity of the circuits. Also, symmetric devices with the same quiescent operating point, for example, the input transistor pair in an amplifier (Q1 and Q2 in our case), have the same trend with changed temperature effects in terms of the SET sensitivity, even though they may have different SET sensitivities at the same temperature.

The effects of quiescent operating point on the SET sensitivity of analog/mixed-signal circuits also facilitate the process of radiation hardened design and testing for different temperatures. Previously, researchers and engineers tend to analysis the SET temperature effects

only from the perspective of current gain ( $\beta$ ) change. This is feasible for single devices or simple circuits where quiescent operating point shift is less effective. However, it is harder for complex analog/mixed signal circuits as the sensitivity variation at a node is a total effect of current gain change and quiescent operating point shift of the related transistors in the circuit. In this case, it is better to analysis also the quiescent operating point shift of the node, which can be easily simulated. As a result, more efforts should be taken to minimize the quiescent operating point shift in the circuit so that the SET sensitivity remains relatively constant and predictable with changed temperatures.

As the Soft-error rate (SER) is highly related to the SET sensitivity of the circuits, this effect of temperature-induced quiescent operating point shift is also supposed to affect the SER of analog/mixed-signal circuits. The tendency of the SER variation can be predicted from circuit simulations in terms of temperature. To be more specific, the decreased sensitivity implies reduced SER and vice versa. As a result, a qualitative expectation on SER variation can be acquired by analyzing the quiescent operating point shift in analog/mixed-signal circuits. However, more work need to be done to correlate the SER variation to temperatures. These will be performed in the future.

## References

- [1] S. Buchner and D. McMorrow, "Single-event transients in bipolarlinear integrated circuits," IEEE Trans. Nucl. Sci., vol. 53, pp. 3079–3102, Dec. 2006.
- [2] C. Poivey, J. Barth, J. McCabe, and K. Label, "A space weather event on the microwave anisotropy probe," in Proc. RADECS Conf., Padova, Italy, Sep. 19–20, pp. 43–46, 2002.
- [3] W.C. Dillard, and R.C. Jaeger, "The temperature dependence of the amplification factor of bipolar-junction transistors," IEEE Trans. Electron Devices, vol. 34, pp. 139 - 142, Jan.

1987.

- [4] G. Guo, T. Hirao, J. S. Laird, S. Onoda, T. Wakasa, T. Yamakawa, and T. Kamiya, “Temperature dependence of single-event transient current induced by heavy-ion microbeam on p+/n/n+ epilayer junctions,” *IEEE Trans. Nucl. Sci.*, vol. 51, pp. 2834–2839, Oct. 2004.
- [5] J. S. Laird, T. Hirao, S. Onoda, H. Mori, and H. Itoh, “Temperature dependence of heavy ion induced current transients in Si epilayer devices,” *IEEE Trans. Nucl. Sci.*, vol. 49, pp. 1389–1395, Jun. 2002.
- [6] D. Truyen, J. Boch, B. Sagnes, J. R. Vaille, N. Renaud, E. Leduc, M. Briet, C. Heng, S. Mouton, and F. Saigne, “Temperature effect on heavy-ion-induced single-event transient propagation in CMOS bulk 0.18  $\mu\text{m}$  inverter chain,” *IEEE Trans. Nucl. Sci.*, vol. 55, pp. 2001–2006, Aug. 2008.
- [7] D. Truyen, J. Boch, B. Sagnes, N. Renaud, E. Leduc, S. Arnal, and F. Saigne, “Temperature Effect on Heavy-Ion Induced Parasitic Current on SRAM by Device Simulation: Effect on SEU Sensitivity,” *IEEE Trans. Nucl. Sci.*, vol. 54, no. 4, pp. 1025 - 1029, Aug. 2007.
- [8] D. Chen, S.P. Buchner, A.M. Phan, H.S. Kim, A.L. Sternberg, D. McMorrow, and K.A. LaBel, “The Effects of Elevated Temperature on Pulsed-Laser-Induced Single Event Transients in Analog Devices,” *IEEE Trans. Nucl. Sci.*, vol. 56, no. 6, pp. 3138 - 3144, Dec. 2009.
- [9] M.J. Gadlage, J.R. Ahlbin, V. Ramachandran, P. Gouker, C.A. Dinkins, B.L. Bhuva, B. Narasimham, R.D. Schrimpf, M.W. McCurdy, M.L. Alles, R.A. Reed, M. H. Mendenhall, L.W. Massengill, R.L. Shuler, and D. McMorrow, “Temperature Dependence of Digital Single-Event Transients in Bulk and Fully-Depleted SOI Technologies,” *IEEE Trans. Nucl. Sci.*, vol. 56, no. 6, pp. 3115 - 3121, Dec. 2009.
- [10] S. Chen, B. Liang, B. Liu, and Z. Liu, “Temperature Dependence of Digital SET Pulse Width in Bulk and SOI Technologies,” *IEEE Trans. Nucl. Sci.*, vol. 55, no. 6, pp. 2914 - 2920, Dec. 2008.
- [11] M.J. Gadlage, J.R. Ahlbin, B. Naeasimham, V. Ramachandran, C.A. Dinkins, B.L. Bhuva, R.D. Schrimpf, and R.L. Shuler, “The effect of elevated temperature on digital single event

- transient pulse widths in a bulk CMOS technology,” IEEE Proceeding of Reliability Physics Symposium., April, 2009.
- [12] M.J. Gadlage, J.R. Ahlbin, B. Naeasimham, V. Ramachandran, C.A. Dinkins, N.D. Pate, B.L. Bhuva, R.D. Schrimpf, L.W. Massengill, R.L. Shuler, and D. McMorrow, “Increased Single-Event Transient Pulsewidths in a 90-nm Bulk CMOS Technology Operating at Elevated Temperatures,” IEEE Trans. Device and Material Reliability, vol. 10, no. 1, pp. 157 - 163, Mar. 2010.
- [13] M.J. Gadlage, J.R. Ahlbin, B.L. Bhuva, R.D. Schrimpf, L.W. Massengill, and R.D. Schrimpf, “Single event transient pulse width measurements in a 65-nm bulk CMOS technology at elevated temperatures,” IEEE Proceeding of Reliability Physics Symposium., May, 2010.
- [14] M.J. Gadlage, J.R. Ahlbin, B. Naeasimham, B.L. Bhuva, L.W. Massengill, and R.D. Schrimpf, “Single-Event Transient Measurements in nMOS and pMOS Transistors in a 65-nm Bulk CMOS Technology at Elevated Temperatures,” IEEE Trans. Device and Material Reliability, vol. 11, no. 1, pp. 179 - 186, Mar. 2011.
- [15] Y. Ren, L. Fan, L. Chen, S.-J. Wen, R. Wong, N. W. van Vonno, A. F. Witulski, and B. L. Bhuva, “Single-Event Effects Analysis of a Pulse Width Modulator IC in a DC/DC Converter,” Springer Journal of Electronic Testing, vol. 28, no. 6, pp. 877–883, Dec. 2012.
- [16] Y. Ren, S.-T. Shi, L. Chen, H.-B. Wang, L.-J. Gao, G. Guo, S.-J. Wen, R. Wong, and N. W. van Vonno, “Correlation of Heavy-Ion and Laser Testing on a DC/DC PWM Controller,” Springer Journal of Electronic Testing, Vol. 29, no. 2, pp. 609-616, Aug, 2013.
- [17] Y. Ren, A.-L. He, S.-T. Shi, G. Guo, L. Chen, S.-J. Wen, R. Wong, N. W. van Vonno, and B. L. Bhuva, “Single-Event Transient Measurements on a DC/DC Pulse Width Modulator Using Heavy Ion, Proton, and Pulsed Laser,” Springer Journal of Electronic Testing: Theory and Applications, online, Jan., 2014.
- [18] P. K. Skorobogatov, A. Y. Nikiforov, O. B. Mavritsky, A. N. Egorov, and A. V. Kirgizova, “Influence of temperature on pulsed laser SEE testing,” in Proc. RADECS Conf., Noordwijk, The Netherlands, Sep. 15–10, pp. 153–155, 2003.

[19]H. Chuang, K. Thei, S. Tsai, and W. Liu, "Temperature-dependent characteristics of polysilicon and diffused resistors," IEEE Trans. Electron Devices, vol. 50, no. 5, pp. 1413 - 1415, May. 2003.

## **5. SET SENSITIVITY DEPENDENCY OF A DC/DC PWM ON LASER REPETITION RATE AND WAVELENGTH**

*Submitted as:*

Y. Ren, and L. Chen, “SET Sensitivity Dependency of a DC/DC PWM on Laser Repetition Rate and Wavelength,” *Springer Journal of Electronic Testing: Theory and Applications*, 2014.

In the previous chapters, a commercial-off-the-shelf DC/DC PWM converter chip sensitive to SET are tested comprehensively using pulsed laser technique. The temperature effect on its sensitivity is studied as well. The root cause for this sensitivity is pinpointed. However, all the evaluation and analysis are performed in fixed repetition rate, which is 10 KHz. The pulsed laser repetition rate decides the temporal interval between each laser pulse. According to the previous study, the repetition rate of the pulsed laser can affect the experiment results significantly. Also, the laser wavelength is another key factor to decide the performance of the SET testing. As a result, attention should be paid to these factors in laser SET experiments.

In this manuscript, multiple repetition rates and wavelengths are used to evaluate the SET responses of the DC/DC PWM chip. As expected, different phenomena are observed as the combination of repetition rate and wavelength changes. These phenomena are compared with previous particle testing results, which indicates that the combination of laser repetition rate and wavelength affect not only the SET shape but also the threshold laser energy per pulse. The reasons are discussed in terms of the circuit structures. A charge accumulation process related to circuit structure is determined to be the main reason. In other words, different wavelengths have

different abilities in terms of generating charges in silicon. Also, a higher repetition rate is accumulating more charges in a specific period. If the circuit structure is not dissipating the charge sufficiently for the specific wavelength and repetition rate combination, the charge accumulation process will affect the laser testing validity. Based on this finding, the wavelength and repetition rate should be properly selected taking the circuit structure into consideration. A low repetition rate is always a preference for all sorts of SEE tests.

# **The SET Sensitivity Dependence of a DC/DC PWM on Laser Repetition Rate and Wavelength**

Y. Ren, and L. Chen

## **Abstract**

The femtosecond pulsed laser was adopted to investigate the sensitive devices in a versatile triple DC/DC PWM controller IC for single event transient (SET) effects. Various wavelengths and a range of repetition rates were used to pinpoint and characterize the SET sensitivity. The dependence of the SET sensitivity on the laser pulse repetition rate and wavelength was observed and analyzed.

## **Index terms**

Single Event Transient (SET), DC/DC PWM, Bandgap Reference, Power-On Reset (POR), Pulsed Laser, Repetition Rate.

## **5.1 Introduction**

The pulsed laser beam has been proven to be a valuable diagnostic tool for single event effects (SEEs) study ever since 1980s [1]-[4]. The laser beams can be focused on the interested devices with high resolution, which provides a complementary method to investigate the SEE. In addition, it is easy to change the average power and energy per pulse by means of modifying laser parameters [5]. Researchers have made a vast study on SEEs via pulsed lasers. However,



the previous work did not specifically investigate the SET dependence of the laser pulse repetition rate and the laser wavelength. In this paper, a complex commercial-off-the-shelf (COTS) controller for DC/DC regulator was used as a testing vehicle for the SET investigation. The schematic for the device under test is shown in Fig. 5.1.

The DC/DC PWM controller chip has a PGOOD output which uses logic high to indicate “Power Good”. The supervisory circuit monitors all blocks in the DC/DC converter to generate the “Power Good” signal. Single events can affect any one of these circuits, but a single event

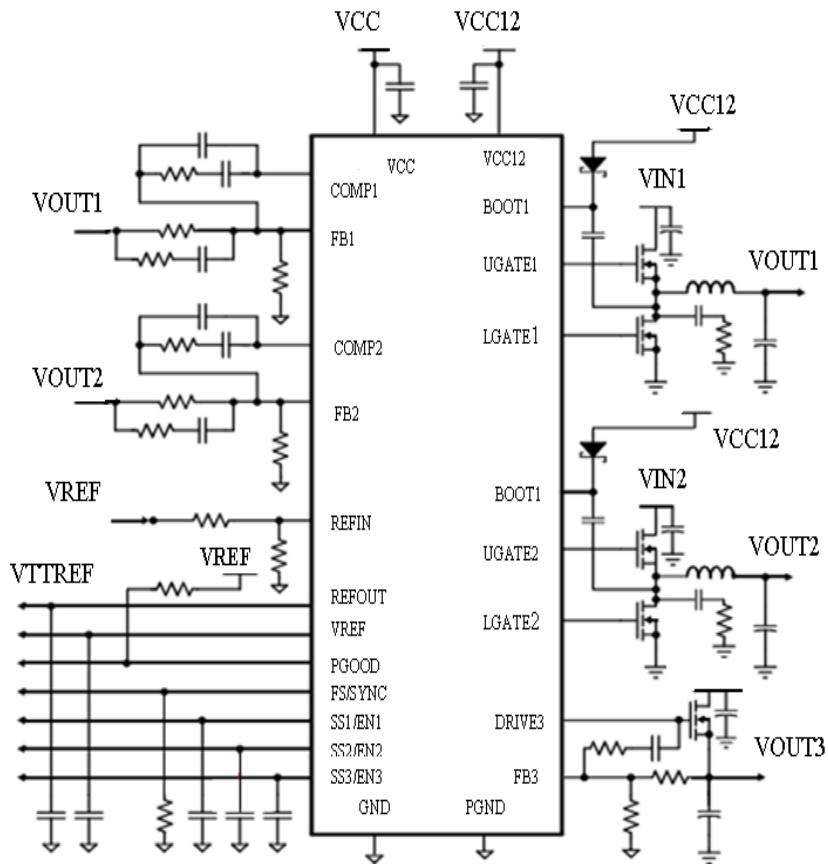


**Figure 5.1** Test circuit for the complete DC/DC PWM converter.

strike in the supervisory circuit or the bandgap reference circuit is particularly serious because it may send a (false) signal to a system controller that shuts down or resets the entire system the DC/DC converter resides in, even though the output voltage of the converter is not seriously affected. An investigation of this particular DC/DC converter have been thoroughly conducted using the pulsed laser with fixed wavelength and repetition rate, the most sensitive areas have been identified to be the bandgap circuits [13]. In this paper, the relationship between the SET responses and the laser pulse repetition rate and wavelength are thoroughly studied. The results show that the SET sensitivity is closely related to the laser repetition rate and wavelength. In addition, different failure mechanisms were observed when changing the pulse repetition rate of the lasers. The phenomena were analyzed and conclusions were summarized at the end of the paper.

## **5.2 Experimental Setups and Laser Parameters**

### ***5.2.1. Laser Facility and Device under Test***

The laser experiments were carried out with a combination of Confocal Microscopy on the Zeiss LSM410 and Mira 900-D laser system with Verdi V-10. The simplified laser path is shown in Fig. 5.2. The system is located on a floating optical table to reduce mechanical vibration transfer to the instrument. Zeiss LSM410 which is an inverted microscope intended for acquisition of fluorescence emission from laser excitation source. The Mira 900-D is a tunable Ti-Sapphire laser system which is capable of emitting wavelengths ranging from 700 nm to 1000 nm. The Mira can emit the continuous wave, picosecond pulses and femtosecond pulses. The mode-lock 130 femtosecond pulsed Ti-Sapphire lasers that emit light at 800 nm, 920 nm and 990 nm in the infrared were used to conduct the experiments. A HeNe 633 nm continuous wave laser

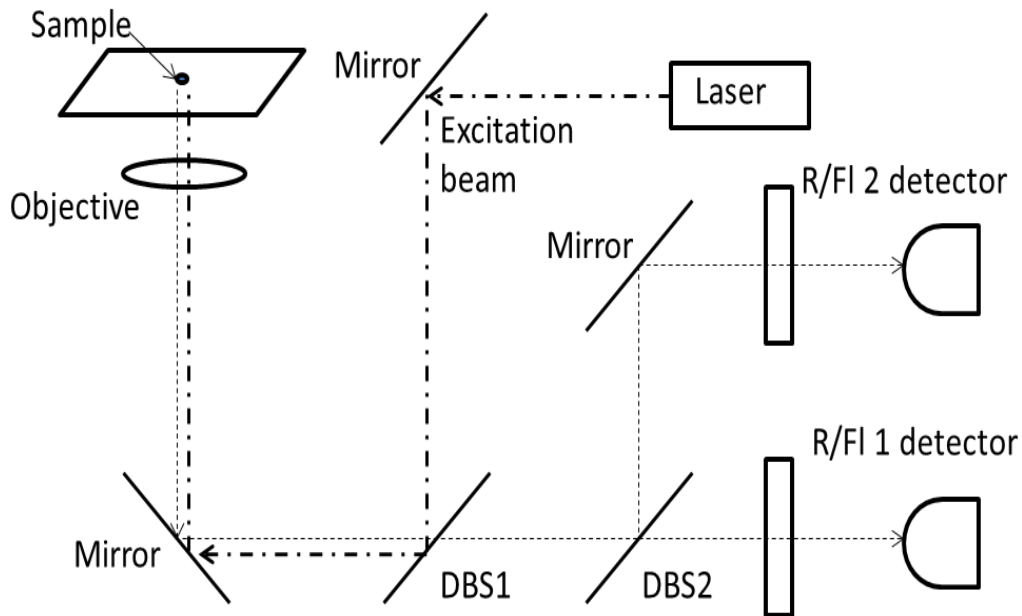


**Figure 5.2** Simplified laser path.

was used to capture the optical image of the chip so that a specific location could be locked. The infrared (IR) laser beams were aligned to the HeNe laser beam in order to irradiate the target spots. The average powers of the IR lasers were controlled by internal polarizers and external neutral density filters.

The laser experiments consisted of applying laser pulse excitations to the decapped chip across the sensitive area of the die. The laser pulse energy was varied continuously to establish a threshold level at any location that was found to exhibit SET sensitivity. This is a 3 metal layer process and all of the transistors targeted for study in this project were accessible for laser hits without any metal layer on top. The waveforms from the device under test (DUT) outputs were captured for SEE event analysis using a high speed oscilloscope triggering on several of the

outputs when they exceeded the limits of normal operations. The PGOOD signal was used as the indicator for SET events.

### ***5.2.2. Laser Wavelength***

Different wavelengths were used in our experiments, namely 800nm, 920nm and 990nm. For one photon absorption, a photon is absorbed only when its energy is larger than the band gap of the semiconductor material. Longer wavelength laser (around 1000nm) is proven to have a small absorption coefficient, which means a deep penetration depth whereas shorter wavelength (around 800nm) laser is on the contrary [5, 9]. However, the absorption coefficient for long wavelength tends to vary a lot at high doping levels because of free carrier absorption and band gap narrowing (band gap shrinkage) effects [10, 11]. It is a different case for short wavelength laser with energy farther above the band gap whose absorption coefficient is less sensitive to different doping concentrations [6]. Given all these facts, three distinct wavelengths, namely 800 nm, 920 nm and 990nm, are selected in our experiment for the sake of precision.

### ***5.2.3. Laser Pulse Duration***

The pulse duration used in the experiments is 130 femtosecond. According to the previous studies on rise time of charge collection [7], this time is at picosecond level with respect to different linear energy transfer (LET) and device resistivity. The pulse width is supposed to be shorter than this charge collection time as a result of carrier diffusion and funneling effect. Based on the above consideration, laser duration of 130 femtoseconds is applied to guarantee the validity of the experiment data.

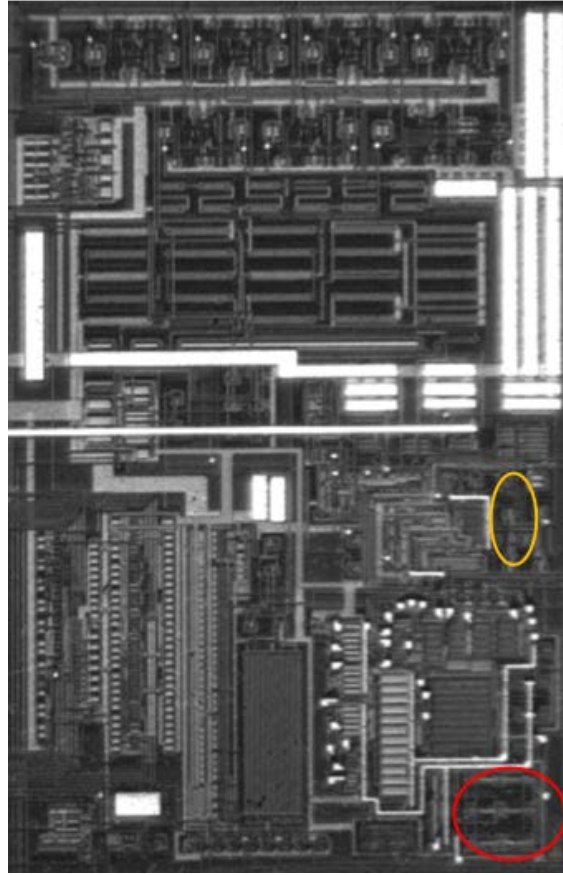


**Figure 5.3** Micrograph of the DC/DC PWM controller.

#### ***5.2.4. Laser Repetition Rate***

The repetition rate decides the interval between every two sequential pulse. In this paper, a wide range of various repetition rates were used from 10 KHz to 4.75 MHz and the results were compared. Obviously repetition rates account for the difference on average power and energy per pulse of the threshold.

### 5.2.5. Laser Spot Size

Compared with ion particle, laser spot size is normally one order magnitude bigger [8, 12]. As a result, it is necessary to make sure the laser spot size is small enough with respect to the testing sensitive transistors. In our case, the spot size is around 1.5 micrometer, which is small enough for the 0.6  $\mu\text{m}$  feature size adopted in the testing DC/DC controller chip.

## 5.3 Experimental Results

Three IR lasers with wavelength of 800 nm, 920 nm and 990 nm were used to irradiate the most sensitive circuits in the chip. The micrograph of the sensitive part of the chip is shown in Fig. 5.3. The upper circle locates the position of the sensitive transistors in Power-On Reset (POR) circuits, whereas the lower circle shows the locations of the sensitive transistors in Bandgap (BG) reference circuits. For each wavelength, repetition rates from 10 KHz to 4.75 MHz were adopted to perform the experiments. The average laser power and energy per pulse

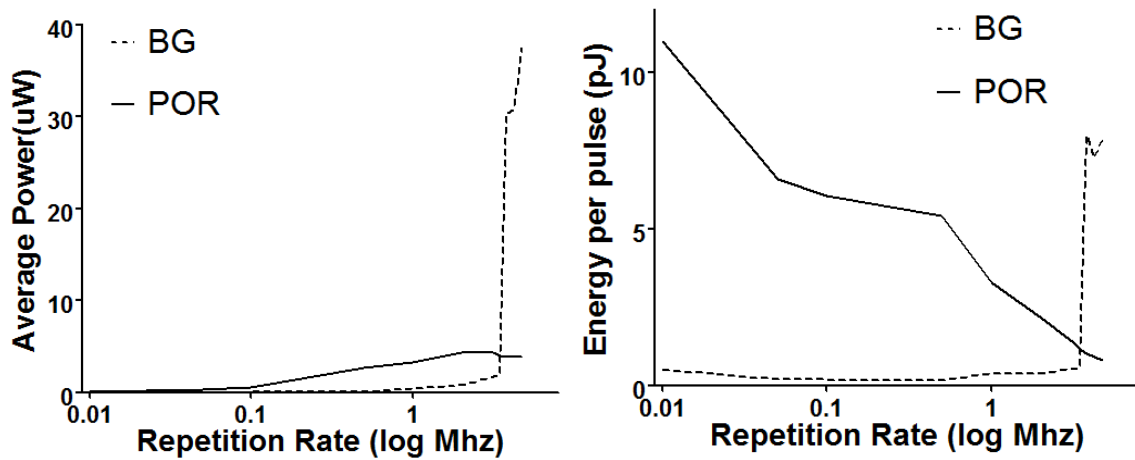


**Figure 5.4** Threshold power and energy per pulse for 800 nm.

versus the pulse repetition rate are shown in Fig. 5.4.

### 5.3.1. 800nm Laser Results

The experiment results for 800 nm are shown in Table 5.1, which indicates the threshold power and energy for SET on the BG and POR, respectively. The BG and POR mean the sensitive transistors in BG and POR circuits. The repetition rate is from 10 KHz to 4.75 MHz. Energy per pulse equals to the average power divided by the repetition rate.

In the experiments, different SET failure phenomena were observed with respect to the repetition rates. For the BG, when the repetition rate is lower than 3.8MHz, the 6- $\mu$ s glitch on PGOOD is captured on the oscilloscope (data in green color). However, when it is equal or higher than 3.8 MHz, the chip directly shuts down without generating the glitches (data in red color). For the POR, when the repetition rate is lower than 500 kHz, the six microsecond glitch is observed (data in green color). When the repetition rate is equal or higher than 500 KHz, irregular glitches with various glitch widths are observed (data in brown color). It is obvious that different repetition rates can trigger different failure mechanisms.

**Table 5.1 Laser Results for 800 nm**

Repetition Rate (Hz)	Average Power ( $\mu$ W)		Energy per Pulse (pJ)	
	BG	POR	BG	POR
10 K	0.005	0.11	0.5	11
50 K	0.01	0.33	0.2	6.6
100 K	0.018	0.605	0.18	6.05
500 K	0.075	2.7	0.15	5.4
1 M	0.385	3.3	0.39	3.3
2 M	0.765	4.3	0.38	2.15
3.12 M	1.7	4.3	0.54	1.36
3.46 M	1.93	3.95	0.56	1.14
3.8 M	30.3	3.89	7.97	1.02
4.22 M	30.7	3.9	7.27	0.92
4.75 M	37.5	3.9	7.89	0.82

### 5.3.2. 920nm Laser Results

The experiment results for 920 nm are as Table 5.2. The general tendency is the same with that of 800 nm. When the repetition rates rose to 4.22 MHz, the failure mechanism changed from 6- $\mu$ s glitch to shut down for the BG. The relative threshold power is a bit different. This is reasonable as the penetration depth differs along with different wavelengths. The similar trend is observed for the POR.

### 5.3.3. 990nm Laser Results

The experiment results for 990 nm are as Table 5.3. For all the repetition rates, the 6- $\mu$ s glitch is observed for the BG. The data in POR column with asterisks mean the maxim power we can have for that repetition rate. Yet no glitch was seen for that maxim power on POR. When repetition rate is higher than 2 MHz, irregular glitches arose on POR. Compared with the previous results of 800 nm and 920 nm, the relation between sensitivity and repetition rate is consistent. However, the relative threshold power is slightly different.

**Table 5.2 Laser Results for 920 nm**

Repetition Rate (Hz)	Average Power ( $\mu$ W)		Energy per Pulse (pJ)	
	BG	POR	BG	POR
10 K	0.017	0.42	1.7	42
50 K	0.025	0.67	0.5	13.4
100 K	0.035	1.04	0.35	10.4
500 K	0.11	3.39	0.22	6.78
1 M	0.222	4	0.222	4
2 M	0.38	4.4	0.19	2.2
3.12 M	1.69	4.8	0.53	1.52
3.46 M	3.2	5.1	0.93	1.48
3.8 M	6.6	5.3	1.74	1.39
4.22 M	34	5.4	8.05	1.28
4.75 M	38	5.1	8	1.07



**Table 5.3 Laser Results for 990 nm**

Repetition Rate (Hz)	Average Power ( $\mu$ W)		Energy per Pulse (pJ)	
	BG	POR	BG	POR
10 K	0.011	0.123*	1.1	12.3*
50 K	0.03	0.34*	0.6	6.8*
100 K	0.055	0.617*	0.55	6.17*
500 K	0.255	2.45*	0.51	5.08*
1 M	0.474	5.7*	0.47	5.7*
2 M	1.03	7.35	0.52	3.675
3.12 M	4.36	7.28	1.38	2.3
3.46 M	6.97	7.7	2.02	2.23
3.8 M	8.97	7.56	2.36	1.99
4.22 M	10.2	7.4	2.41	1.75
4.75 M	19.6	7.31	4.13	1.54

## 5.4 Discussions

The results clearly implied that different pulse repetition rates can trigger different SET failure phenomena for BG and POR circuits as shown in Table 5.1, 5.2 and 5.3. At low repetition rates, it will generate the 6- $\mu$ s glitch on the PGOOD signal, whereas it will induce irregular pulses on the PGOOD signal or shutdown of the chip for higher repetition rates. It is also noted that the sensitivity distribution tended to vary with respect to different repetition rates. For low repetition rates, transistors in BG circuits are the most vulnerable, which is in accordance with the alpha particle experiment results. However, as the repetition goes high, POR circuit requires least power to cause the 6- $\mu$ s glitch on PGOOD. This tendency is consistent in all three wavelength experiments.

In addition, the laser energy per pulse remains relatively low and constant until it switches to another failure mode for BG transistors as shown in Fig. 5.4. On the contrary, the laser energy per pulse decreases gradually over the repetition rates for POR transistors. This tendency is also consistent with all three wavelength experiments.

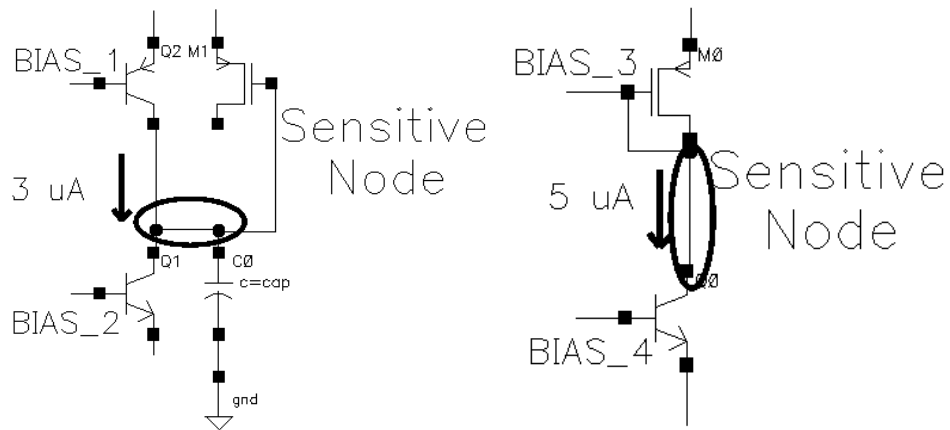


**Figure 5.5** Sensitive node schematic for POR and Band Gap.

The aforementioned phenomena can be explained with circuit schematic operations. The schematic simulation results imply that the root cause for the glitch is a voltage drop in the sensitive nodes, which need a continuous deposit of charges (holes or electrons depending on the type of device components). Once the voltage drop reaches a threshold level, it will change the state of some subsequent buffers and inverters, which eventually generate the PGOOD pulses. So the correlation could be explained with the accumulation process of laser power on semiconductor and the recovery time of circuits.

As is shown in Fig. 5.5, the sensitive transistors in POR circuits are connected to a capacitor, the gate of a PMOS transistor and the collector of a bipolar whereas the sensitive node in BG transistors is the collector of a bipolar. In addition, the discharge current in BG transistors is almost twice as much as of that in POR, which means the BG transistor will recover faster. In that case, when repetition rate is low, the interval between each laser pulse is long enough for the

POR node to discharge the SET charges and recover, when the energy per pulse is not big enough to cause a SEE on POR node. However, it is large enough to upset the bandgap transistor, which is what we observed in low repetition rate. As the repetition rate goes up, energy per pulse keeps going down. And finally, it is too small to cause a SEE on band gap transistor. Also, because the discharge of band gap transistor is quicker, an accumulation is not likely. On the contrary, for high repetition rate, the charges begin to store on the POR capacitor and generate a glitch at the end. That is why POR is most sensitive in high repetition rate. Based on the above analysis, it is obvious that band gap transistor actually needs less energy to have a SEE whereas the POR sensitivity turns out to be dependent on charge accumulation in high repetition rates. Also, consider the practical applications of the DC/DC PWM controller, where the radiation particles strike the chip in very low frequency, low repetition results are more convincing.

## **5.5 Conclusions**

In this paper, a versatile triple DC/DC PWM controller was tested using femtosecond pulsed laser beams to locate the most sensitive spot. IR lasers of three different wavelengths with different repetition rates were selected to guarantee the validity of the experiment results. Different failure mechanisms were observed along with the increasing of the repetition rate. The relationship between the SET sensitivity and the laser repetition rate was observed and investigated. A conclusion is drawn that low the repetition rate should be adopted for laser-based SET experiments for complex analog/mixed signal integrated circuits.

## **References**

- [1] S.P. Buchner, D. McMorrow, J.S. Melinger, and A.B. Campbell, "Laboratory tests for single event effects," IEEE Trans. Nuc. Sci. Vol. 43, No. 2, April 1996.

- [2] D. McMorro, J.S. Melinger, and S. Buchner, "Application of a pulsed laser for evaluation and optimization of SEU hard designs," *IEEE Trans. Nuc. Sci.* Vol. 47, No. 3, June 2000.
- [3] F. Darracq, H. Lapuyade, N. Buard, F. Mounsi, B. Foucher, P. Fouillat, M.C. Calvet, and R. Dufayel, "Backside SEU laser testing for commercial off-the-shelf SRAMs," *IEEE Trans. Nuc. Sci.* Vol.49, No. 6, December 2002.
- [4] J.A. Mazer, K. Kang, and S. Buchner, "Laser simulation of single event in a p-Well CMOS counter," *IEEE Trans. Nuc. Sci.* Vol.36, No. 1, February 1989.
- [5] S.P. Buchner, D. Wilson, K. Kang, D. Gill, and J.A. Mazer, "Laser simulation of single event upsets," *IEEE Trans. Nuc. Sci.* Vol. NS-34, No. 6, December 1987.
- [6] J.S. Melinger, S. Buchner, D. McMorro, W.J. Stapor, T. R. Weatherford, and A.B. Campbell, "Critical evaluation of the pulsed laser method for single event effects testing and fundamental studies," *IEEE Trans. Nuc. Sci.* Vol. 41, No. 6, December 1994.
- [7] R.S. Wagner, N. Bordes, J.M. Bradley, and C.J. Maggiore, "Alpha-, boron-, silicon- and iron-ion-induced current transients in low-capacitance silicon and GaAs diodes," *IEEE Trans. Nuc. Sci.* Vol. 35, No. 6, December 1988.
- [8] A.H. Johnston, "Charge generation and collection in p-n junctions excited with pulsed infrared lasers," *IEEE Trans. Nuc. Sci.* Vol. 40, No. 6, December 1993. 1987, pp. 740–741 [Dig. 9th Annu. Conf. Magnetism Japan, 1982, p. 301].
- [9] Cecile Weulersse, Françoise Bezerra, Florent Miller, Thierry Carrière, Nadine Buard, and William Faló, "Probing SET Sensitive Volumes in Linear Devices Using Focused Laser Beam at Different Wavelengths," *IEEE Trans. Nuc. Sci.* Vol. 55, No.4, August 2008.
- [10] D.A. Kleinman, and R.C. Miller, "Band-gap renormalization in semiconductor quantum wells containing carriers," *Phys. Rev. B* 32, 2266–2272 (1985).

- [11] E.D. Jones, M. Blount, W. Chow, H. Hou, and J.A. Simmons, "Bandgap renormalization studies of n-type GaAs/AlGaAs single quantum wells," *IEEE Trans. Nuc. Sci.*, September 1997.
- [12] F. Miller, N. Buard, T. Carriere, R. Dufayel, R. Gaillard, P. Poirot, J.M. Palau, B. Sagnes, and P. Fouillat, "Effects of beam spot size on the correlation between laser and heavy ion SEU testing," *IEEE Trans. Nuc. Sci.* Vol. 51, No.6, December 2004.
- [13] Y. Ren, L. Fan, L. Chen, S.-J. Wen, R. Wong, N. W. van Vonno, A. F. Witulski, and B. L. Bhuvu, "Single-Event Effects Analysis of a Pulse Width Modulator IC in a DC/DC Converter," *Springer Journal of Electronic Testing: Theory and Applications*, vol. 28, no. 6, pp. 877–883, Dec., 2012.

## 6. CORRELATION OF HEAVY-ION AND LASER TESTING ON A DC/DC PWM CONTROLLER

*Published as:*

Y. Ren, S.-T. Shi, L. Chen, H.-B. Wang, L.-J. Gao, G. Guo, S.-J. Wen, R. Wong, and N. W. van Vonno, "Correlation of Heavy-Ion and Laser Testing on a DC/DC PWM Controller," *Springer Journal of Electronic Testing: Theory and Applications*, Vol. 29, no. 4, pp. 609-616, Aug., 2013.

In the previous chapters, comprehensive studies are performed on the SET sensitive DC/DC PWM chip using pulsed laser technique. Both the root cause for the sensitivity and its dependency on temperatures, wavelengths and repetition rates are discussed. The analysis is also verified taking the advantages of circuit level simulation. As we can see, bandgap circuit can be very sensitive to SET. And temperatures can have different effects on SET sensitivity considering the quiescent point shift. However, the correlation of the laser testing to the standard heavy ion testing is not established yet. This correlation potentially makes pulsed laser technique more versatile in SEE evaluations.

In this manuscript, the correlation between pulsed laser technique and standard heavy ion testing is established based on the DC/DC PWM experimental data. To be specific, the heavy ion data is correlated to those of pulsed laser testing by means of threshold LET and laser energy per pulse. As a result, the equivalent LETs for different laser wavelengths, namely, 750 nm, 800 nm, 850 nm and 920 nm, are acquired. The equivalent LETs for the four wavelengths are determined to be 0.44 MeV•cm<sup>2</sup>/mg, 0.36 MeV•cm<sup>2</sup>/mg, 0.29 MeV•cm<sup>2</sup>/mg and 0.18 MeV•cm<sup>2</sup>/mg,

respectively. The significance of this finding is also presented. For example, based on the laser equivalent LETs, the laser cross-section can be easily acquired from that of heavy ion testing. In return, the heavy ion cross-section of some sub-circuits inside the chip can also be calculated from the pulsed laser data, making it much more convenient. In this way, it can be used to develop the cross-section of any specific area inside the circuit using pulsed laser technique. This can also facilitate the future SEE testing with pulsed laser.

# **Correlation of Heavy-Ion and Laser Testing on a DC/DC PWM Controller**

Y. Ren, S.-T. Shi, L. Chen, H.-B. Wang, L.-J. Gao, G. Guo, S.-J. Wen, R. Wong, N. W. van

Vonno

## **Abstract**

Pulsed laser and heavy-ion experiments were carried out on a commercial-off-the-shelf DC/DC pulse width modulation controller to study the equivalent laser Linear Energy Transfer (LET) at wavelengths of 750 nm, 800 nm, 850 nm and 920 nm. The laser experiments showed that the shorter wavelength laser has smaller threshold energy to generate single-event transient pulses. The cross-sections versus heavy-ion LET and laser energy per pulse were obtained and correlated. The heavy-ion and laser cross-sections fit well considering the effects of metal layers on the chip. The results of this research facilitate the future pulsed laser testing by providing explicit coefficients to evaluate the equivalent laser LET, which can be used to replace costly heavy-ion testing.

## **Index terms**

Single-event transient, pulse-width modulator, pulsed laser technique, heavy-ion, cross-section, correlation.

## **6.1 Introduction**

The pulsed laser is a powerful tool to study Single-Event Effects (SEEs). It offers numerous advantages for SEE testing compared to the conventional heavy-ion technique. For example,



laser testing does not cause radiation-induced degradation. In addition, the pulses can be generated at well-controlled time and location, and the amount of charges deposited per unit depth can be varied over a wide range during the testing. The pulsed laser technique is very effective in debugging and evaluating Single-Event Transients (SETs) in linear devices [1-3] and Single-Event Upsets (SEUs) in digital integrated circuits (ICs) [4, 5]. The laser energy of several specific wavelengths (mostly around 600 nm) has been correlated to the Linear Energy Transfer (LET) of heavy-ions in silicon material with reasonable accuracy [6-9]. These relatively short wavelengths have large absorption coefficient and equivalent laser LET. In our paper, a wide range of longer wavelengths from 750 nm to 920 nm were analyzed. The small equivalent laser LETs results from the longer wavelengths enable more margin and accuracy in controlling the laser energy, and hence make them especially suitable for sensitive device testing, like the DC/DC PWM controller in our case. The longer wavelength also features deeper penetration depth. For example, the penetration depth of 600 nm is around 3  $\mu\text{m}$  while that of 920 nm can be around 100  $\mu\text{m}$ . This is important for studying the bipolar transistors in BiCMOS processes, since bipolar transistors have shown the sensitivity to the laser penetration depth [6].

In this work, a commercial mixed-signal controller chip for a DC/DC converter fabricated in a 0.6  $\mu\text{m}$  BiCMOS process was used to correlate data between heavy-ion beams and the pulsed laser with wavelengths of 750 nm, 800 nm, 850nm and 920 nm. This controller chip is sensitive to neutrons and alpha particles on ground level testing. The most sensitive area was determined to be nine bipolar transistors (used as a delta  $V_{be}$  generator) inside a bandgap sub-circuit with a pulsed laser in our previous studies [10]. This controller chip requires low critical charge to generate the SET pulses, making it an ideal study case for low LET particles. The SET cross-sections versus laser energy per pulse were produced with wavelengths of 750

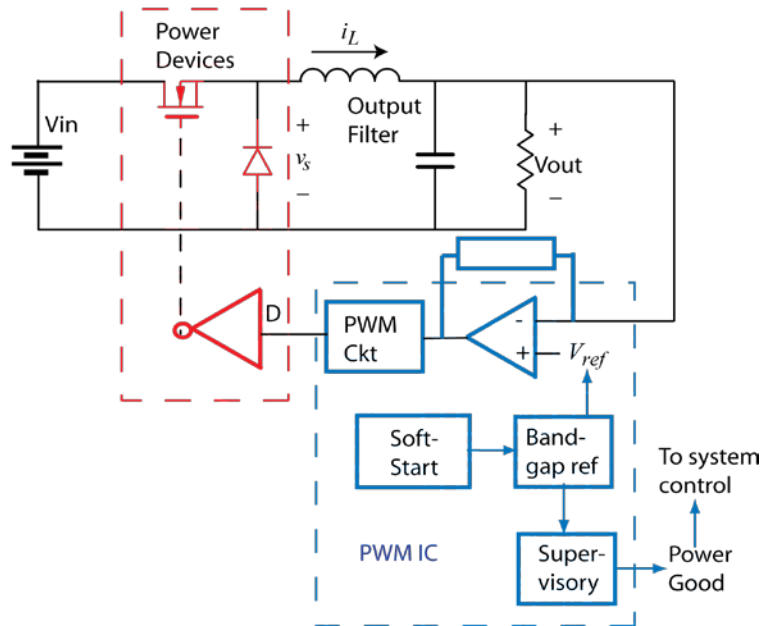


**Figure 6.1** Block level circuit diagram for a DC/DC converter.

nm, 800 nm, 850 nm, and 920 nm, respectively. The heavy-ion experiment was performed to get the SET cross-section versus LET curve. The laser cross-sections are consistently smaller than heavy-ion counterparts because unlike the heavy-ions, the laser cannot access the areas underneath the metal layers. After considering the metal coverage percentage, the laser cross-section curves from all four wavelengths fit well with that from the heavy-ion experiment. It demonstrates that pulsed lasers with different wavelengths can have equivalent cross-sections to that of the heavy-ion. Finally, an equivalent laser LET versus wavelength curve was acquired from our experimental data.

## 6.2 DC/DC PWM Controller IC

Fig. 6.1 shows the major components of a DC/DC converter containing the controller IC (blue box), power devices (red box), and passive components. The controller IC contains a Pulse-Width Modulation (PWM) circuit, a bandgap reference circuit, a soft-start circuit, a supervisory circuit, and an error amplifier. It includes both digital and analog circuits. The PWM circuit generates the signal that controls the percentage of the clock period that the power transistor is “ON”. The soft-start circuit limits the duty cycle at the start up to limit the load current, shown as  $i_L$  in Fig. 6.1. The supervisory circuit monitors all other blocks to generate the “Power Good” signal, which is used to monitor the health of the DC/DC converter. Single events can affect any one of these circuits [11-16]. However, hits to the PWM often do not significantly disturb the output voltage of the converter because perturbations of individual duty cycles are filtered by the LC low-pass filter on the output of the converter. The output voltage responds only to the average duty cycle. The pulsed laser or heavy-ions can induce a voltage perturbation at the output of the bandgap sub-circuit. When this voltage perturbation is big enough, it resets a low pass filter inside the PWM chip and hence causes a 6- $\mu$ s SET. This 6- $\mu$ s SET eventually propagates to the PGOOD output pin. The cross-section calculation in this paper is based on the error rates of SETs (negative glitches) at the PGOOD pin. The following sections describe an investigation of SETs in the DC/DC PWM controller chip by monitoring the PGOOD output.

## 6.3 Experimental Details

### 6.3.1 Device under Test (DUT)

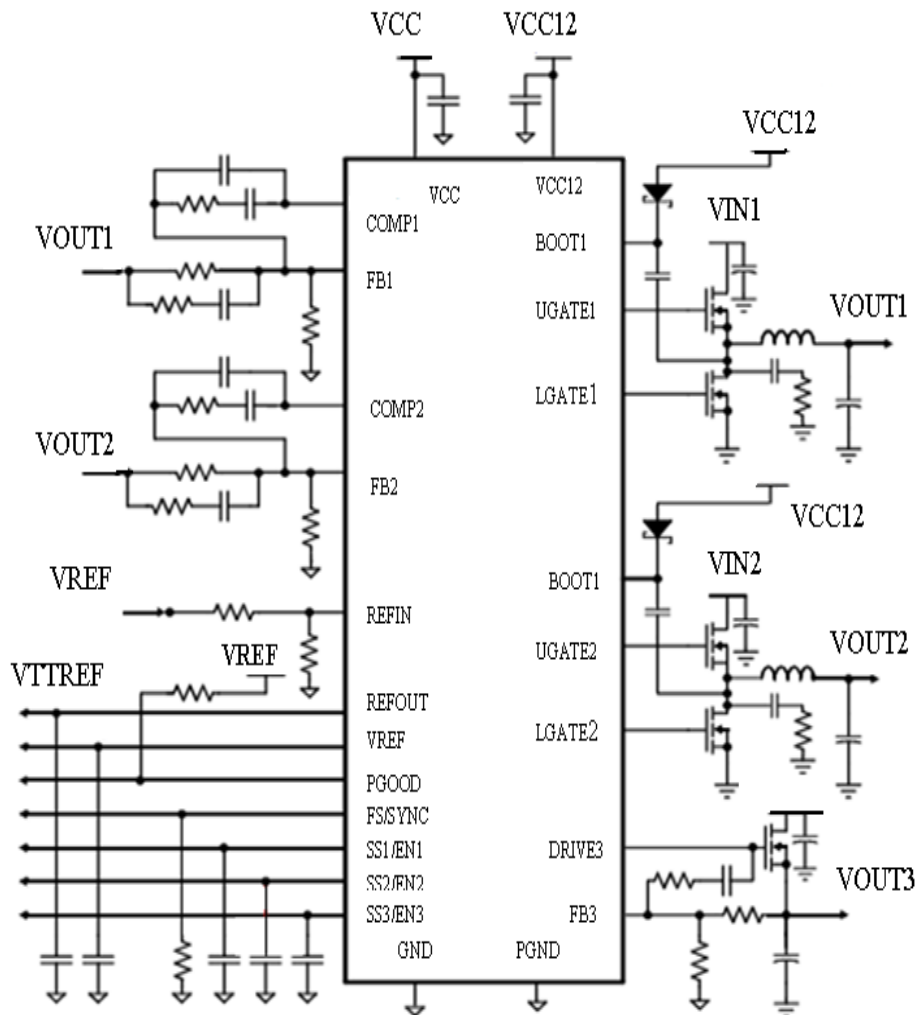


**Figure 6.2** Test circuit for the complete DC/DC PWM controller.

The DC/DC controller under test is a triple regulator. It has two independent synchronously-rectified buck controllers (OUT1 and OUT2) and a linear controller (OUT3) to offer precise regulation of up to three voltage rails. The test circuit is shown in Fig. 6.2 [10]. The three soft-start pins, namely SS1/EN1, SS2/EN2 and SS3/EN3, are grounded through a capacitor for each pin. The PGOOD pin is an open-drain pull-down device output connected to VCC and

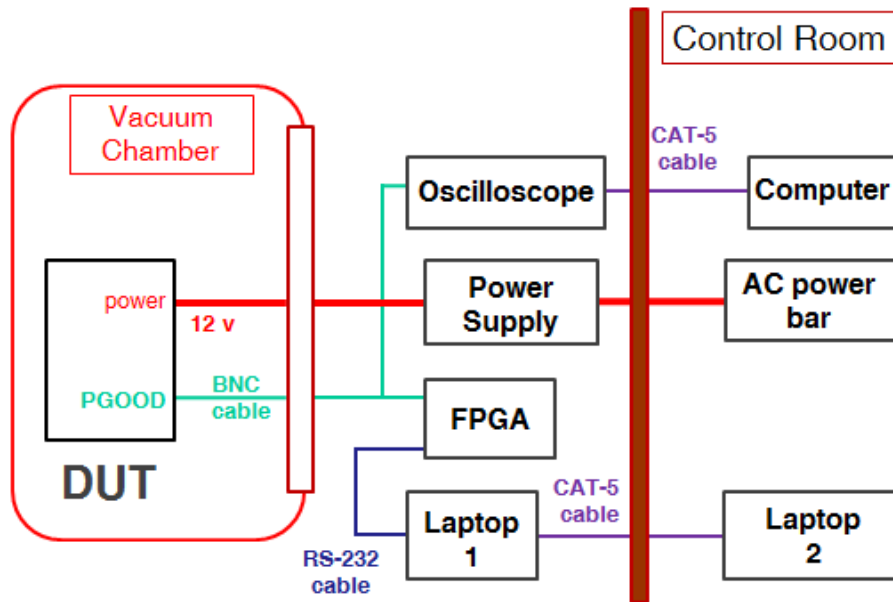


**Figure 6.3** Block diagram for heavy-ion testing.

provides high level voltage monitoring for almost every circuit in the controller IC. When power is first applied to the IC, the PGOOD output is pulled low indicating an initial condition. After all three soft-start pins complete their ramp up with no faults (no short detected on switchers), the power is considered “GOOD” as indicated by a high PGOOD pin. The DC/DC controller IC was used in the above configuration for all tests presented in this paper.

### 6.3.2 Setups

A general block diagram for heavy-ion testing is shown in Fig. 6.3. A pre-programmed FPGA was used to record SET pulses and to calculate their durations from the PGOOD pin. A BNC cable coupled the PGOOD signal from the DUT to the FPGA. The DUT was located in a

**Table 6.1 Heavy ions in use and cross section data**

Heavy ion	Energy (MeV)	Range in Si ( $\mu\text{m}$ )	LET ( $\text{MeV}\cdot\text{cm}^2/\text{mg}$ )	Cross-section ( $\text{cm}^2$ )
Li	45	259.6	0.44	$1.03 \times 10^{-4}$
C	78	122.2	1.77	$4.73 \times 10^{-4}$
F	100	72.7	4.43	$1.2 \times 10^{-3}$
Si	120	43.9	9.82	$1.3 \times 10^{-3}$
Cl	145	41.2	13.6	$1.36 \times 10^{-3}$

vacuum chamber to extend the available range of the heavy-ion beam. A high speed oscilloscope was also used to monitor the shape of SET pulses. All the data was sent to laptop 1 in the irradiation room through an RS-232 cable. Laptop 2 in the control room controlled all the equipment in the radiation room by means of a CAT-5 cable. The laser testing used a similar setup to record SET pulses, differing only in that it was performed in air rather than in vacuum.

### **6.3.3 Irradiation Facilities**

The heavy-ion irradiation was carried out using HI-13 tandem electrostatic Van de Graaff accelerator at China Institute of Atomic Energy (CIAE) in Beijing [17]. This broad beam facility is capable of accelerating almost all the elements of the periodic table with the non-uniformity of beam less than 10% over an area of  $10 \text{ cm} \times 10 \text{ cm}$ . A sample holder capable of holding four  $254 \text{ mm} \times 254 \text{ mm}$  test boards resides in the vacuum testing chamber whose diameter and height are both 1100 mm. The multiple choices of interfaces on the chamber wall, such as BNC and Sub D-9, facilitate the experiments. The particles used are shown in Table 6.1. The fluence of the

particles ranges from  $9 \times 10^4 \text{ cm}^{-2}$  to  $9.9 \times 10^5 \text{ cm}^{-2}$  with the beam size of  $2 \text{ cm} \times 2 \text{ cm}$ . The system setup inside the vacuum chamber is shown in Fig. 6.4.

The laser induced SET testing facility used in this work is located at the Saskatchewan Structural Sciences Centre (SSSC) in University of Saskatchewan. The basis of the laser scanning system is a Zeiss LSM410 confocal microscope which is located on a floating optical table to reduce mechanical vibration transfer to the instrument. The laser system is a Mira 900-D

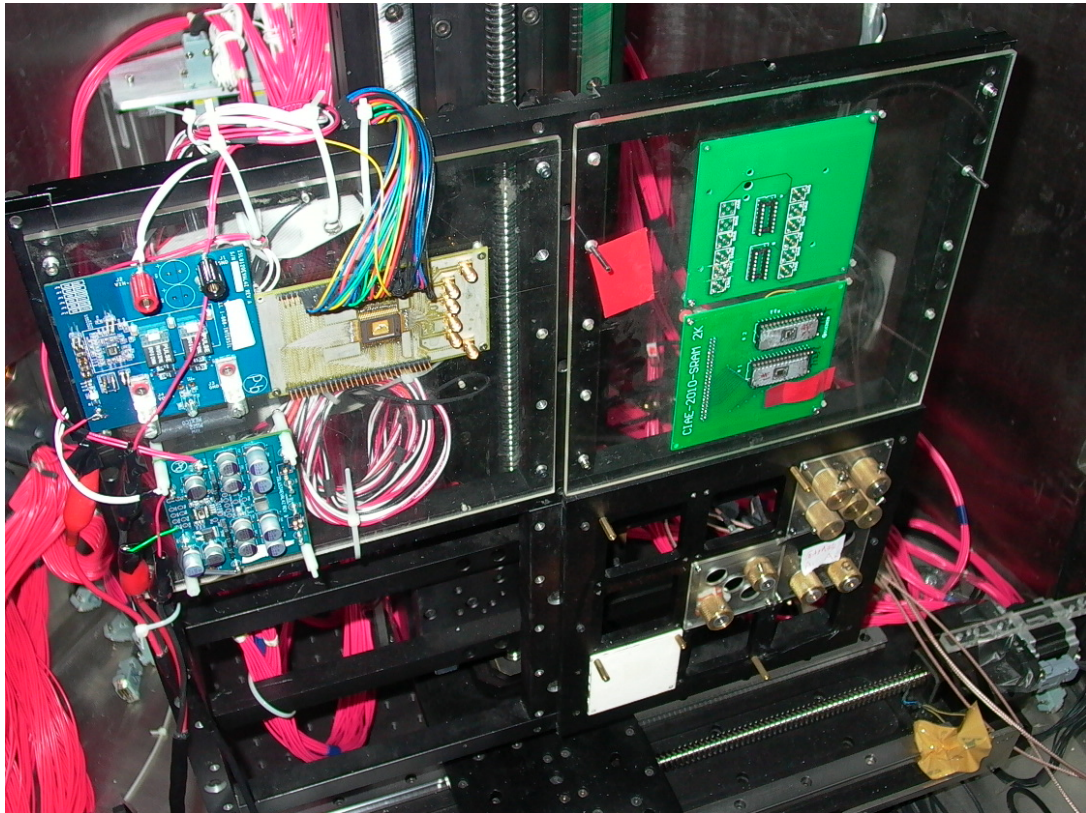


**Figure 6.4** Experimental heavy-ion testing setup in the vacuum chamber.

pumped by a Verdi V-10 (made by Coherent). It has a tunable Ti:sapphire laser with wavelengths ranging from 700 nm to 1000 nm. The laser system is capable of emitting a continuous wave beam or picosecond and femtosecond pulses. It has a Pulse Picker 9200 which is a stand-alone accessory for the laser system to change the pulse repetition rate over the wide range available. It gives a repetition rate selection from 10 kHz to 75 MHz.

In the scanning process, the DUT was fastened on the testing plate. The laser beam was focused on the surface of the die through the objective of the microscope. The laser spot size diameter and pulse duration are  $1.6\ \mu\text{m}$  and 130 fs, respectively. The Zeiss 10X objective in use has a working distance of 5.5 mm. The scanning area displayed on the monitor is divided into

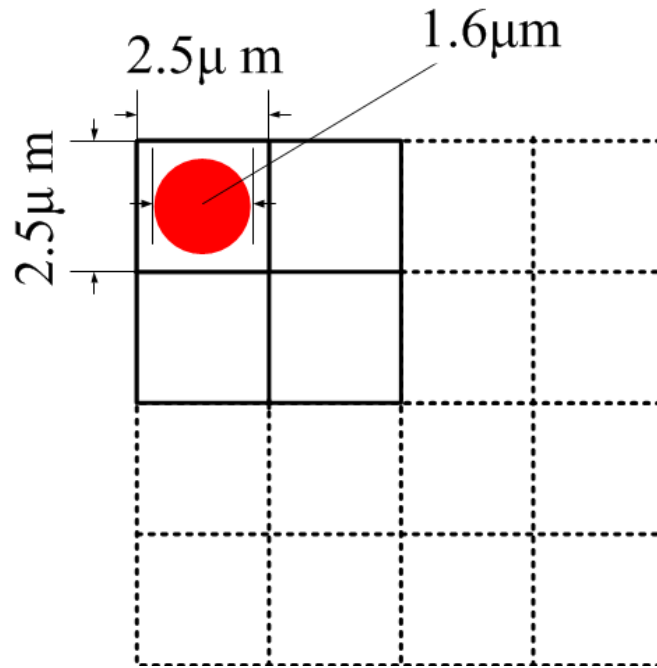


**Figure 6.5** Scanning block units and laser spot size.



512 × 512 pixels. Each pixel measures 2.5 μm × 2.5 μm, which is a little larger than the laser spot size (the red dot) as is shown in Fig. 6.5. The laser coming out of the objective scans the DUT pixel by pixel with a step size of 2.5 μm. The dwelling time on each pixel is around 244 μs.

## 6.4 Experimental Results

### 6.4.1 Heavy-Ion Data

The heavy-ion experimental results are shown in Table 6.1. Five different heavy-ions with LETs in silicon ranging from 0.44 MeV•cm<sup>2</sup>/mg to 13.6 MeV•cm<sup>2</sup>/mg were selected to perform the experiment. As expected, the cross-section curve shows the conventional shape (Fig. 6.6). The cross-section of Li ion in Table 6.1 is 1.03 × 10<sup>-4</sup> cm<sup>2</sup> and the sensitive area (nine bipolar transistors in bandgap sub-circuit) is around 1 × 10<sup>-4</sup> cm<sup>2</sup> according to the layout of the chip. So we can see the LET for Li is around the threshold and make 0.44 MeV•cm<sup>2</sup>/mg the threshold

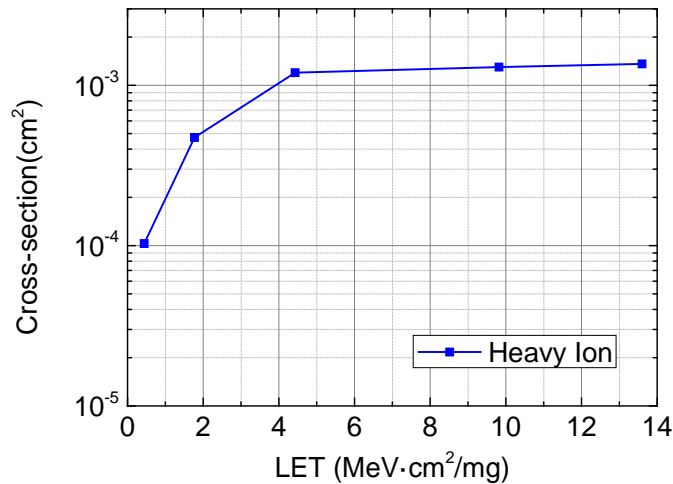


**Figure 6.6** Cross-section for heavy-ion testing.

LET. The saturation value of the cross-section was reached around an LET of 4.43 MeV•cm<sup>2</sup>/mg. Note that the experiment was performed only once for each LET as a result the error bar is not included.

#### **6.4.2 Laser Data**

A range of wavelengths (750 nm, 800 nm, 850 nm and 920 nm) were used in our laser testing with the repetition rate of 10 kHz. The time interval between each laser pulse is 100 μs for the 10 kHz repetition rate, which is much longer than the SET pulse width (6 μs) we were recording. This guarantees that the system has enough time to recover from the 6-μs SET glitch and no overlaps between the effects.

To calculate the laser cross-section, a similar equation (6.1) was developed in analogy to the calculation of cross-section as used in particle irradiations. The cross-section is normally acquired through dividing the number of times that an effective single-event was observed by the incident particle fluence [18]. In our pulsed laser irradiation, every single pulse is considered as an equivalent incident particle. In this case, the pulsed laser cross-section is calculated below as (6.1)

$$\sigma = \frac{\#}{\frac{f \times t}{A}} \quad (6.1)$$

Where  $\sigma$  is laser cross-section, # is the number of times that a SET was observed, f is the laser pulse repetition rate, t is the scanning time and A is the scanning area.  $\frac{f \times t}{A}$  gives the concept of pulse fluence (pulses per unit area). To obtain the overall cross-section versus laser energy curve for the whole chip, the chip surface was divided into two sub-areas for laser

**Table 6.2 Laser Threshold and equivalent LET over wavelength**

Wavelength (nm)	Threshold Energy (pJ)	Equivalent LET per 1 pJ (MeV·cm <sup>2</sup> /mg)
750	1	0.44
800	1.2	0.36
850	1.5	0.29
920	2.55	0.18

scanning. Each sub-area scan was completed in 64 seconds. Both areas were scanned separately and their error cross-sections were summed up mathematically. The threshold energies of different wavelengths were described in Table 6.2. As we can see, the threshold energy increases along with the increasing wavelength. The energy points are set by changing the optical density

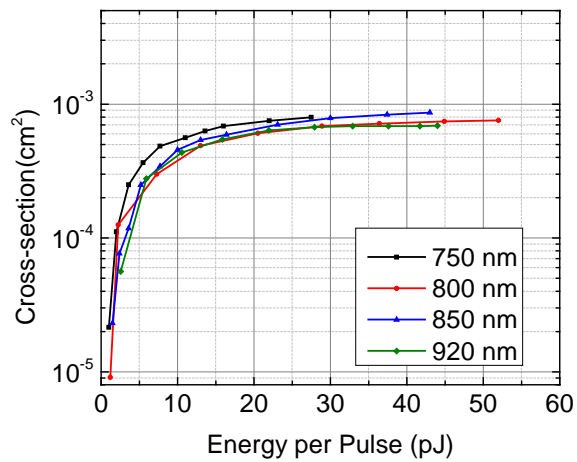


**Figure 6.7** Cross-sections for 750 nm, 800 nm, 850 nm and 920 nm laser.

with a relative constant step size. Laser energy was increased until the cross-section sees saturation. The laser cross-section curve in Fig. 6.7 clearly shows that the four lasers give very similar saturated cross-sections.

## 6.5 Analyses and Discussions

Table 6.2 shows that the threshold energy of 920 nm wavelength is the largest while that of 750 nm is the smallest. This is reasonable because the 750 nm wavelength requires the least energy to have the same LET compared with other wavelengths, since the absorption coefficient of the 750 nm wavelength laser exceeds those of the other three wavelengths. This was also proved theoretically in [19], in which the equivalent laser LET equations are listed below as (6.2), (6.3)

$$L_e = K_e E_L \quad (6.2)$$

$$K_e = T \frac{E_p}{E_\gamma} \frac{1 - e^{-\alpha d}}{d} \quad (6.3)$$

Where,

$L_e$  is equivalent laser LET

$E_L$  is laser energy per pulse

$K_e$  is equivalent coefficient

$T$  is transmission coefficient

$E_p$  is average energy to generate one hole-electron pair

$E_\gamma$  is energy of the photon

$\alpha$  is absorption coefficient

$d$  is the device sensitive depth to the laser

The relatively large absorption coefficient ( $\alpha$ ) for the 750 nm wavelength results in the largest equivalent coefficient ( $K_e$ ) in the four wavelengths.

First, we will correlate the 750 nm wavelength data with that of the heavy-ion. By comparing Fig. 6.6 and Fig. 6.7, we can see that the heavy-ion saturation cross-section is higher than that of the 750 nm wavelength. Actually, this is the fact for all four wavelengths. This can be explained by the metal layers covering the active areas of the chip. These metal layers will not pose any hindrance to the heavy-ions. The heavy-ions will be able to penetrate the metal layers and reach active silicon areas whereas the laser beam will not be able to penetrate these metal layers. Since the laser cross-section was obtained by dividing the number of SETs observed by the number of laser pulses during the scanning and multiplying by the scanning area, areas covered by metal layers must be compensated for. The DC/DC controller chip under study is fabricated using a three-layer metal process. The total metal layer coverage for the whole chip is around 40%. The saturation cross-sections for the heavy-ion and the 750 nm wavelength laser are  $0.00136 \text{ cm}^2$  and  $0.00079 \text{ cm}^2$ , which show a difference of around 41.9%. This difference is very consistent with the metal coverage percentage of the chip. The correlation between laser energy and heavy-ion LET can be obtained by comparing the thresholds [8, 9]. In this situation, a laser energy of 1 pJ (energy per pulse for 750 nm) is equivalent to around  $0.44 \text{ MeV}\cdot\text{cm}^2/\text{mg}$  (equivalent LET). Once we apply this conversion coefficient to the whole cross-section curve and consider the metal coverage compensation, the cross-section curves for 750 nm wavelength and heavy-ion can be re-plotted as Fig. 6.8. The curves show the same shape and tendency. The

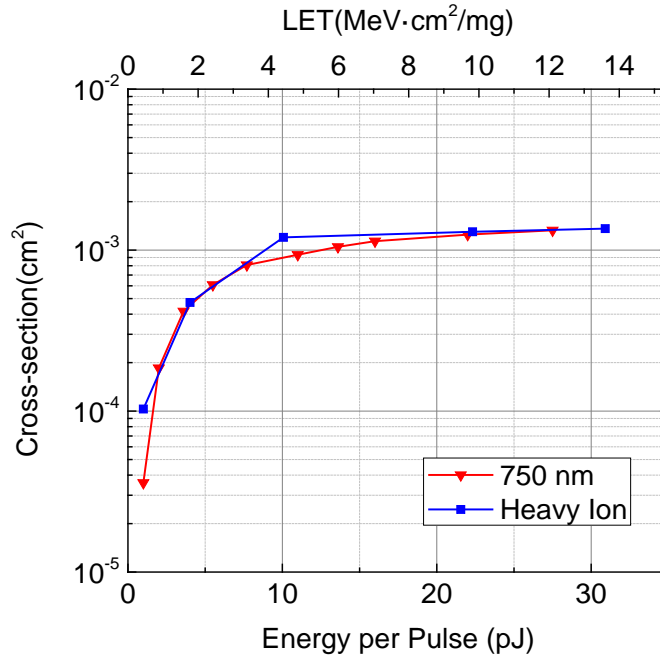


**Figure 6.8** Cross-section curve fitting for heavy ion and 750 nm wavelength.

saturation levels also fit well. However, this laser cross-section scale-up according to the chip metal coverage percentage is only reasonable for large feature size like our DUT which is fabricated in a 0.6  $\mu\text{m}$  BiCMOS process. For example, the size for one bipolar transistor in the most sensitive area (bandgap sub-circuit) is 20  $\mu\text{m}$   $\times$  16  $\mu\text{m}$ . The transistors are fairly large compared to the metal lines and there are always sensitive areas exposed to the laser irradiation. For advanced technology, this method may introduce more errors due to more metal layers and larger metal coverage as well as the sensitivity distribution uncertainty of the areas underneath the metal layers. This will be confirmed in the future using our backside Two-Photon Absorption (TPA) irradiation laser facility under construction, which can get rid of the metal coverage issue by applying laser from the backside of the chip.

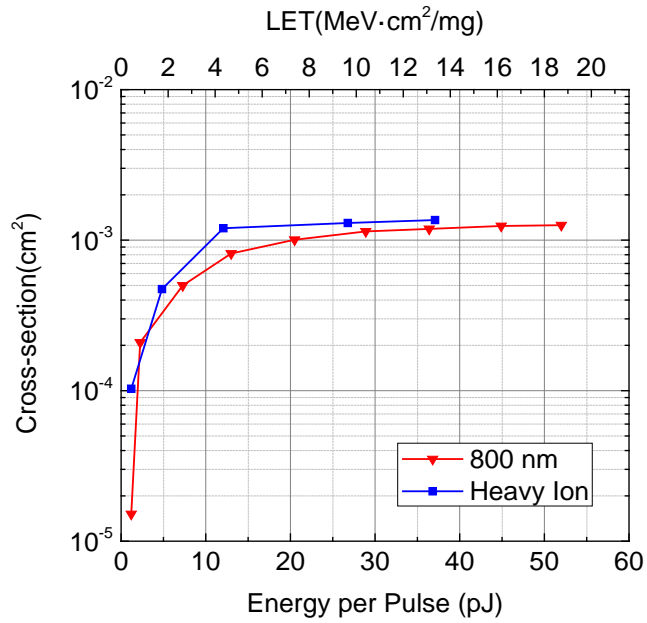


**Figure 6.9** Cross-section curve fitting for heavy ion and 800 nm wavelength.

The equivalent laser LETs for 800 nm, 850 nm and 920 nm wavelengths were acquired in the same procedure. In these situations, each 1 pJ laser energy is equivalent to around 0.36 MeV·cm<sup>2</sup>/mg, 0.29 MeV·cm<sup>2</sup>/mg and 0.18 MeV·cm<sup>2</sup>/mg for 800 nm, 850 nm and 920 nm, respectively. These numbers were acquired by comparing the thresholds between laser and heavy- ion. For the same energy per pulse, the 750 nm wavelength shows the largest equivalent laser LET as it has the largest absorption coefficient ( $\alpha$ ). The cross-section curves for 800 nm, 850 nm and 920 nm wavelengths and heavy-ion are re-plotted in Fig. 6.9, Fig. 6.10 and Fig. 6.11. Finally, an equivalent laser LET vs. wavelength curve was plotted in Fig. 6.12.

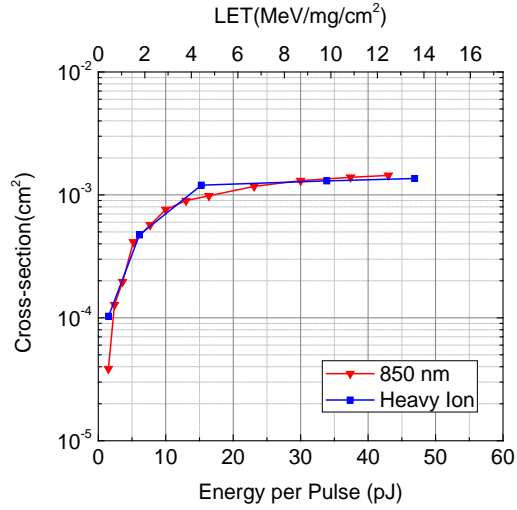


**Figure 6.10** Cross-section curve fitting for heavy ion and 850 nm wavelength.

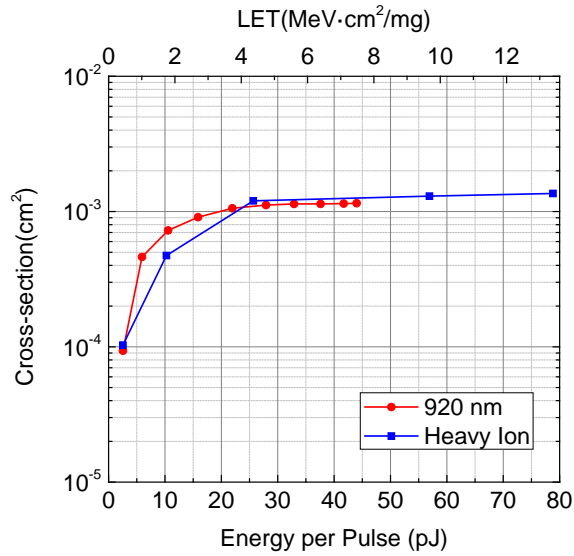


**Figure 6.11** Cross-section curve fitting for heavy ion and 920 nm wavelength.

Now it is interesting to compare our data with those of previous work [8, 9] which are shown in Table 6.3. The equivalent LETs for [8] and [9] were explicitly given in their papers.



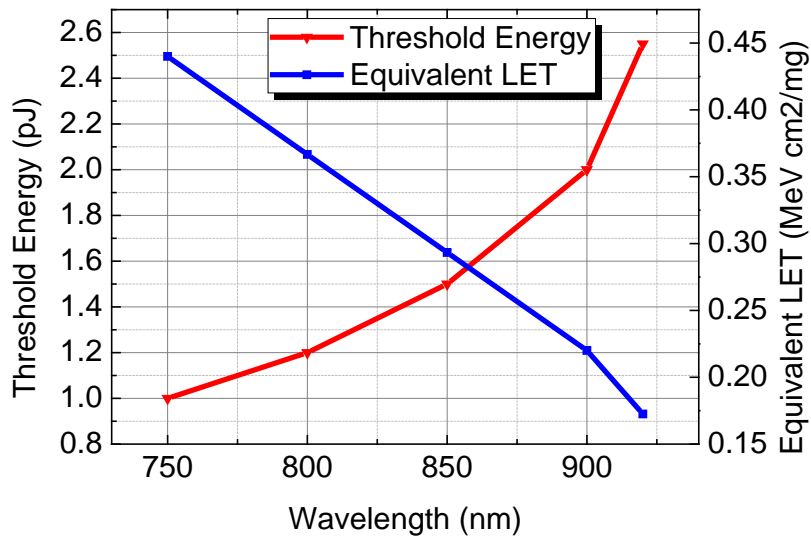


**Figure 6.12** Laser threshold and equivalent LET in terms of wavelength.

**Table 6.3** Comparison with previous work.

Ref.	Wave length (nm)	Pulse duration (s)	Repetition Rate (Hz)	Equivalent LET Per 1 pJ (MeV·cm <sup>2</sup> /mg)
[8]	600	10p	5 M	3
[9]	605	1p	1 k	3.05
Our paper	750	130f	10 k	0.44
Our paper	800	130f	10 k	0.36
Our paper	850	130f	10 k	0.29
Our paper	920	130f	10 k	0.18

Our data values are less than those reported in [8, 9]. This is mainly because of the longer laser

wavelengths we used. In addition, previous studies have compared the experimental results on a basic component (a single diode) from several mainstream laser facilities and have found that different laser characteristics tend to affect the transient amplitudes and charge collection [20]. The results from our experiments may not be directly applied to other laser facilities. Further studies are to be carried out to fully understand the charge collection mechanism induced by lasers and establish the correlations among different laser facilities.

## 6.6 Applications

As we know, a laser is much more accessible and flexible compared with heavy-ion beams. There are valuable applications for the equivalent laser LETs presented in our paper, such as accurately estimating the cross-sections of heavy-ion LETs for the overall IC and arbitrary

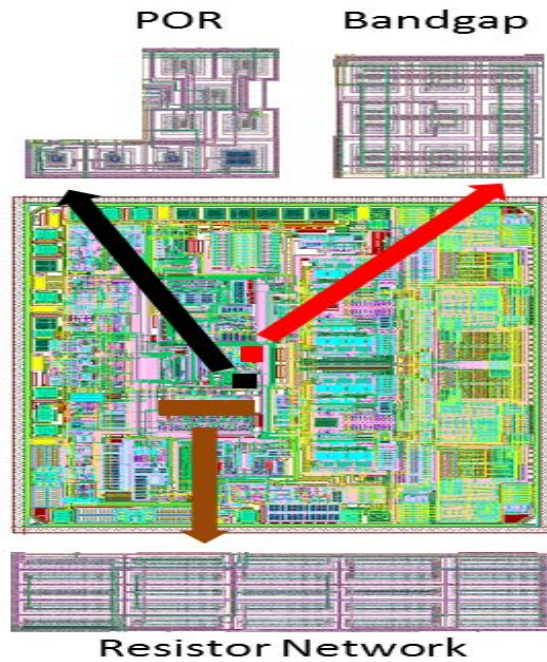


**Figure 6.13** Layout of the controller IC and each individual blocks.

sub-circuits, and providing guidance on radiation-hardened-by-design techniques. The correlation is proven to be accurate for the circuits implemented with the 0.6  $\mu\text{m}$  BiCMOS process. More experiments are to be carried out to obtain the accurate correlation for more advanced CMOS technologies.

The cross-section versus LET curves for arbitrary sub-circuits can be easily acquired by calculating from the laser data. Normally, it is hard to have the cross-section vs. LET curves of arbitrary sub-circuits directly from heavy-ion testing as heavy-ion cross-section data do not differentiate between each sub-circuits. On the contrary, it is easy for pulsed laser to irradiate arbitrary sub-circuits. An example was shown in Fig. 6.13, which is the layout of the DC/DC PWM controller. In this example, the 920 nm wavelength was used to irradiate three sub-circuits sensitive to SET in the DC/DC PWM controller. The first sub-circuit is noted as bandgap (red area) which is composed of nine NPN bipolar transistors (the most sensitive devices according to our previous study [10]). It is used to generate a delta  $V_{be}$  voltage in the bandgap reference circuit. The second one is the resistor network (orange area) which is made up of twenty-five resistors. Its function is to divide the initial bandgap voltage into several different ones. The third one is the Power-on Reset (POR) sub-circuit (black area). The POR is using one of the bandgap reference voltages as an input. So its sensitivity derives from the bandgap variations and it takes more laser energy to trigger SEE at POR directly. The pulsed laser cross-section and the calculated cross-section versus LET curve were shown in Fig. 6.14 and Fig. 6.15. This shows the convenience of getting cross-section vs. LET curves for arbitrary sub-circuits. These individual sub-circuits cross-section also gives direct information to designers to mitigate SEEs by design.

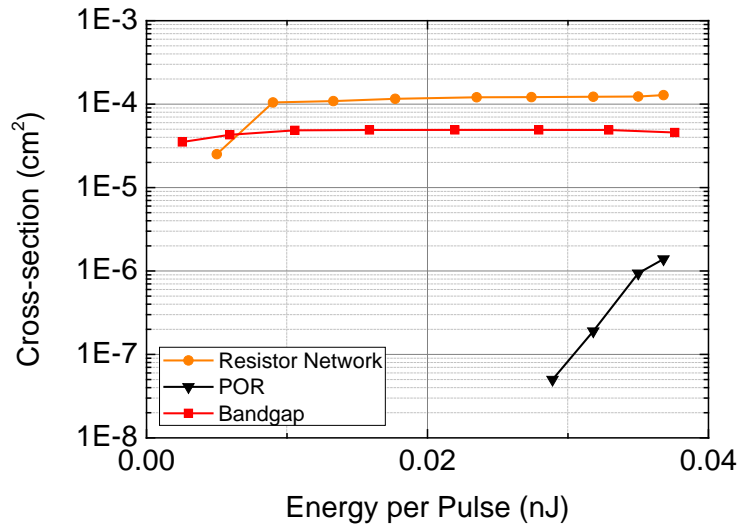


**Figure 6.14** Cross-sections for individual areas laser testing.

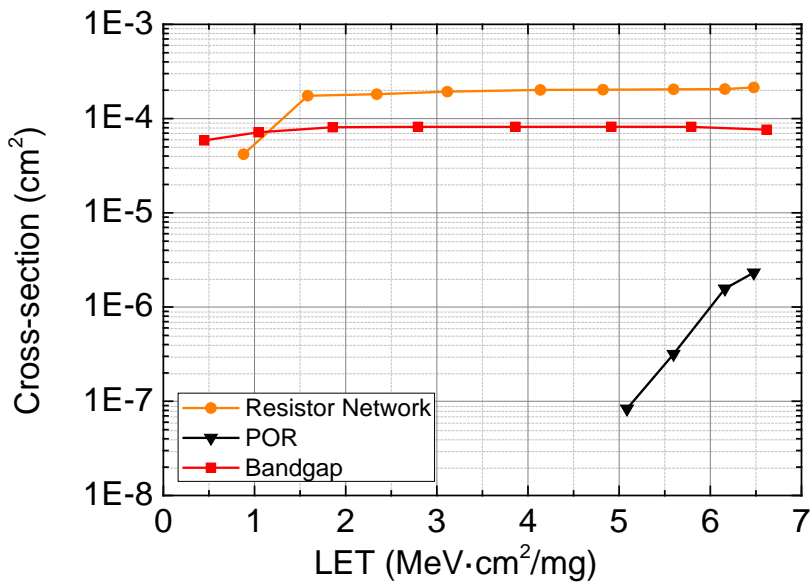


**Figure 6.15** Calculated heavy-ion cross-sections for individual areas.

## 6.7 Conclusions

Correlations between laser energy and heavy-ion LET were established based on our experiments of a mixed-signal controller chip with 0.6  $\mu\text{m}$  BiCMOS process. A wide range of laser wavelengths, from 750 nm to 920 nm, were used. The equivalent laser LETs of every 1 pJ (energy per pulse) for 750 nm, 800 nm, 850 nm and 920 nm wavelengths are 0.44  $\text{MeV}\cdot\text{cm}^2/\text{mg}$ , 0.36  $\text{MeV}\cdot\text{cm}^2/\text{mg}$ , 0.29  $\text{MeV}\cdot\text{cm}^2/\text{mg}$  and 0.18  $\text{MeV}\cdot\text{cm}^2/\text{mg}$ , respectively. These conversion coefficients were applied to the whole cross-section curves and proven to be reasonable. These explicit conversion coefficients can facilitate the future pulsed laser experiments using similar wavelengths. With our correlated equivalent laser LET, general heavy-ion data can be easily obtained from the laser testing data with reasonable accuracy for the similar technologies.

## **Acknowledgement**

The authors would like to thank Saskatchewan Structural Science Center (SSSC) for providing the laser facility and services for the laser experiments. The authors are also grateful that CMC Microsystems provided the simulation tools for the research.

## **References**

- [1] S. Buchner, D. McMorrow, C. Poivey, J. Howard Jr, Y. Boulghassoul, L.W. Massengill, R. Pease, and R.M. Savage, "Comparison of single-event transients induced in an operational amplifier (LM124) by pulsed laser light and a broad beam of heavy ions," IEEE Trans. Nucl. Sci., vol. 51, no. 5, pp. 2776 -2781, Oct. 2004.
- [2] S.D. LaLumondiere, R. Koga, P. Yu, M.C. Maher, and S.C. Moss, "Laser-induced and heavy ion-induced single-event transient (SET) sensitivity measurements on 139-type comparators," IEEE Trans. Nucl. Sci., vol. 49, no.6, pp. 3121 -3128, Dec. 2002.
- [3] S. Buchner, D. McMorrow, A. Sternberg, L. Massengill, R.L. Pease, and M. Maher, "Single-event transient (SET) characterization of an LM119 voltage comparator: an approach to SET model validation using a pulsed laser," IEEE Trans. Nucl. Sci., vol. 49,

- no.3, pp. 1502 -1508, Jun. 2002.
- [4] J.A. Mazer, S. Buchner, and K. Kang, "Laser simulation of single-event upset in a p-well CMOS counter," *IEEE Trans. Nucl. Sci.*, vol. 36, no. 1, pp. 1330 -1332, Feb. 1989.
- [5] F. Darracq, H. Lapuyade, N. Buard, F. Mounsi, B. Foucher, P. Fouillat, M.C. Calvet, and R. Dufayel, "Backside SEU laser testing for commercial off-the-shelf SRAMs," *IEEE Trans. Nucl. Sci.*, vol. 49, pp. 2977 -2983, Dec. 2002.
- [6] C. Weulersse, F. Bezerra, F. Miller, T. Carriere, N. Buard, and W. Falo, "Probing SET sensitive volumes in linear devices using focused laser beam at different wavelengths," *RADECS Conference*, 2007.
- [7] J.R. Schwank, M.R. Shaneyfelt, D. McMorrow, V. Ferlet-Cavrois, P.E. Dodd, D.F. Heidel, P.W. Marshall, J.A. Pellish, K.A. LaBel, K.P. Rodbell, M. Hakey, R.S. Flores, S.E. Swanson, and S.M. Dalton, "Estimation of Heavy ion LET Thresholds in Advanced SOI IC Technologies From Two-Photon Absorption Laser Measurements," *IEEE Trans. Nucl. Sci.*, vol. 57, pp. 1827 -1834, Aug. 2010.
- [8] S.C. Moss, S.D. LaLumondiere, J.R. Scarpulla, K.P. MacWilliams, and R. Koga, "Correlation of picosecond laser-induced latchup and energetic particle-induced latchup in CMOS test structures," *IEEE Trans. Nucl. Sci.*, vol. 42, no. 6, pp. 1948 - 1956, Dec. 1995.
- [9] D. McMorrow, J.S. Melinger, and N.F. Haddad, "Application of a pulsed laser for evaluation and optimization of SEU-hard designs," *IEEE Trans. Nucl. Sci.*, vol. 47, no. 3, pp. 559 - 565, Jun. 2000.
- [10] Y. Ren, L. Fan, L. Chen, S.-J. Wen, R. Wong, N. W. van Vonno, A. F. Witulski, and B. L. Bhuvu, "Single-Event Effects Analysis of a Pulse Width Modulator IC in a DC/DC Converter," *Springer Journal of Electronic Testing Theory and Applications (JETTA)*, vol. 28, no. 6, pp. 877-883, Dec. 2012.
- [11] K. Label, R.K. Barry, K. Castell, H.S. Kim, and C.M. Seidleck, "Implications of single event effect characterization of hybrid dc/dc converters and a solid state power controller," *IEEE Trans. Nucl. Sci.*, vol. 38, pp. 1957-1963, Dec. 1995.
- [12] N.W. van Vonno, L.G. Pearce, J.S. Gill, H.W. Satterfield, E.T. Thomson, T.E. Fobes,

- A.P.Williams and P.J.Chesley, "Total Dose and Single Event Testing of a Hardened Point of Load Regulator," Radiation Effects Data Workshop (REDW), 2010 IEEE.
- [13] N.W.van Vonno, L.G.Pearce, G.M.Wood, J.D.White, E.J.Thomson, T.M.Bernard, P.J.Chesley and R.Hood, "Total Dose and Single Event Testing of a Hardened Single-Ended Current Mode PWM Controller,," Radiation Effects Data Workshop (REDW), 2010 IEEE.
- [14] S. H. Penzin, W. R. Crain, K. B. Crawford, S. J. Hansel, J. F. Kirshman, and R. Koga, "Single event effects in pulse width modulation controllers," IEEE Trans. Nucl. Sci., vol. 43, no. 6, pp. 2968–2973, Dec. 1996.
- [15] S.H. Penzin, W.R. Crain, K.B. Crawford, S.J. Hansel, and R. Koga, "The SEU in pulse width modulation controllers with soft start and shutdown circuits," Proc. IEEE Radiation Effects Data Workshop, 1997, pp. 73–79.
- [16] P.C. Adell, R.D. Schrimpf, B.K. Choi, W.T. Holman, J.P. Attwood, C.R. Cirba, and K.F. Galloway, "Total-dose and single-event effects in switching DC/DC power converters," IEEE Trans. Nucl. Sci., vol. 49, no. 6, pp. 3217–3221, Dec. 2002.
- [17] G. Guo, D. Shen, S. Shi, Q. Chen, J. Liu, J. Xu, X. Lu, N. Hui, L. Cai, L. Gao, H. Wang, R. Teng, B. Wu, D. Wang, S. Du, and H. Fan, "Irradiation facility and technique to increase LET for SEE testing on tandem accelerator," Radiation and Its Effects on Components and Systems (RADECS), pp. 724 -728, Sept. 2011.
- [18] E. Petersen, "Soft Error Results Analysis and Error Rate Prediction," IEEE NSREC Short Course, 2008.
- [19] V. Pouget, H. Lapuyade, P. Fouillat, D. Lewis, and S. Buchner, "Theoretical investigation of an equivalent laser LET," Microelectronics Reliability, pp. 1513 - 1518, 2001.
- [20] S. Buchner, J. Warner, D. McMorrow, F. Miller, S. Morand, V. Pouget, C. Larue, P. Adell, and G. Allen, "Comparison of single event transients generated at four pulsed-laser test facilities - NRL, IMS, EADS, JPL," Radiation and Its Effects on Components and Systems (RADECS), pp. 430 - 433, Sept. 2011.

## **7. SINGLE-EVENT TRANSIENT MEASUREMENTS ON A DC/DC PULSE WIDTH MODULATOR USING HEAVY ION, PROTON, AND PULSED LASER**

*Published as:*

Y. Ren, A.-L. He, S.-T. Shi, G. Guo, L. Chen, S.-J. Wen, R. Wong, N. W. van Vonno, and B. L. Bhuvu, "Single-Event Transient Measurements on a DC/DC Pulse Width Modulator Using Heavy Ion, Proton, and Pulsed Laser," *Springer Journal of Electronic Testing: Theory and Applications*, Vol. 30, no. 1, pp. 149-154, Feb., 2014.

In the previous chapters, the applications of pulsed laser and heavy ions in SET evaluation are discussed. The pulsed laser is discussed in more details in terms of different wavelengths and repetition rates, which indicate that the parameters of the pulsed laser should be properly set in order to be used in the SEE evaluation. The correlation between pulsed laser and heavy ion is also presented, which gives the equivalent LETs of pulse laser with different wavelengths. These conclusions will facilitate the future testing. They can also be used to verify the testing results from one method to the other. However, as a crucial SEE evaluation methodology, the proton irradiation is not used to study the SEE response. And its relationship to heavy ion and laser is not studied.

In this manuscript, proton irradiation is adopted to study to SEE response of a DC/DC PWM chip. The data are compared with those from the previous heavy ion and pulsed laser. The SET glitch has the same shape as those of heavy ion and pulsed laser testing. However, its level of cross section is several orders lower than that of heavy ion testing. This difference is explained from the



perspective of different SEE principles between heavy ions and protons. The former is direct ionization while the latter is nuclear reaction. To further quantify their error rates, a physics model is also used to correlate the proton and heavy ion data. The results show that theoretical calculations can precisely match those from experiments. This relationship also gives hints on SER calculation between heavy ions and protons.

# **Single-Event Transient Measurements on a DC/DC Pulse Width Modulator Using Heavy Ion, Proton, and Pulsed Laser**

Y. Ren, A.-L. He, S.-T. Shi, G. Guo, L. Chen, S.-J. Wen, R. Wong, N. W. van Vonno,  
B. L. Bhuva

## **Abstract**

This paper discusses multiple methods of Single-Event Transient (SET) measurements on a commercial DC/DC Pulse Width Modulator (PWM). Heavy ion, proton, and pulsed laser are used in the experiments. The correlations between the heavy ion, pulsed laser and proton data are analyzed and presented. A proton cross-section model is used to derive proton cross-section from heavy ion test data. The calculated result is close to the real proton data, which means the heavy ion and proton data fit well. The relationship between pulsed laser and proton are also analyzed through heavy ion as a medium.

## **Index terms**

single-event transient (SET), heavy ion, proton, pulsed laser, DC/DC pulse width modulator (PWM).

## **7.1 Introduction**

Single-event transients (SETs) have always been a main source of soft errors in electronic devices [1-2]. It is the interaction between particles and atoms in the material (usually silicon)

when particles penetrate the sensitive regions of a device, such as the reversed biased p-n junction. To be more specific, the energized particle ionizes the material atom and generates electron-hole pairs, which are collected by the electric field in the p-n junction. This causes current and voltage perturbations in electronic devices, which propagate through the circuitry and hinder the system function, or even lead to system failures. As a result, it is necessary to fully study the SET sensitivity of electronic devices.

Heavy ion and proton are frequently used in SET evaluations. However, the basic SET mechanisms caused by them are quite different. SET by heavy ion is caused by direct ionization from incident particles, whereas SET by proton is due to both direct and indirect ionizations [3]. High-energy proton interacts with the silicon nucleus to generate secondary particles. These secondary particles generate charge tracks through direct ionization. Low-energy protons are known to generate carriers in semiconductor material through direct ionization also [4]. The probability of nuclear reactions for high-energy protons is quite small. As a result, probability of an SET generation for heavy ions and low-energy protons are orders of magnitude higher than that for high-energy protons. Since space environment contains all of these particles, it is important to evaluate SET performance of all space-bound electronic circuits for heavy ions and protons.

The pulsed-laser technique has also been widely used as a complementary tool for SET investigations ever since 1990s [5-6]. It features well-controlled temporal and spatial information. When the absorbed photon energy is larger than the bandgap energy of the semiconductor material, it will ionize the material atom and generate electron-hole pairs.

Previously, we have studied a radiation sensitive DC/DC pulse width modulator using heavy ion and pulsed laser technique [7-8]. The DC/DC PWM is observed to malfunction on

ground level application. To be more specific, negative 6- $\mu$ s glitches are observed at Power Good (PGOOD) pin, which resets the system the DC/DC PWM resides in. The laser evaluation indicates that the most sensitive area is a bipolar input pair ( $\Delta V_{be}$  generator) in a bandgap sub-circuit. Also, the correlation between heavy ion and pulsed laser results are developed.

This work extends the SET evaluations of the DC/DC converter IC by providing the proton exposure results. These results are compared with and correlated to the previous heavy ion and pulsed laser data.

## **7.2 Experimental Details**

### ***7.2.1 DUT and Setups***

The DC/DC converter IC is fabricated in 600-nm Bi-CMOS technology. The nominal power supply for the test IC is 12 V and it is capable of providing DC voltages from 0.6 V to 6 V. During the test, the nominal values of the three output voltages are 1.2V, 3.3 V and 2.5 V, respectively. The nominal PGOOD voltage is 5.8 V. The currents output for the whole chip is around 240 mA in our test configuration, which is also monitored using a digital multi-meter.

The general block diagram for the heavy ion test is shown in Fig. 7.1. A Spartan-3 series FPGA from Xilinx is pre-programmed to record the SET pulses (6- $\mu$ s glitches) and its duration from the PGOOD pin. The FPGA features a 50 MHz crystal oscillator on-board, which has enough frequency margins to monitor the 6- $\mu$ s glitch in our test. The data are sent to the laptop in the radiation room through an RS-232 cable. Due to the limited transmission distance of RS-232 and the purpose of better fidelity, another laptop in control room is used to control all the equipment in radiation room by means of a CAT-5 cable. The proton and pulsed laser testing

setups are similar to that of heavy ion with the only difference being they are performed in the air rather than the vacuum chamber.

### 7.2.2 Irradiation Facilities

The heavy ion irradiation is carried out using HI-13 tandem electrostatic Van de Graaff accelerator at China Institute of Atomic Energy (CIAE) in Beijing [9]. This broad beam facility is designed for single-event effect study, especially for ground level simulation.

The pulsed laser testing is performed at the Saskatchewan Structural Sciences Centre (SSSC). Zeiss LSM410 confocal microscope is used along with a Ti:Sapphire laser [7]. It gives a tunable wavelengths ranging from 700 nm to 1000 nm with a repetition range from 10 KHz to 4.75 Mhz.

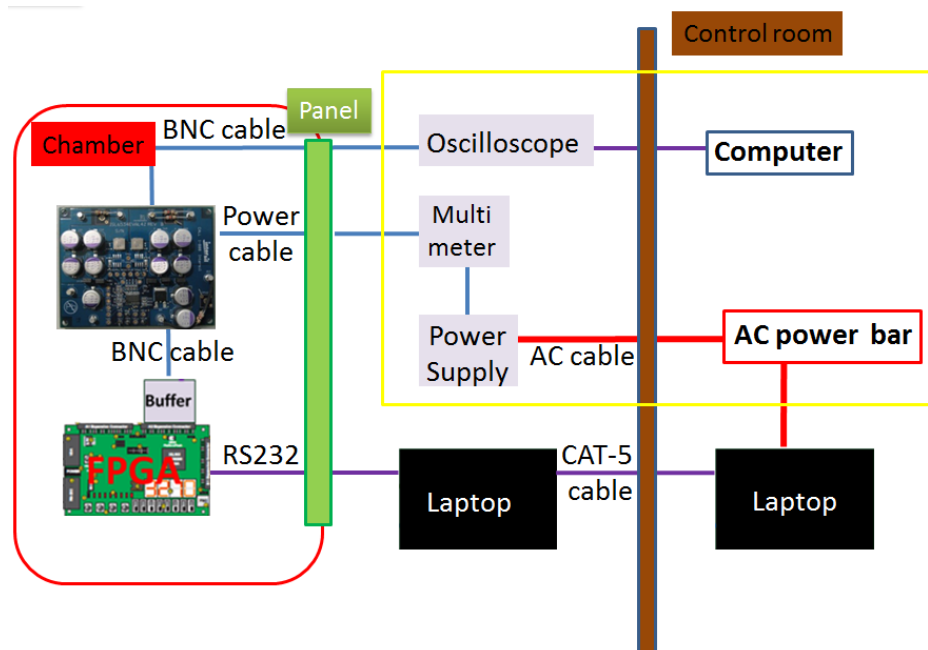


**Figure 7.1** Block diagram for the heavy ion test.

The proton irradiation is performed using the Proton Irradiation Facility (PIF) at TRIUMF, Vancouver, Canada. TRIUMF proton beam from a cyclotron yields protons from 65 to 500 MeV energies [10]. A range shifter is used as a degrader to decrease the initial proton energy to desired levels. One side effect of the degrader is that the distribution of proton energies becomes wider. The proton flux from  $10^5$  particles  $\text{cm}^{-2}\text{s}^{-1}$  to  $10^8$  particles  $\text{cm}^{-2}\text{s}^{-1}$  was used during testing. The beam spot size diameter is from 1 cm to 7.5 cm.

### 7.3 Experimental Data

As the secondary ion LET created by neutrons in terrestrial application environment is usually limited to no more than 15 MeV-cm<sup>2</sup>/mg [11], ion particles with five different LET values, which range from 0.44 MeV cm<sup>2</sup>/mg to 13.6 MeV cm<sup>2</sup>/mg (Table 7.1), are initially used in our heavy ion test. The results show that these LET values properly characterized the cross-section curve of the DC/DC chip. The SET pulses on PGOOD output are monitored using the programmed FPGA board to record the SET error information. We put down the fluence when the SET errors reached around 100. Table 7.2 shows the number of SET pulses observed

**Table 7.1 Heavy ions in the experiment**

Heavy Ion	Energy (MeV)	Range in Si ( $\mu\text{m}$ )	LET (MeV cm <sup>2</sup> /mg)
Li	45	259.6	0.44
C	78	122.2	1.77
F	100	72.7	4.43
Si	120	43.9	9.82
Cl	145	41.2	13.6

**Table 7.2 Heavy ions test data**

LET (MeV cm <sup>2</sup> /mg)	SET	Fluence (#/cm <sup>2</sup> )	Cross-section (cm <sup>2</sup> )
0.44	102	9.9×10 <sup>5</sup>	1.03×10 <sup>-4</sup>
1.77	123	2.6×10 <sup>5</sup>	4.73×10 <sup>-4</sup>
4.43	102	8.5×10 <sup>4</sup>	1.2×10 <sup>-3</sup>
9.82	100	7.7×10 <sup>4</sup>	1.3×10 <sup>-3</sup>
13.6	122	9.0×10 <sup>4</sup>	1.36×10 <sup>-3</sup>

along with the particle fluence and the resulting cross-section for heavy ion exposures. As expected, the cross-section of the circuit increases with an increase in the particle LET values and tends to reach the plateau in the end.

In the laser testing, multiple wavelengths (750 nm, 800 nm, 850nm and 920 nm) are selected as the laser penetration depth (absorption coefficient) differs with wavelength. Cross-section curves similar to that of heavy ion are acquired as is in [8]. The only difference for the four wavelengths is the threshold energy. As a result, only the data for 920 nm is selected in this paper to compare with the proton data. The calibrated cross-section for 920 nm laser is shown in Fig. 7.2.

The experiment results of the proton test are shown in Table 7.3. As relatively less SET errors are expected in the proton test, we record the fluence once the SET errors reached around 50. Considering the terrestrial application environment of this chip, a primary energy of 65 MeV is used in our irradiation test. Range shifter is used to change the proton energy. The proton energy in Table 7.3 is the value after degrading. It must be noted that the use of degrader spread the distribution of proton energies. Two types of beam currents, namely 1 nA and 5 nA, are used.

**Table 7.3 Proton test data**

Current (nA)	Energy (MeV)	SET	Fluence (#/cm <sup>2</sup> )	Cross-section (cm <sup>2</sup> )
1	57.6	58	$5.8 \times 10^9$	$9.99 \times 10^{-9}$
1	48.8	53	$6.64 \times 10^9$	$7.98 \times 10^{-9}$
1	35.5	51	$7.42 \times 10^9$	$6.87 \times 10^{-9}$
1	27.1	49	$7.68 \times 10^9$	$6.38 \times 10^{-9}$
1	20.7	38	$8.08 \times 10^9$	$4.7 \times 10^{-9}$
1	13.7	15	$9.13 \times 10^9$	$1.64 \times 10^{-9}$
5	9.0	9	$1.62 \times 10^{10}$	$5.57 \times 10^{-10}$
5	4.8	4	$0.582 \times 10^{10}$	$6.87 \times 10^{-10}$
5	3.9	0	$4.17 \times 10^{10}$	0

We increased the current for the low energy test to increase the particle flux. The proton cross-sections are generally several orders of magnitudes below heavy ion and pulsed laser data as they mainly reflect the possibility of elastic reaction between proton and silicon atom rather than the real sensitive areas of the device. This is the mechanism especially for energy higher than 20 MeV.

#### **7.4 Analyses and Discussions**

Previous research has correlated the heavy ion and pulsed laser. Now, it will be very interesting to compare the proton data to those of heavy ion and pulsed laser.



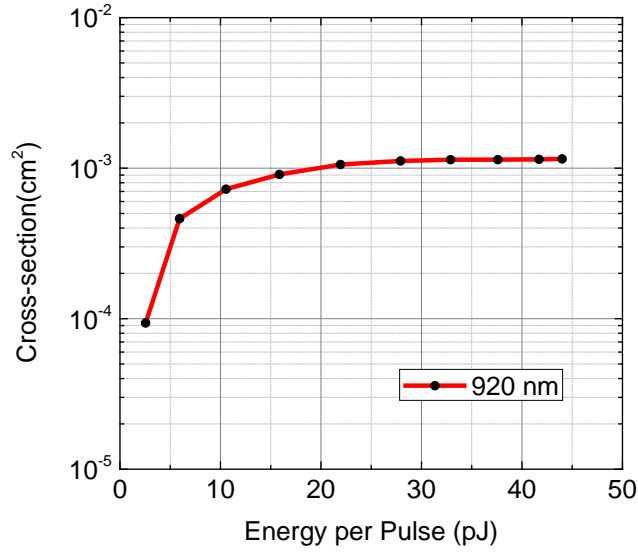
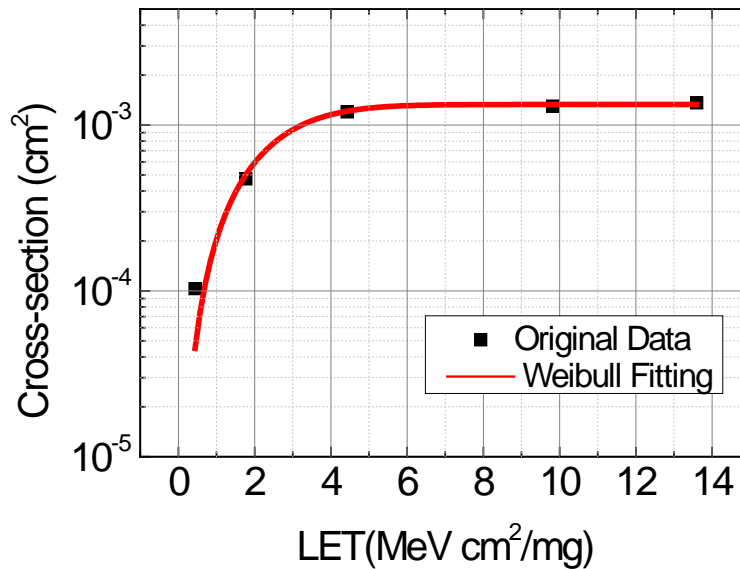


**Figure 7.2** Calibrated energy vs. cross-section for 920 nm laser.

#### 7.4.1 Heavy Ion vs. Proton Data

Fig. 7.3 presents the total SET cross-section as a function of heavy ion LET values for the DC/DC PWM IC. The stopping range of the particles we used here are all more than 40  $\mu\text{m}$  while the sensitive volume depth of the DUT is under 1  $\mu\text{m}$ . In this case, the LET variation along with the penetration depth in silicon is ignorable. The black dots are the original data while the red curve is after Weibull Fitting. The heavy ion cross-section  $\sigma_{HI}(L)$  given by Weibull Fitting Function is usually as:

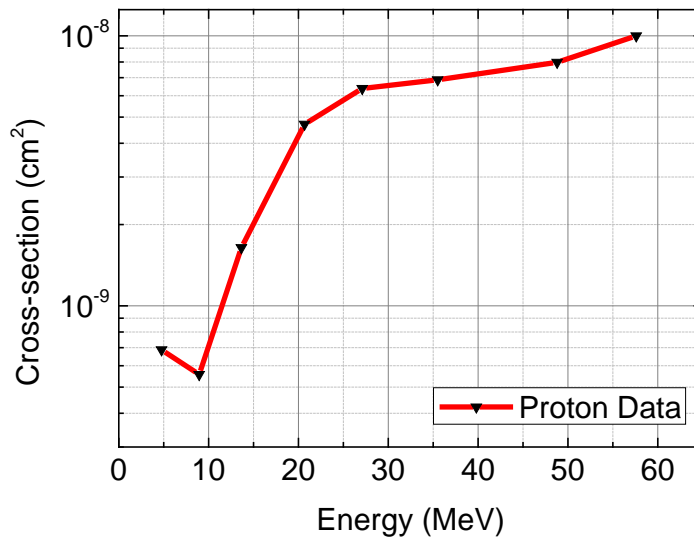
$$\sigma_{HI}(L) = \begin{cases} \sigma_{HI-Sat} \{1 - \exp[-(L - L_{th})/W]^s\}, & L \in [L_{th}, +\infty) \\ 0, & L \in (-\infty, L_{th}) \end{cases} \quad (7.1)$$



**Figure 7.3** LET vs. cross-section for heavy ion.

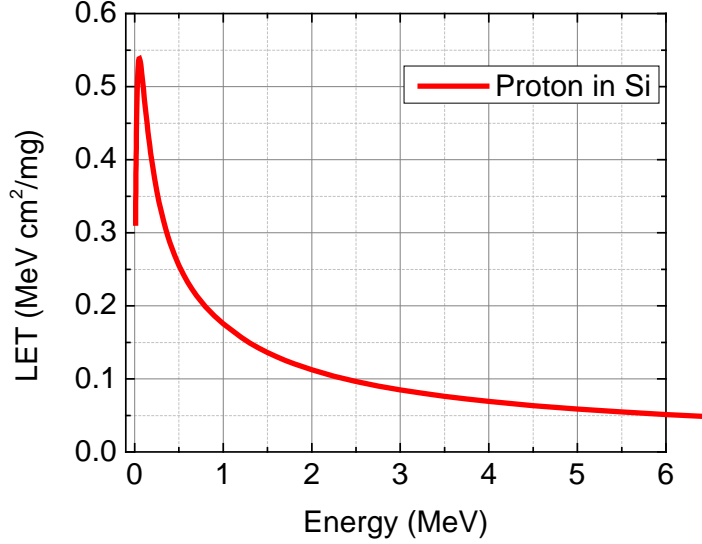
Where  $\sigma_{HI-Sat}$  is the saturation cross-section value of the device,  $L_{th}$  is the threshold LET value to trigger an SET, and W and S are the width parameter and the dimensionless exponent, respectively. The saturated cross-section for this circuit is reached around an LET value of 5 MeV-cm<sup>2</sup>/mg. When the LET value is larger than 5 MeV-cm<sup>2</sup>/mg, saturation cross-section is reached at around  $1.3 \times 10^{-3}$  cm<sup>2</sup>.

Fig. 7.4 gives the general SET cross-section as a function of proton energy (the degraded energy using range shifter). The smallest and biggest cross-sections are seen at 9 MeV and 57.6 MeV, respectively. The saturated cross-section from proton irradiation is  $1 \times 10^{-8}$  cm<sup>2</sup> which is five orders of magnitude lower than that of heavy ion. This is expected as the probability of a secondary reaction between proton and silicon nucleus is very small, whereas each and every heavy ion will cause direct ionization to generate a charge track. The curve shows the same tendency as that of heavy ion for proton energy larger than 9 MeV. One interesting thing is, as



**Figure 7.4** Proton energy vs. cross-section for proton.

the energy decreases from 9 MeV to 4.8 MeV, an increase in the cross-section is observed. However, no error is recorded at an even lower energy of 3 MeV. Considering the small error numbers at 4.8 MeV and 3 MeV, which are 4 and 0 respectively, the inconsistency can be the statistical error. Also from the equivalent LET vs. proton energy curve (Fig. 7.5) which was obtained by using the SRIM [12], it is seen that the LET values for proton energy of 9 MeV, 4.8 MeV and 3 MeV are close to each other. As a result, the increase in the cross-section is unlikely because of the proton direct ionization. However, further proton evaluation needs to be performed between 1 MeV and 3 MeV to confirm and explain this phenomenon.



**Figure 7.5** Proton LET vs. energy in silicon.

In spite of the different mechanisms, there is relationship between the heavy ion and proton induced soft error rates. Previous studies have presented all kinds of models to calculate and correlate heavy ion and proton error rates [13 - 17]. As our DUT is based on an large feature size (600 nm), we simply chose a classic Rectangular Parallel Piped (RPP) (shown in Fig. 7.6) model to validate our data by estimating proton cross-section values from heavy ion data. As most models differ mainly by their cross-section at low proton energy [13], it is more meaningful to correlate the saturation cross-section values of heavy ion and proton. The model used here assumes that the sensitive volume of a transistor is equivalent to a rectangle with thickness  $d$ . In this case, the probability ( $p$ ) for proton to have a nuclear reaction is

$$p = 1 - \exp(-n \times \sigma_{Si} \times d) \quad (7.2)$$



**Figure 7.6** Rectangular Parallelepiped (RPP) model for proton.

Where  $n$  is the number of silicon atoms per unit volume ( $5 \times 10^{22} \text{ cm}^{-3}$ ) and  $\sigma_{Si}$  is the cross-section of proton having elastic interactions with silicon. If the proton fluence for a unit area is  $\Phi/\text{cm}^2$ , ( $p \cdot \Phi$ ) number of protons will cause nuclear reactions. If  $\varepsilon$  indicates the ratio of interactions with deposited energy higher than the threshold energy over all interactions, the number of SET observed,  $N$ , is given by

$$N = p \times \Phi \times \varepsilon = \Phi \times \varepsilon \times [1 - \exp(-n \times \sigma_{Si} \times d)] \quad (7.3)$$

As a result, the proton cross-section will be

$$\sigma_p = N/\Phi = \varepsilon \times [1 - \exp(-n \times \sigma_{Si} \times d)] \quad (7.4)$$

Normally,  $n \times \sigma_{Si} \times d \ll 1$ , so

$$\sigma_p = n \times \sigma_{Si} \times d \times \varepsilon \quad (7.5)$$

Since  $\varepsilon$  has the similar meaning as heavy ion cross-section  $\sigma_{HI}$ , therefore we can calculate the proton cross-section by replacing  $\varepsilon$  with  $\sigma_{HI}(L)$ . Using (7.1), proton cross-section is given by

$$\sigma_p = n \times \sigma_{Si} \times d \times \sigma_{HI-sat} \{1 - \exp[-(L - L_{th})/W]^s\} \quad (7.6)$$

Using this model, the proton saturated cross-section is calculated using heavy ion data. The calculations indicate that proton cross-section should be approximately  $0.78 \times 10^{-8} \text{ cm}^2$ . The experiment proton saturation cross-section is  $1 \times 10^{-8} \text{ cm}^2$ . These results agree well within the experimental errors, proving the validity of the model and the experiment data. Such a model will allow designers to estimate the proton as well as heavy ion SET vulnerabilities with just one set of heavy ion data.

#### **7.4.2 Pulsed Laser vs. Proton Data**

Previously, the heavy ion and pulsed laser data were correlated to each other by means of comparing the threshold energy and LET [8]. In that way, the equivalent LETs for energy per pulse for different wavelengths are developed. However, it is not easy to correlate the proton energy to the laser energy in the same method as proton induced SET has different mechanisms at high and low energy periods (indirect and direct ionizations).

On the other hand, pulsed laser has the ability to develop similar cross-sections to that of heavy ion according to previous research [8], which means the saturated cross-sections for laser

and proton has the similar relationship as that between heavy ion and proton mentioned before. This relationship makes it straightforward to estimate the proton saturated cross-section from laser data as laser testing is relatively time and cost efficient compared with proton testing.

## **7.5 Conclusions**

In this chapter, the SET sensitivity of a DC/DC converter IC is evaluated using heavy ion, proton and pulsed laser. As expected, the measured cross-sections for heavy ion and pulsed laser are orders of magnitude higher than that for high-energy protons. A model correlating heavy ion data with proton cross-section is evaluated to show a very good match with experimental data. The correlation of saturated cross-sections for pulsed laser and proton can be acquired through the heavy ion data as a medium. These set of data will allow designers to understand the SET vulnerability of DC/DC converter circuits for space applications.

The very low LET threshold as well as high cross-section of the DC/DC PWM circuit presents a challenge for the designers for space and ground applications. Since stable DC power supplies are absolutely necessary for proper system-level operations, care must be taken to ensure that DC/DC converter circuits are properly evaluated and hardened for space environments.

## **References**

- [1] S. Buchner and D. McMorrow, "Single-event transients in bipolarlinear integrated circuits," *IEEE Trans. Nucl. Sci.*, vol. 53, pp. 3079–3102, Dec. 2006.
- [2] C. Poivey, J. Barth, J. McCabe, and K. Label, "A space weather event on the microwave anisotropy probe," in *Proc. RADECS Conf.*, Padova, Italy, Sep. 19–20, 2002, pp. 43–46.
- [3] E. L. Peterson, "Effects of Terrestrial Radiation on Integrated Circuits," *IEEE Trans. Nucl. Sci.*, vol. 43, no. 2, pp. 496 - 504, Apr. 1996.

- [4] E. H. Cannon, M. Cabanas-Holmen, J. Wert, T. Amort, R. Brees, J. Koehn, B. Meaker, and E. Normand, "Heavy Ion, High-Energy, and Low-Energy Proton SEE Sensitivity of 90-nm RHBD SRAMs," *IEEE Trans. Nucl. Sci.*, vol. 57, pp. 3493-3499, Dec. 2010.
- [5] S. Buchner, D. McMorrow, C. Poivey, J. Howard, Y. Boulghassoul, L. W. Massengill, R. Pease, and M. Savage, "Comparison of single-event transients induced in an operational amplifier (LM124) by pulsed laser light and a broad beam of heavy ions," *IEEE Trans. Nucl. Sci.*, vol. 51, pp. 2776-2781, Dec. 2004.
- [6] J. S. Melinger, S. Buchner, D. McMorrow, W. J. Stapor, T. R. Weatherford, and A. B. Campbell, "Critical evaluation of the pulsed laser method for single event effects testing and fundamental studies," *IEEE Trans. Nucl. Sci.*, vol. 41, pp. 2574-2584, Dec. 1994.
- [7] Yi. Ren, L. Fan, L. Chen, S.-J. Wen, R. Wong, N. W. van Vonno, A. F. Witulski, and B. L. Bhuva, "Single-Event Effects Analysis of a Pulse Width Modulator IC in a DC/DC Converter," *Springer Journal of Electronic Testing: Theory and Applications*, vol. 28, no. 6, pp. 877-883, Dec. 2012.
- [8] Y. Ren, S.-T. Shi, L. Chen, H.-B. Wang, L.-J. Gao, G. Guo, S.-J. Wen, R. Wong, and N. W. van Vonno, "Correlation of Heavy-Ion and Laser Testing on a DC/DC PWM Controller," *Springer Journal of Electronic Testing: Theory and Applications*, Vol. 29, no. 2, pp. 609-616, Aug, 2013.
- [9] G. Guo, D. Shen, S. Shi, Q. Chen, J. Liu, J. Xu, X. Lu, N. Hui, L. Cai, L. Gao, H. Wang, R. Teng, B. Wu, D. Wang, S. Du, and H. Fan, "Irradiation facility and technique to increase LET for SEE testing on tandem accelerator," *Radiation and Its Effects on Components and Systems (RADECS)*, pp. 724-728, Sept. 2011.
- [10] E. W. Blackmore, "Operation of the TRIUMF (20-500 MeV) proton irradiation facility," *Radiation Effects Data Workshop, 2000, TRIUMF, Vancouver, BC*.
- [11] R. Baunmann, "Effects of Terrestrial Radiation on Integrated Circuits," in *Handbook of Semiconductor Manufacturing Technology, 2000, CRC Press*.
- [12] J. Ziegler, J. Biersack, and U. Littmark, "The Stopping and Range of Ions in Solids," *New York: Pergamon, 1996*.



- [13]J. Barak, "Simple Calculations of Proton SEU Cross Sections from Heavy Ion Cross Sections," IEEE Trans. Nucl. Sci., vol. 53, no. 6, pp. 3336-3342, Dec. 2006.
- [14]A. Akkerman, J. Barak, and Y. Lifshitz, "Nuclear models for proton induced upsets: A critical comparison," IEEE Trans. Nucl. Sci., vol. 49, no. 3, pp. 1539-1546, Jun. 2002.
- [15]J. Barak, "Analytical microdosimetry model for proton-induced SEU in modern devices," IEEE Trans. Nucl. Sci., vol. 48, no. 6, pp. 1937-1945, Dec. 2001.
- [16]J. Barak, "Empirical modeling of proton induced SEU rates," IEEE Trans. Nucl. Sci., vol. 47, no. 3, pp. 545-550, Jun. 2000.
- [17]V. V. Miroshkin, and M. G. Tverskoy, "Two parameter model for predicting SEU rate," IEEE Trans. Nucl. Sci., vol. 41, no. 6, pp. 2085 -2092, Dec. 1994.

## **8. SINGLE-EVENT TRANSIENT MEASUREMENT ON A DC/DC PWM CONTROLLER USING PULSED X-RAY TECHNIQUE**

*Published as:*

Y. Ren, S.-T. Shi, L. Chen, R.-F. Feng, G. Guo, S.-J. Wen, R. Wong, N. W. van Vonno, and B. L. Bhuvu, “Single-Event Transient Measurement on a DC/DC PWM Controller Using Pulsed X-ray,” *Journal of Microelectronics and Solid State Electronics*, vol. 3, no. 1A, pp. 30-35, 2014.

In the previous chapter, three main stream SEE evaluation methods are used to study the SEE response of a DC/DC PWM chip. The pulsed laser technique features well-controlled spatial and temporal precision while proton and heavy ion give more accurate nuclear irradiation responses. These methods dominate the SEE study field nowadays. However, these methods have limitations, respectively. For example, the pulsed laser is unable to penetrate metal layers on top of the die, which makes it difficult to study the devices under metal layers. While for proton and heavy ion testing, it is not easy to identify the exact irradiation spots.

Recently, the pulsed X-ray begins to find its applications in SEE testing. It features metal penetration ability as well as precise spatial and temporal information. In this manuscript, the potential application of X-ray on the SEE testing of silicon-based devices is presented. Its advantages, such as much smaller resolution and metal penetration ability, are elaborated. The possible side effects of this technique are also discussed. These disadvantages include low absorption coefficient in material and total ionizing dose (TID) effect. The pulsed X-ray testing results are also compared with those of pulsed laser and heavy ion testing. The comparison

indicates that the pulsed X-ray technique has equivalent ability with pulsed laser and heavy ion in terms of generating SEE. In addition, it can also detect the sensitive devices underneath metal layers, which is a significant benefit over the pulsed laser technique. However, some different phenomena are also observed, which are not observed in the previous pulsed laser and heavy ion experiments. This difference in irradiation response is believed to be the results of some side effects from X-ray irradiation. To sum up, pulsed X-ray technique can be a good complementary tool to study SEEs, who possesses several obvious advantages over other counterparts. Yet some side effects need to be dealt with in the future study.

# **SINGLE-EVENT TRANSIENT MEASUREMENT ON A DC/DC PWM CONTROLLER USING PULSED X-RAY TECHNIQUE**

Y. Ren, L. Chen, S.-T. Shi, G. Guo, R.-F. Feng, S.-J. Wen, R. Wong, N. W. van Vonno, and B.

L. Bhuva

## **Abstract**

Pulsed X-rays were used to perform Single-Event Transient (SET) measurements on a COTS DC/DC PWM controller. The results were consistent with those of the previous heavy ion and pulsed laser tests, which indicates that the pulsed X-ray technique is a complementary tool to investigate SET. However, there are some limitations, such as low energy absorption of X-rays in silicon and total ionizing dose (TID) effects due to the X-ray irradiation, which need to be considered during X-ray applications.

## **Index terms**

Pulsed X-ray Technique, Single-Event Transient, Pulse-Width Modulator (PWM), DC/DC Converter, Pulsed Laser, Heavy Ion.

## **8.1 Introduction**

Currently, multiple testing techniques have been developed to perform Single-Event Transient (SET) investigation on electronic devices, such as heavy ion and pulsed laser techniques [1-3]. However, they both have some limitations. Heavy ion irradiation cannot provide precise time and physical location information of the ion hit, while the spot size of the pulsed laser is limited by its wavelength. A previous study showed that a picosecond pulsed

X-ray technique, which features metal penetration and sub-micrometer resolution, can induce SET in GaAs/GaN High Electron Mobility Transistors (HEMTs) [4]. This result suggests a potential application of pulsed X-rays in SET investigation in modern electronic devices. In addition, the pulsed X-ray technique has a potential to achieve much better spatial resolution (less than 50 nm) for generating a more precise sensitivity map for circuits. However, it is still not clear whether pulsed X-rays can induce SET pulses that are big enough to affect the system function in silicon based CMOS technology. In this paper, a commercial-off-the-shelf (COTS) DC/DC PWM controller based on 600 nm BiCMOS silicon technology was used to investigate the practical application of pulsed X-rays on SET measurement. This DC/DC PWM controller was previously studied using heavy ion and pulsed laser irradiations [5] and was found to have a low threshold Linear Energy Transfer (LET) . In other words, it requires a very low linear energy for the particles to trigger an SET. This makes it an ideal case to perform this study. Comparisons were made between the pulsed X-ray testing results and those from the previous heavy ion and laser experiments.

The DC/DC PWM controller is the key part of the DC/DC converter circuit based on the pulse-width modulation technique shown in Fig. 8.1. The circuit contains a Pulse-Width Modulation (PWM) block, power switching transistors and passive components. The PWM block further contains a PWM controller, a bandgap reference circuit, a soft-start circuit, and an error amplifier. The PWM block generates the signal that controls the duty cycle (designated as  $D$ ) of the power transistor (or percent of time that the power transistor is ON). The converter topology determines the relationship between the DC input and output voltages. For the commonly used buck converter, the relationship is described by [6].

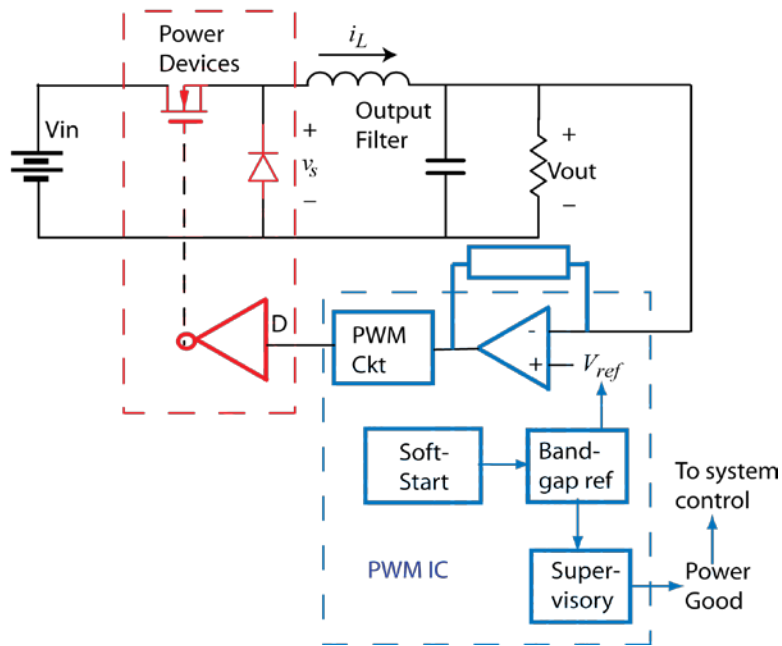


**Figure 8.1** Block level circuit diagram for a DC/DC converter.

$$V_{out} = DV_{in} \quad (8.1)$$

The soft-start circuit limits the load current, shown as  $i_L$  in Fig. 8.1, by means of modulating the duty cycle at the start up. PWM block also generates a “Power Good” signal through a Supervisory circuit (also shown in Fig. 8.1) to monitor the health of the DC/DC PWM controller. The supervisory circuit monitors all other blocks to generate the “Power Good” signal. System-level controllers monitor this “Power Good” signal with the assumption that any transitions represent faulty operation of the DC/DC converter.

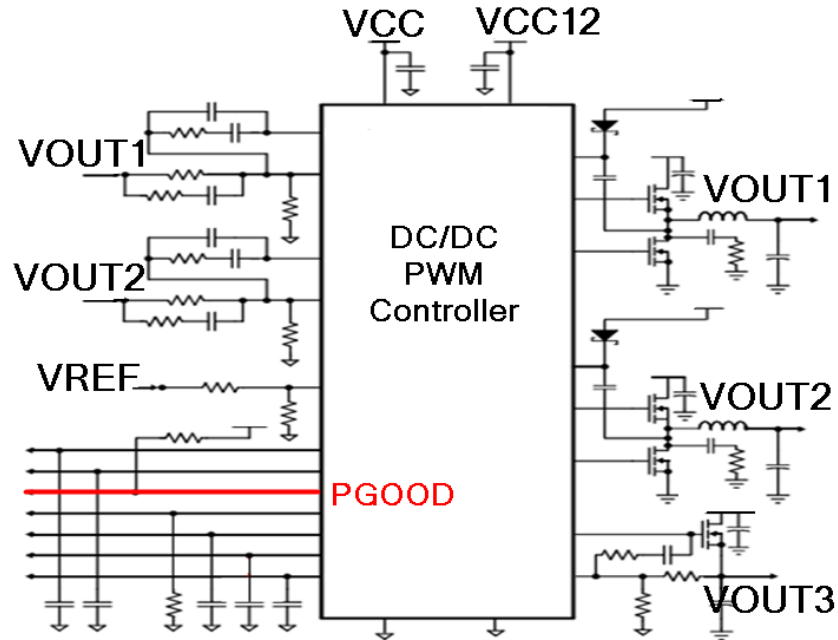


**Figure 8.2** Test circuit for the complete DC/DC PWM controller.

## 8.2 Experimental Details

### 8.2.1 Device under Test (DUT)

The DC/DC PWM controller under study is a triple regulator. It has two independent synchronously-rectified buck controllers and a linear controller to offer precise regulation of up to three voltage rails. The test circuit is shown in Fig. 8.2. Each of the three soft-start pins is connected to a capacitive load. The PGOOD pin is an open-drain pull-down device. When power is first applied to the IC, the PGOOD output is pulled low indicating an initial condition. After all three soft-start pins complete their ramp up with no faults (no shorts detected on the switchers), the power is considered “GOOD” as indicated by a high PGOOD pin. The nominal output voltage for PGOOD is 5.7 V for this DC/DC PWM. Our previous testing [5] showed that a 6- $\mu$ s SET pulse appeared on the PGOOD pin when the chip was irradiated with either heavy ions or

pulsed laser beams. Our further analyze indicated that this is because the irradiation causes SET inside the PWM, which will cut off a NMOS current mirror on its propagation path when it is large enough. In this case, a 6- $\mu$ s pulse is observed on PGOOD pin. On the other hand, if the SET inside the PWM is not large enough to cut off the NMOS current mirror, it will not propagate out and 6- $\mu$ s pulse will not be observed on PGOOD pin. The 6- $\mu$ s constant is the charging constant for a RC delay circuit connected to the current mirror. To sum up, a 6- $\mu$ s pulse is only observed on PGOOD pin when the irradiation-induced SET inside the PWM is larger than a threshold. As a result, the PGOOD pin was used as an indicator in the pulsed X-ray experiments.

### ***8.2.2 Irradiation Facilities***

The pulsed X-ray facility used for this study is the Very Sensitive Elemental and Structural Probe Employing Radiation from a Synchrotron (VESPERS) [7] beam line located at the Canadian Light Source (CLS, Saskatoon, SK, Canada). VESPERS has a hard X-ray microprobe capable of providing high level complementary structural and analytical information. The machine was operated at “single-bunch” mode to produce X-ray pulses with a pulse duration of ~540 ps and dark-gap of 570 ns (i.e., 1.75MHz). The energy of X-ray photons within the pulse ranges from 6 keV to 30 keV. Multi-bandpass and pink beam capabilities are built in to meet variable requirements. The spot size is around (2-4)  $\mu$ m by (2-4)  $\mu$ m. The sample setup for X-ray testing is shown in Fig. 8.3. The test board was screwed to the acrylic sample holder which was placed at 45 degrees with respect to the X-ray beam vertically for better illumination and irradiation. Note that this incident angle can affect the X-ray spot profile and degrade its resolution.



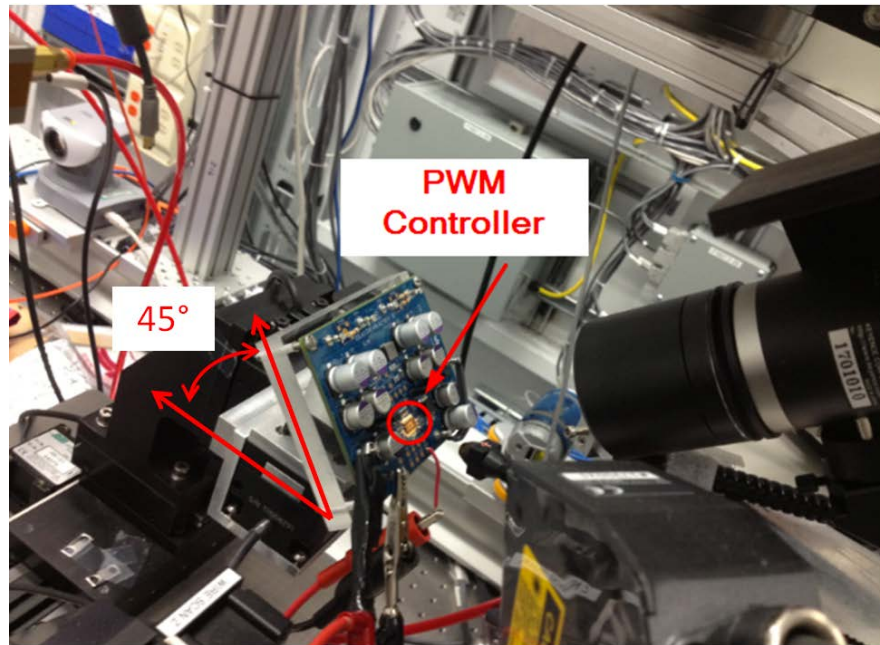


**Figure 8.3** The sample setup in the pulsed X-ray testing.

The heavy ion irradiation was carried out using the HI-13 tandem electrostatic Van de Graaff accelerator at China Institute of Atomic Energy (CIAE) in Beijing [8]. This broad beam facility is designed for single-event effect studies. It is capable of accelerating almost all the elements of the periodic table with a beam non-uniformity of less than 10% over an area of 10 cm × 10 cm. A sample holder capable of holding four 254 mm × 254 mm test boards resides in the vacuum testing chamber whose diameter and height are both 1100 mm. The multiple choices of interfaces on the chamber wall, such as BNC and Sub D-9, facilitate the experiments. The fluence of the particles ranges from  $9 \times 10^4 \text{ cm}^{-2}$  to  $9.9 \times 10^5 \text{ cm}^{-2}$  with a beam size of 2 cm × 2 cm. The heavy ion testing was performed in a vacuum chamber, which is shown in Fig. 8.4. As we can see, a metal frame is fixed onto the motorized plate inside the vacuum chamber. The DUTs are fastened onto the frame using screws. The PWM evaluation board in our testing is circled in red.

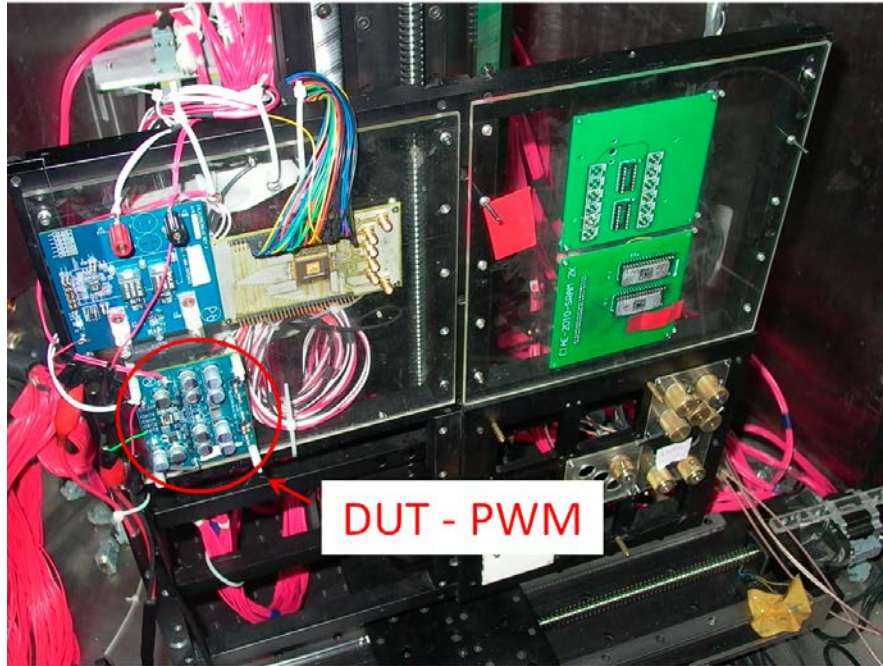


**Figure 8.4** Experimental heavy ion testing setup in the vacuum chamber.

The laser induced SEE testing facility used in this work is located at the Saskatchewan Structural Sciences Centre (SSSC) at the University of Saskatchewan [5]. The basis of the laser scanning system is a Zeiss LSM410 confocal microscope which is located on a floating optical table to reduce mechanical vibration transfer to the instrument. The laser system is a Mira 900-D pumped by a Verdi V-10 (made by Coherent). It has a tunable Ti:Sapphire laser with wavelengths ranging from 700 nm to 1000 nm. The laser system is capable of emitting a continuous wave beam or picosecond and femtosecond pulses. It has a Pulse Picker 9200 which is a stand-alone accessory for the laser system to change the pulse repetition rate over the widest range available. It gives a repetition rate selection from 10 kHz to 75 MHz.

### **8.3 Experimental Results**

In the X-ray experiment, a monochromatic X-ray pulse was applied to some sensitive nodes of the DUT (as determined by the laser scanning experiment [5]). The photon energy was varied from 7 keV to 20 keV. However, no SET (which is defined as a 6- $\mu$ s or greater negative transient on the PGOOD pin) was observed on PGOOD pin of the DUT for these tests. For the next set of experiments, pink (polychromatic) X-ray pulses, which were composed of multiple bands and hence had much higher energy, were used to repeat the same experiments. 6- $\mu$ s SET signatures were observed (Fig. 8.5) on the PGOOD pin only when the X-ray pulse struck the most sensitive region of the circuit. This sensitivity of different regions was determined through laser testing [5]. These results showed that the nine bipolar transistors (used as a delta  $V_{be}$  generator) inside a bandgap sub-circuit was the most sensitive region to single-event effects, as shown in Fig. 8.6.

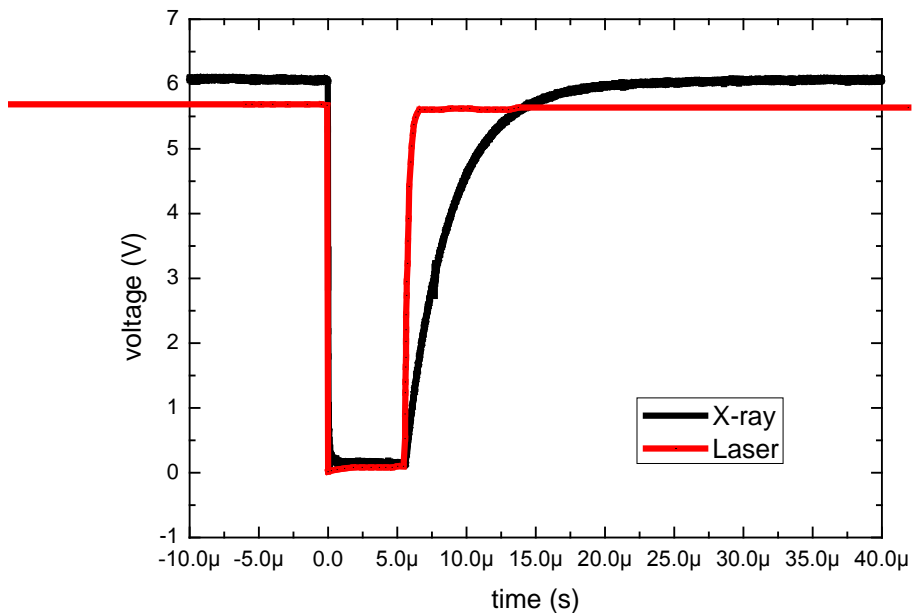


**Figure 8.5** SET induced at PGOOD output by X-ray and laser.

Each one of the nine square blocks is a bipolar junction transistor. During this testing, the X-ray is not only applied to the active area, but also the different layers of metals. The 6- $\mu$ s SET is observed all the time if only the X-ray is within the nine bipolar area. However, after 10 minutes of exposure, the X-ray beam failed to trigger any SET event even with maximum pink X-ray energy. As the experiment went on, it was also observed that the PGOOD output high voltage increased gradually from 5.7 V to 7.4 V. Later on, the PGOOD signal oscillated when X-rays were applied (Fig. 8.7). To be more specific, the PGOOD signature started to oscillate when the X-ray pulse was applied. The time durations of the negative glitches were in the order of several seconds. In addition, after the X-ray irradiation was stopped, the PGOOD went through an oscillation process for about 20 minutes before it was finally stabilized at 7.4V. The time duration of the glitches decreased gradually along with this oscillation until they reached several

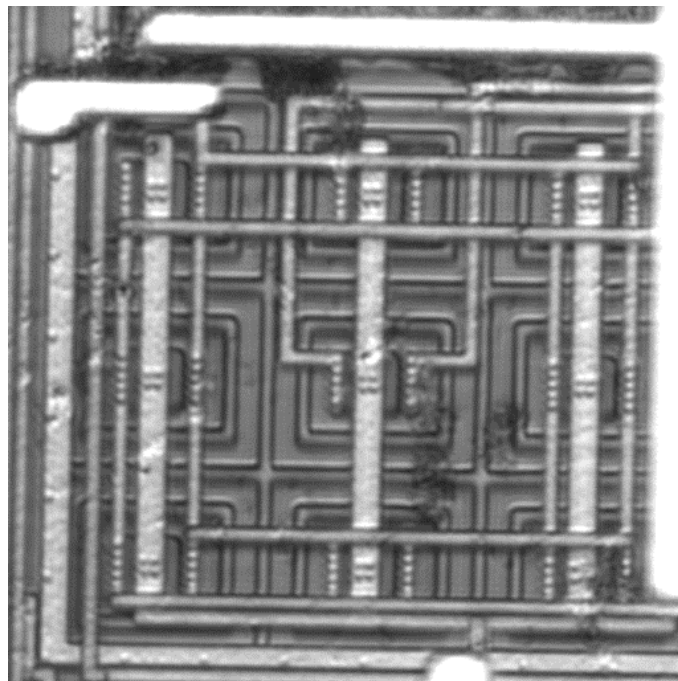


**Figure 8.6** Sensitive areas in the pulsed X-ray testing.

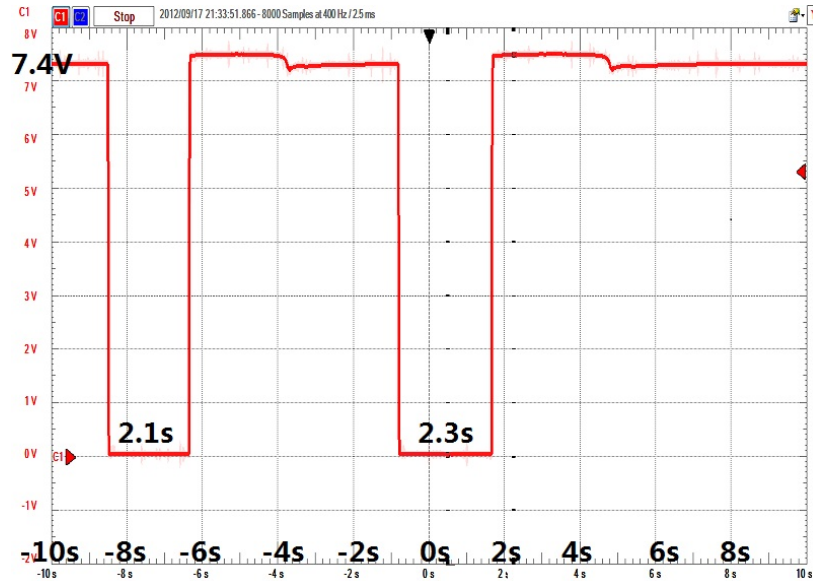


**Figure 8.7** Irregular oscillations at PGOOD pin.

hundred milliseconds. This complex phenomenon was not observed for previous heavy ion and laser experiments. This time-dependent phenomenon is a direct result of total dose effects as discussed below.

The heavy ion (HI) and laser (800 nm) experiment results are shown for reference in Fig. 8.8. The HI cross-section was acquired by divided the SET counts (the number of the 6- $\mu$ s glitch) by the HI fluence. The laser cross-section was acquired based on the same principle by considering each pulse as a particle hit. The cross-section curves both show the conventional Weibull shape. The LET threshold was so low that a significant number of errors were recorded even at an incident LET of 0.44 MeV-cm<sup>2</sup>/mg. The saturation value of cross-section was reached at particle LET of 4.43 MeV-cm<sup>2</sup>/mg.

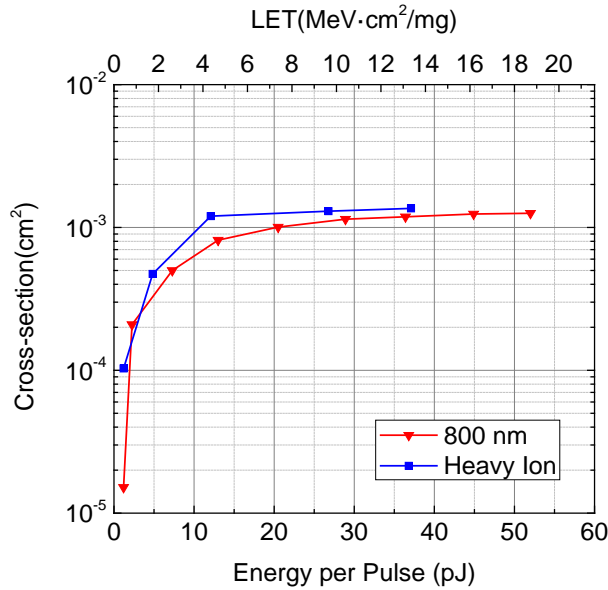


**Figure 8.8** The heavy ion and laser experiment results.

## 8.4 Discussions

From the X-ray experiment results, it is observed that the pulsed X-rays generally have the same ability as the pulsed laser and heavy ion in terms of inducing SET in the DC/DC PWM controller fabricated in 600 nm BiCMOS technology. It is obvious from our experiment that pulsed X-ray technique has its own advantages over both pulsed laser technique and heavy-ions in terms of SET evaluation. For example, when the pulsed laser is applied to the metal layers of the die, no SET will be ever observed because the pulsed laser will be blocked by the metal. It is a different situation for pulsed X-ray who has the capability to penetrate the metal. This advantage is supported by our testing when the pulsed laser is applied to metal layers and the SET appears. The pulsed X-ray is much more convenient in locate the sensitive devices compared with its heavy-ion counterpart. Our experiment clearly showed that the nine bipolar is

most sensitive while it will be harder for heavy-ion testing to get this information. However, there are some aspects that need further study.

First, the X-ray charge deposition level in the sensitive volume is different from that observed for heavy ion and pulsed laser tests. The X-ray photon has higher energy than the pulsed laser photon. However, its absorption is much lower. The X-ray absorption mainly depends on the target material, the sensitive volume thickness and the X-ray energy. For example, the energy absorption of a 30 KeV X-ray photon in 1  $\mu\text{m}$  silicon is around 0.027% [9]. This low absorption coefficient reduces the charge deposition in the sensitive volume of the chip. As a result, it is difficult to generate an effective chip-level SET unless the required critical charge at the specific node is small. In our testing, monochromatic X-rays failed to cause SET in the PWM chip. Our pulsed laser experiments showed that the PGOOD SET threshold laser energy for this DC/DC PWM controller is 1.2 pJ for 800 nm laser wavelength, and heavy ion experiments showed a threshold LET of less than 0.4 MeV-cm<sup>2</sup>/mg. The results imply that samples have to have low threshold LET in order to be suitable for pulsed X-ray study. These results also imply that the pulsed X-ray diagnostic technique is applicable only to low SET threshold commercial devices and is at least for the present of limited utility for investigating formally SET hardened part types. Further experiments are required to correlate the X-ray energy in silicon technologies to other experimental results using pulsed laser and HI irradiation. We are correlating the energy using a diode fabricated in the IBM 130 nm CMOS technology.

Second, total ionizing dose (TID) affects the validity of the SET test results. TID is a potential limitation to SET investigation using the pulsed X-ray technique. In our testing, the laser instead of X-ray fluorescence was used to image the chip, which diminished the X-ray irradiation. However, TID effects were observed during the testing, with the maximum PGOOD

SET voltage level increasing for successive tests, especially when the pink X-ray beam was used. This maximum voltage level increase was found to be non-recoverable even when a power cycle is applied or the DUT was powered off for five days. TID also changed the X-ray pulse threshold energy of the DUT. As a result, even the pink (higher energy) X-ray pulse was unable to induce a 6- $\mu$ s SET after the X-ray irradiation. This is believed to be due to gain degradation of the bipolar transistor devices in the bandgap sub-circuit caused by the X-ray irradiation. The TID effect is more serious in complex analog/mixed signal system as the changes in device parameters along with the complex circuit architecture tend to cause unexpected system responses such as the oscillation we observed in our case.

## **8.5 Conclusions**

This paper compares SET testing results using the pulsed X-ray technique with earlier results using the heavy ion and the pulsed laser. The advantages and limitations of the pulsed X-rays as a practical method for SET investigation were presented and analyzed. The results show that the pulsed X-ray technique is a potential tool to study SEE, especially for devices with low threshold LET. It has its own advantages over both pulsed laser technique and heavy-ions evaluation method. It is easier to locate the sensitive devices with pulsed X-ray than heavy-ions evaluation. Also, it is more accurate than pulsed laser technique in terms of pinpoint the sensitive area due to its capability to penetrate metal layers. For example, the laser will not detect the sensitive area if it is underneath metal layers while pulsed X-ray can make it as well. However, its low effective LET and the effects of TID may present potential problems for general applications. Also, future work including testing of a diode structure will be done to correlate pulsed X-ray results with those obtained earlier for pulsed laser simulation in silicon technology.



The diode has the advantage of simple structure over the DC/DC PWM controller in SET investigations. In other words, the diode can show the initial width and amplitude of the SET while the DC/DC PWM controller is blocking the information due to the components on the SET propagation path. As a result, more insights on X-ray induced SET will be gained in our future study using the diodes.

## References

- [1] D. Lewis, V. Pouget, F. Beaudoin, P. Perdu, H. Lapuyade, P. Fouillat, and A. Touboul, "Backside laser testing of IC's for SET sensitivity evaluation," *IEEE Trans. Nucl. Sci.*, vol. 48, pp. 2193–2201, Dec. 2001.
- [2] R. L. Ladbury, J. Benedetto, D. McMorrow, S. P. Buchner, K. A. LaBel, M. D. Berg, H. S. Kim, A. B. Sanders, M. R. Friendlich, and A. Phan, "TPA laser and heavy-ion SEE testing: complementary techniques for SDRAM single-event evaluation," *IEEE Trans. Nucl. Sci.*, vol. 56, no. 6, pp. 3334-3340, Dec. 2009.
- [3] A. Bougerol, F. Miller, N. Guibbaud, R. Gaillard, F. Moliere, and N. Buard, "Use of Laser to Explain Heavy Ion Induced SEFIs in SDRAMs," *IEEE Trans. Nucl. Sci.*, vol.57, pp. 272-278. Feb. 2010.
- [4] D.M. Cardoza, S.D. LaLumondiere, M.A. Tockstein, S.C. Witczak, Y. Sin, B.J. Foran, W.T. Lotshaw, and S.C. Moss, "Single Event Transients Induced by Picosecond Pulsed X-Ray Absorption in III–V Heterojunction Transistors," *IEEE Trans. Nucl. Sci.*, vol. 59, pp. 2729–2738, Dec. 2012.
- [5] Y. Ren, L. Fan, L. Chen, S.-J. Wen, R. Wong, N. W. van Vonno, A. F. Witulski, and B. L. Bhuva, "Single-Event Effects Analysis of a Pulse Width Modulator IC in a DC/DC Converter," *Springer Journal of Electronic Testing*, vol. 28, No. 6, pp. 877–883, Dec. 2012.
- [6] R.W. Erickson, D. Maksimovic, "Fundamentals of Power Electronics," Second Edition, 2004.

- [7] R. Feng, A. Gerson, G. Ice, R. Reininger, B. Yates, and S. McIntyre, “VESPERS: a beamline for combined XRF and XRD measurements”, AIP Conf. Proc., vol. 879, pp. 872-874, 2007.
- [8] G. Guo, D. Shen, S. Shi, Q. Chen, J. Liu, J. Xu, X. Lu, N. Hui, L. Cai, L. Gao, H. Wang, R. Teng, B. Wu, D. Wang, S. Du, and H. Fan, “Irradiation facility and technique to increase LET for SEE testing on tandem accelerator,” Radiation Effects on Components and Systems (RADECS) Proc., pp. 724 -728, Sept. 2011.
- [9] X-Ray attenuation & absorption calculator,  
[http://web-docs.gsi.de/~stoe\\_exp/web\\_programs/x\\_ray\\_absorption/index.php](http://web-docs.gsi.de/~stoe_exp/web_programs/x_ray_absorption/index.php)

## 9. THE SINGLE-EVENT TRANSIENT STUDY OF A CMOS BGR USING PULSED LASER TECHNIQUE

*Submitted as:*

Y. Ren, and L. Chen, “The Single Event Transient Study of a CMOS BGR Using Pulsed Laser Technique,” *IEEE Transaction of Nuclear Science*, 2014.

In the previous chapter, a commercial-off-the-shelf DC/DC PWM converter chip based on BiCMOS technology was evaluated using multiple irradiation methods, such as heavy ion, proton, pulsed laser and X-ray. And the bandgap reference sub-circuit was determined to be the most vulnerable block to SET. The SPICE simulations and TCAD modeling were also used to verify the conclusions. However, as the CMOS technology becomes increasingly dominant in modern IC design, it is both significant and necessary to study the SET sensitivity of the CMOS bandgap reference circuits.

In this chapter, a bandgap reference circuit similar to the one in the DC/DC PWM chip was redesigned and fabricated in IBM bulk CMOS 130nm technology. The SET sensitivity of different devices was studied using the pulsed laser technique. Unlike the previous study in the BiCMOS DC/DC PWM chip, the PTAT generator transistors (previously mentioned as 3 by 3 areas) are not the most sensitive devices. The reason is determined to be the different bipolar structures in BiCMOS and bulk CMOS technologies. Further analysis is performed to explain the difference between the two technologies. This knowledge also gives hints to radiation hardened by design techniques.

# **The Single Event Transient Study of a CMOS BGR Using Pulsed Laser Technique**

Y. Ren, and L. Chen,

## **Abstract**

This paper investigates the single event transient (SET) response of a bandgap reference (BGR) circuit fabricated in standard CMOS technology using pulsed laser technique. Our experiment shows that CMOS substrate PNP transistors can dramatically decrease SET sensitivity of BGR circuits when being used to generate proportional to absolute temperature (PTAT) current. The mechanisms for this phenomenon are discussed and analyzed. This also gives hints on the radiation hardened by design (RHBD) techniques. For example, the substrate PNP transistor is a preference in BGR circuits design and fabrication, especially when SET is a concern.

## **Index terms**

single-event transient (SET), bandgap reference (BGR), pulsed laser, CMOS, BiCMOS, radiation hardened by design (RHBD), substrate bipolar transistor, current gain.

## **9.1 Introduction**

Single event transients (SETs) have always been a main source of soft errors in modern electronic devices [1-2]. It takes the form of a temporal current or voltage perturbation when energetic particles hit and traverse the sensitive nodes in the circuits. To be specific, the particle ionizes the material and generates electron-hole pairs along its track. These extra carriers cause

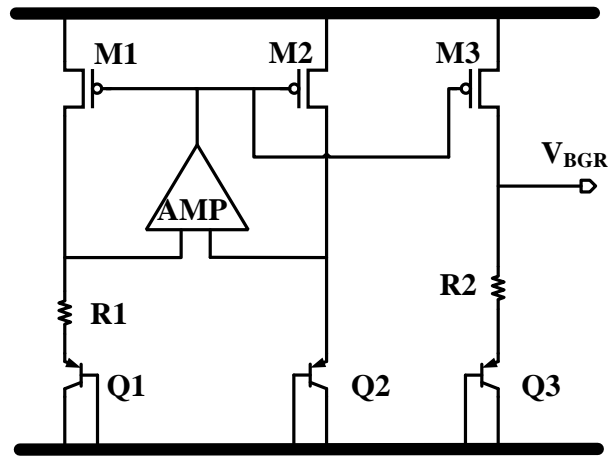
temporary voltage or current variations.

SETs affect the performance or function of many kinds of electronic devices, one important type of which is the BGR circuit [3-4]. The basic function of BGR is to provide a stable voltage reference independent of the voltage and temperature variations. It finds a wide range of applications in modern electronic devices. For example, it can be used to provide a voltage standard for comparator circuits. Also, in an analog-to-digital converter (ADC) system, the accuracy of BGR severely limits the resolution of ADC. As a result, the SET in the BGR is a threat to the whole electronics system.

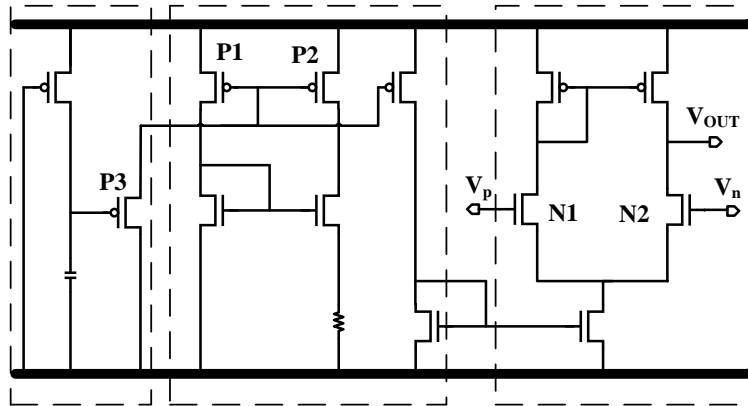
Our previous study indicates that a BGR circuit failure caused by SET seriously affects the function of the DC/DC PWM chip it resides in [4]. In other words, when the energetic particle hits the BGR and SET arises, a subsequent POR circuit receiving voltage reference from BGR is affected and sends fault reset signals to the DC/DC chip. As a result, a voltage glitch will be observed at its PGOOD pin. Our further study indicated that the most sensitive devices were two analog bipolar NPN transistors working as proportional to absolute temperature (PTAT) current generator. Note that this BGR was based on BiCMOS technology.

In this paper, the previous tested BiCMOS BGR circuit is redesigned and fabricated in standard CMOS technology, where the PTAT current generator is realized using CMOS substrate PNP transistors. The CMOS technology has dominated the IC fabrication industry due to its lower power dissipation, larger integration capability, and lower cost compared to its BiCMOS counterpart. As a result, it is both significant and necessary to investigate the SET response of the BGR based on the CMOS process. The CMOS BGR is investigated with pulsed laser technique. However, unlike in the BiCMOS BGR, the PTAT current transistors in the

CMOS BGR are not sensitive to SET any more. In fact, no SET was observed when the laser is applied to them. This phenomenon is mainly because the CMOS substrate PNP transistor has much smaller current gain  $\beta$  than the analog bipolar NPN transistor. A significantly smaller  $\beta$  means a smaller amplification of the base region SET current. As a result, it dramatically suppresses the current and voltage variations at the emitter node. This understanding also finds its applications in RHBD technique, where CMOS substrate PNP



(a)



(b)

**Figure 9.1** (a) The schematic of the BGR circuit; (b) The schematic of the AMP circuit.

transistors can be used as much as possible to mitigate the potential SET effects in the BGR circuit.

## 9.2 Device under Test

The schematic of the CMOS BGR under test is shown in Fig. 9.1(a). Q1, Q2, and R1 generate the PTAT current, which is injected into R2 by means of the current mirror composed of M1, M2, and M3. The output of the BGR circuit is the voltage sum of R2 and VBE3, which is expressed in (9.1)

$$V_{BGR} = V_{BE3} + \frac{R_2}{R_1}(V_{BE2} - V_{BE1}) \quad (9.1)$$

As is known, the base-emitter voltage VBE3 has a negative temperature coefficient (TC). Meanwhile, the voltage difference between VBE2 and VBE1 provides a positive TC. As a result, if the ratio of R1 and R2 is properly set, a temperature independent output voltage can be acquired (VBGR). Note that Q1, Q2, and Q3 are designed by CMOS substrate PNP transistors here while they are realized using analog bipolar NPN transistors in the previously tested BiCMOS BGR circuit [4].

For better presentation of the data in the following sections, the schematic of the amplifier (AMP) is also elaborated in Fig. 9.1(b). As we can see, this AMP is composed of three parts. The first part is a startup circuit. It prevents the circuit from going into zero current state in the power-on process by drawing a small current from P2. When the power supply reaches its designated value, P3 will be turned off. As a result, there is no extra power dissipation. The second part is a current source. It generates a current which is mirrored to bias the subsequent core AMP circuit. The third part is a classic five-transistor AMP circuit.

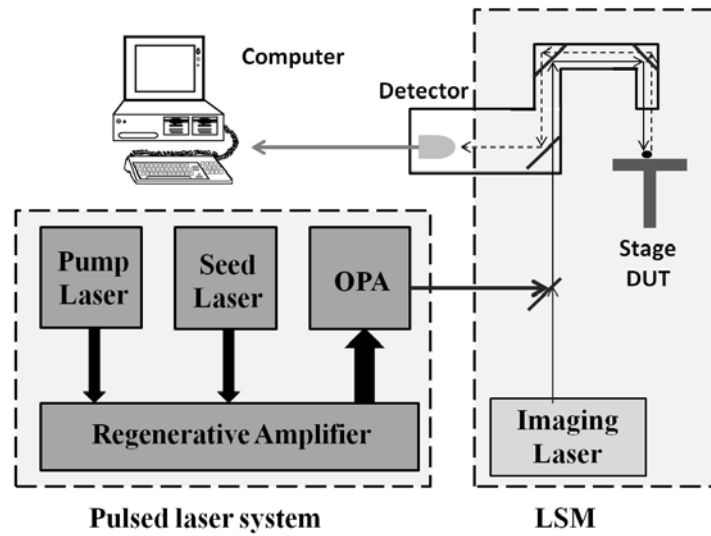


**Figure 9.2** The laser facility setup.

## 9.3 Experimental Details

### 9.3.1 Irradiation Facility

The irradiation facility used here is the pulsed laser system located in SSSC at University of Saskatchewan. It includes a Ti:Sapphire pulsed laser facility and a Laser Scanning Microscope (LSM). The schematic for the laser facility is described in Fig. 9.2.

The pulsed laser system uses a continuous wave (CW) green diode-pumped solid-state (DPSS) laser as the pump laser, which provides 18W output at 532 nm. Its output goes into a regenerative amplifier (RegA) who uses Ti:Sapphire as its gain medium. The RegA can provide a repetition rate from 10 KHz to 300 KHz internally. To achieve an even lower repetition rate for the testing, an external signal generator is connected to its time controller. In fact, 1 KHz is used in our experiments. Note that the RegA is also seeded with a femtosecond pulsed laser. The pulse energy of the seed laser is amplified dramatically by the RegA. After that, it will be injected into



an optical parametric amplifier (OPA) which extends the wavelength coverage. In our experiment, the 800 nm laser is adopted. The final output of the pulsed laser system is merged with imaging laser and sent to the optical path of the LSM as is shown in Fig. 9.2. The imaging laser is applied on the DUT and its reflection photons are collected by a detector and sent to the computer for image processing. The X-Y-Z directions are fully controlled from the computer end with a step size of 0.05  $\mu\text{m}$  for XY and 0.1  $\mu\text{m}$  for Z. During the scanning, the area is divided into 256 by 256 pixels with a dwell time of 5  $\mu\text{s}$  on each pixel. Thanks to the 50X objective, the minimum area can reach to 3.84  $\mu\text{m}$  by 3.84  $\mu\text{m}$ , which gives us decent accuracy in the experiments. An Agilent DSA90404A high speed oscilloscope with 4 GHz bandwidth is used to trigger the SET on the output of the BGR circuit.

### ***9.3.2 Experimental Results***

Normally, SET is characterized by two parameters, which are transient amplitude and duration [5]. Following this idea, the laser beam is applied to each device separately and the BGR circuit output change on the oscilloscope is monitored. Considering the relatively simple structure of the circuit, this testing procedure is feasible. Also, during our circuit design, the exclusive layer was set on the circuit layout. This means no metal filling is allowed inside the area defined by it. In this way, all the devices of interest are exposed and ready to the laser irradiation. The minimum irradiation area for the laser system is 3.84  $\mu\text{m}$  by 3.84  $\mu\text{m}$ . This value is comparable with or smaller than the device dimensions. For example, the dimension for Q2 is 5  $\mu\text{m}$  by 10  $\mu\text{m}$ . This provides us with enough resolution to isolate the effect of each device.

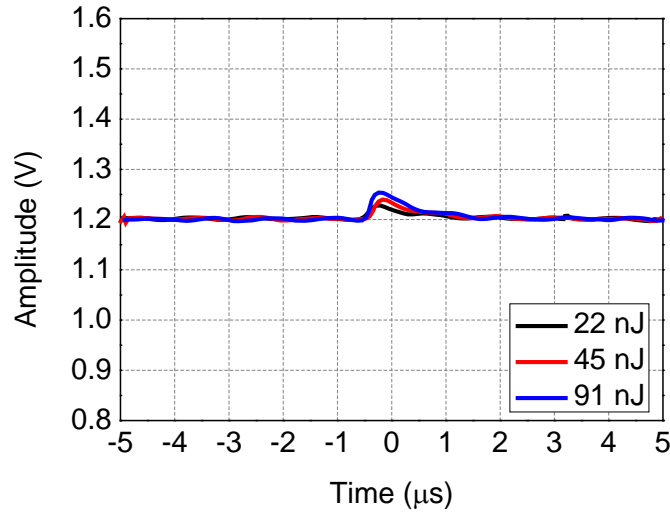


**Figure 9.3** SETs for transistors Q1 (Q2) at laser energies of 22 nJ, 45 nJ and 91 nJ.

As we can see from Fig. 9.3, no measurable SETs were observed when the laser beam was applied to Q1 and Q2 until the laser energy reached around 22 nJ. As the energy went to 91 nJ, the SET amplitude increased to around 50 mV. For N1 (N2) and P1 (P2), a measurable SET can be observed at 0.55 nJ and 2.4 nJ, respectively (Fig. 9.4 and Fig. 9.5). However, N1 (N2) exhibited positive SET while P1 (P2) was negative. When the laser energy increased, the amplitudes for N1 (N2) and P1 (P2) also saw a fast trend compared with Q1 and Q2. To sum up, the CMOS transistors, such as N1 (N2), and P1 (P2) exhibits larger SET response to the laser irradiation. This sensitivity response is different from our previous tested BiCMOS BGR, where Q1 and Q2 were fabricated in bipolar NPN transistors. In our previous testing, Q1 and Q2 were most sensitive to laser irradiations.

## 9.4 Discussions

The experiment data indicates that Q1 and Q2 are the least sensitive transistors in the

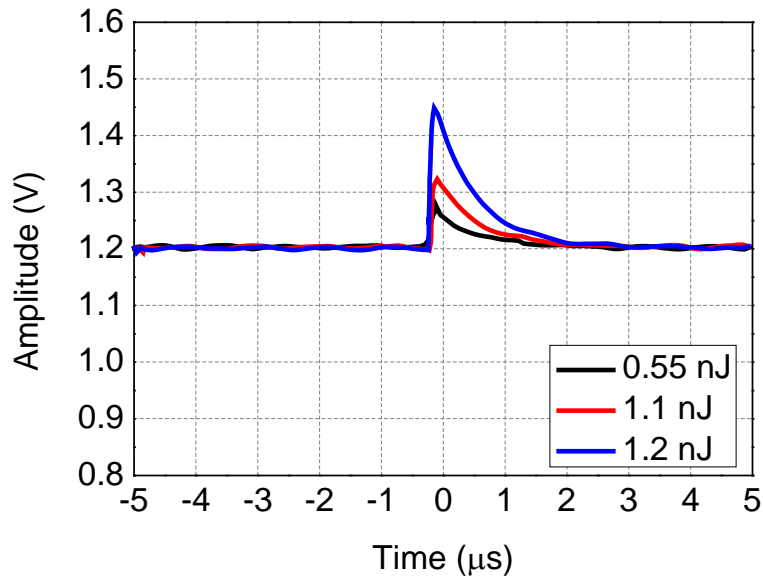


**Figure 9.4** SETs for transistors N1 (N2) at laser energies of 0.55 nJ, 1.1 nJ and 1.2 nJ.

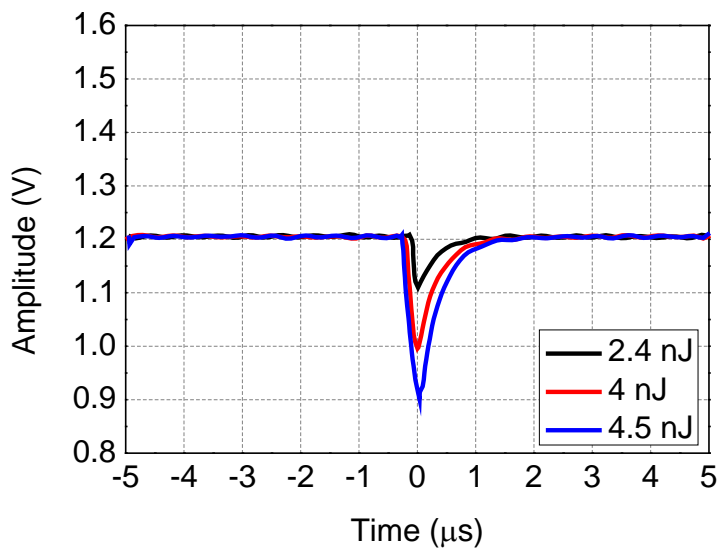


**Figure 9.5** SETs for transistors P1 (P2) at laser energies of 2.4 nJ, 4 nJ and 4.5 nJ.

CMOS BGR. However, they were the most sensitive devices in our previously tested BiCMOS

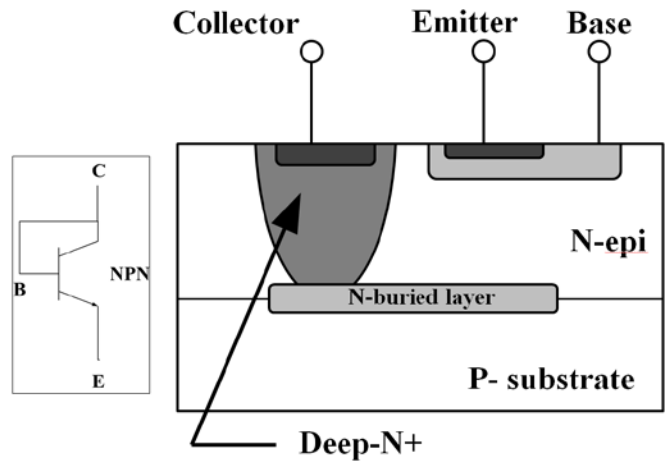


**Figure 9.6** Cross-section for bipolar NPN transistor.

BGR. The two BGR circuits have similar architecture. As a result, the difference is caused by the internal differences between BiCMOS and CMOS bipolar transistors.

Before further discussion, it is necessary to illustrate the SET mechanism in a bipolar transistor. We can elaborate this point based on a typical bipolar NPN. The cross-section and schematic of the device is shown in Fig. 9.6. Note that the vertical scales for all the device cross sections are exaggerated for clarity. When the transistors work as PTAT current generator, the base-collector junction is short while the base-emitter junction is biased in forward active region. In the case of a particle penetration in the base-emitter junction, extra carriers will be deposited. This phenomenon is shown in Fig. 9.7. As the base-emitter junction is forward biased and the base node is connected to relatively high voltage, the electrons quickly escape from the base contact leaving the holes. Some holes will be consumed in base recombination while the rest will be swept from base to emitter by the electric field and recombined there. Generally, during

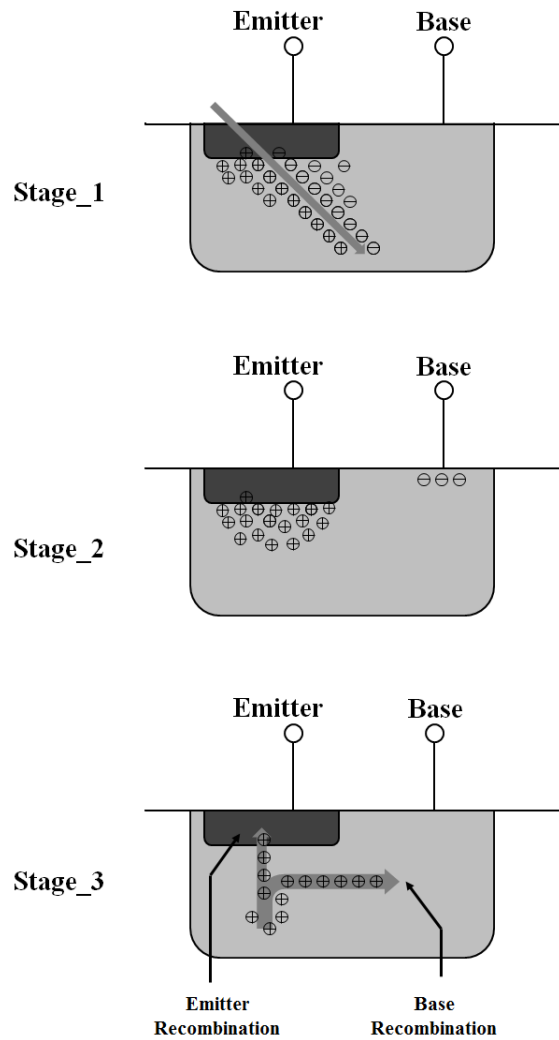


**Figure 9.7** SET process in the base-emitter region of a bipolar NPN transistor.

particle penetration, a temporary current injection happens in the base region. This current will be amplified according to the following equation:

$$I_C = \beta I_B \quad (9.2)$$

Beta ( $\beta$ ) is the current gain of the transistor. As a result, a larger current conduction happens between collector and emitter. And a voltage variation is observed in the circuit.

From the foregoing discussion we can see, beta ( $\beta$ ) plays a critical role in the amplification of SET current in bipolar transistors. In other words, a smaller beta can mitigate the SET glitch to some sense. In fact, the beta of CMOS substrate PNP transistor (5-10) is much smaller than the analog bipolar NPN transistor (200 -1000). The big difference is mainly derives from the following facts:

1. The thick and heavily doped N-well in modern CMOS technology increases the Gummel number. As is shown in Fig. 9.8, a substrate PNP transistor uses N-well as its base region. Compared with the base of typical bipolar transistor shown in Fig. 9.6, the N-well is thicker, which decreases the possibility of carriers being swept from emitter to collector. Also, the N-well is more heavily doped than the base region in a typical bipolar transistor, which increases the possibility of carrier recombination. In other words, when the majority carriers flow through emitter to base, they become minority carriers. These minority carriers become more likely to recombine if the base region is heavily doped. All these facts increase the base Gummel number. Since this value is inverse proportional to beta, a smaller beta is acquired.
2. Thinner and more lightly doped source/drain region in CMOS technology. As we can see from Fig. 9.8, the CMOS substrate transistor is taking source/drain region as its emitter. The even thinner source/drain region will decrease the emitter injection efficiency. Commonly, if the emitter is thin enough, the carriers injecting into the emitter from base will traverse over it before they recombine in the emitter region. This will decrease the minority concentration in emitter

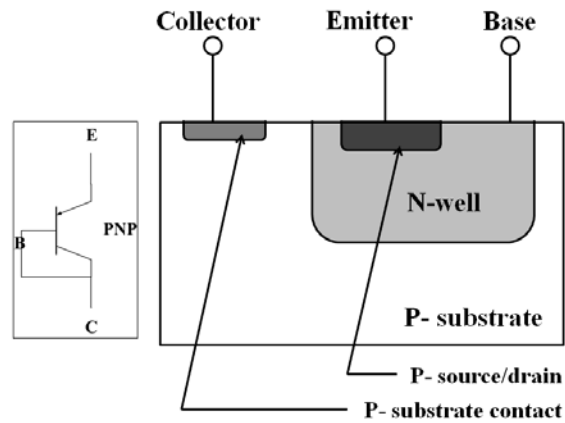


**Figure 9.8** Cross-section for bipolar PNP transistor.

and hence increase the carrier gradient. As a result, it draws more current from base in the form of an increasing diffusion current. Note that the increases in diffusion current also accelerate the dissipation of the extra carriers deposited by particle strike. Fig. 9.9 shows a TCAD simulation result of an SET current generated by the ion penetration based on the bipolar NPN transistor model we designed. The sharp peak current is contributed by the drift collection while the subsequent wide current is caused by diffusion collection. As a result, the increase in diffusion current will accelerate the diffusion charge collection and hence decrease the SET duration.

3. Holes have smaller mobility than electrons. The PNP transistor has smaller beta compared with their NPN counterpart because the mobility of the hole is around one third of the electron mobility. For PNP transistors, the holes are collected at the collector while it is electrons for NPN. The smaller mobility of holes makes them slower in the transition and hence more likely to recombine in the base region.

To sum up, all these evidences explain how the CMOS substrate PNP transistor exhibits a

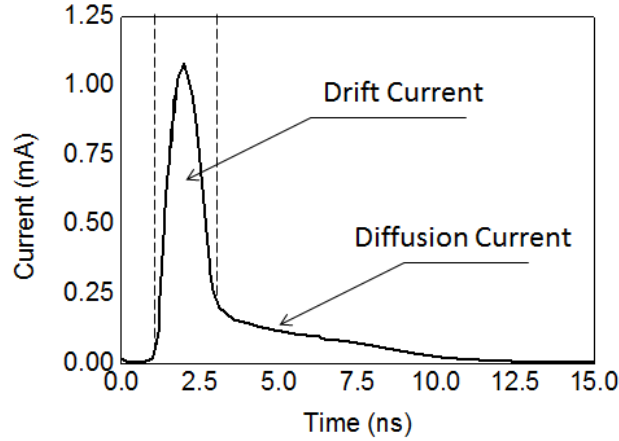


**Figure 9.9** TCAD simulation of SET current in a bipolar NPN model.

much smaller beta than the typical bipolar NPN one. The degradation in beta helps to mitigate the SET glitch.

## 9.5 Applications

The SET immunity of substrate PNP transistor also finds its application in RHBD field. Normally, designers of analog/mix signal ICs seek large beta bipolar transistors to take the advantage of their excellent amplification capability. But for the BGR circuit design, we utilize the well predicted linear temperature coefficient of base-emitter voltage rather than their current amplification capability. The base-emitter voltage can be expressed as follows [6]:

$$V_{BE} = V_{g0} + \frac{kT}{q} \ln\left(\frac{I_C}{A_E C T^\eta}\right) \quad (9.3)$$

Where  $V_{g0}$  is the extrapolated bandgap voltage at 0K,  $k$  is Boltzmann's constant,  $q$  is the electron charge,  $A_E$  is the emitter area,  $C$  and  $\eta$  are process dependent constants. As we can see,



the main parameters affecting the temperature coefficient of the base-emitter voltage are the process dependent  $C$  and  $\eta$ . However, different processes, such as CMOS and BiCMOS, will not affect its first order linearity over temperature. As a result, BGR with CMOS substrate transistors can have a temperature coefficient as good as that of analog bipolar transistors. Also, the cost of CMOS substrate transistors is lower. In addition, the substrate PNP transistor has much better SET immunity according to our study in this paper. To sum up, the CMOS substrate PNP transistor is a preference for BGR circuit designing and fabrication, especially when SET is a concern.

## 9.6 Conclusions

This paper discussed the SET response of a CMOS BGR circuit. The investigations were performed via pulsed laser irradiation facility. The results were compared with a previously tested BiCMOS BGR circuit. The PTAT voltage generator in CMOS BGR was not sensitive to laser irradiation while it was the most sensitive device in the BiCMOS BGR. The reason for this difference is the much lower current gain ( $\beta$ ) of a CMOS substrate PNP transistor than that of an analog bipolar NPN transistor in BiCMOS technology. Comprehensive analysis is presented in terms of device physics and fabrication process to explain this phenomenon. In summary, the substrate PNP transistor in CMOS technology has better SET immunity than the analog bipolar NPN transistor in BiCMOS.

The application of this SET immunity in the RHBD of BGR is also elaborated in this paper. The effect of different processes, such as BiCMOS and CMOS, on the temperature dependence of base-emitter voltage was discussed. As far as is concerned, the CMOS substrate PNP transistor has temperature linearity as good as the analog bipolar NPN transistor. As a result, the

CMOS substrate PNP transistor is suggested for BGR design and fabrication, especially when SET immunity is taken into consideration.

## **Acknowledgements**

The authors would like to thank CMC for its support in the BGR chip fabrication. Also, we appreciate the effects from SSSC at University of Saskatchewan. Their hard work guarantees the smooth operation of the pulsed laser system used all through our experiments.

## **References**

- [1] S. Buchner and D. McMorrow, "Single-event transients in bipolarlinear integrated circuits," *IEEE Trans. Nucl. Sci.*, vol. 53, pp. 3079–3102, Dec. 2006.
- [2] C. Poivey, J. Barth, J. McCabe, and K. Label, "A space weather event on the microwave anisotropy probe," in *Proc. RADECS Conf.*, Padova, Italy, Sep. 19–20, 2002, pp. 43–46.
- [3] A. Zanchi, S. Buchner, C. Hafer, S. Hisano, and D. B. Kerwin, "Investigation and mitigation of analog SET on a bandgap reference in triple-Well CMOS using pulsed laser techniques," *IEEE Trans. Nucl. Sci.*, vol. 58, no. 6, pp. 2570-2577, Dec. 2011.
- [4] Y. Ren, L. Fan, L. Chen, S.-J. Wen, R. Wong, N. W. van Vonno, A. F. Witulski, and B. L. Bhuvu, "Single-Event Effects Analysis of a Pulse Width Modulator IC in a DC/DC Converter," *Springer Journal of Electronic Testing*, vol. 28, no. 6, pp. 877–883, Dec. 2012.
- [5] S. Buchner and D. McMorrow, "Single-event transients in bipolarlinear integrated circuits," *IEEE Trans. Nucl. Sci.*, vol. 53, pp. 3079–3102, Dec. 2006.
- [6] M. A.P.Pertijis, G. C. M. Meijer, and J. H. Huijsing, "Precision Temperature Measurement Using CMOS Substrate PNP Transistors," *IEEE Sensors Journal*, vol. 4, no. 3, pp. 294-300, Jun. 2004.

## 10. A RHBD BANDGAP REFERENCE UTILIZING SINGLE EVENT TRANSIENT ISOLATION TECHNIQUE

*Submitted as:*

Y. Ren, L. Chen, and J.S. Bi, “A RHBD Bandgap Reference Utilizing the Single Event Transient Isolation Technique,” *IEEE Transaction of Nuclear Science*, 2014.

In the previous chapters, the SET sensitivity of a commercial-off-the-shelf DC/DC PWM IC has been comprehensively studied using multiple irradiation methods, such as heavy ion, proton, pulsed laser and X-ray techniques. The results indicated that the SET sensitivity of a bandgap reference circuit can dramatically affect the performance or function of the system it resides in. Even though many RHBD techniques are developed by researchers, little work is done to mitigate the SET in bandgap reference circuits. As a result, it is particular meaningful to seek a method to mitigate the SET sensitivity of bandgap reference circuits.

In this chapter, a novel SET hardened bandgap circuit based on SET isolation technique is proposed and tested. The sample circuit is fabricated in IBM bulk CMOS 130nm technology. The structure can dramatically suppress the SET amplitude by temporarily isolating the output from the bandgap core circuit. In this way the majority of the SET glitch will be prevented from propagating to the output. The pulsed laser technique is used to verify the test structures. The experimental data show a decent mitigation of the SET effects. The SPICE simulation is also performed, whose results are consistent with those of the pulsed laser test. This structure

provides more choices in designing RHBD bandgap reference circuits for engineers and researchers in this area.

# **A RHBD Bandgap Reference Utilizing Single Event Transient Isolation Technique**

Y. Ren, and L. Chen,

## **Abstract**

A novel radiation hardened by design (RHBD) structure to reduce the single event transient (SET) amplitude in analog circuits is presented in this paper. This structure features a SET isolation technique, which contains a sensor and a switch. The sensor turns off a switch on the detection of a voltage transient in the sensitive node, in which case the core circuit is isolated with the output temporarily. Once the voltage at the sensitive node recovers, the sensor turns on the switch again to connect the core circuit to the output. This structure is integrated and validated on a typical bandgap reference circuit, which is fabricated in IBM 130 nm technology. The simulation results show a significant reduction in the SET amplitude, which is also verified with the pulsed laser. The additional sensor and switch in the circuit do not bring extra power dissipation if they are properly chosen. The area overhead is neglectable by selecting the appropriate size for the RHBD structure.

## **Index terms**

Radiation hardened by design (RHBD), single-event transient (SET), bandgap reference, pulsed laser, SET isolation.

## **10.1 Introduction**

Single event transients (SETs) have been a main source of soft errors in electronic devices

[1-2]. It is the interaction between particles and atoms in the material (usually silicon) when particles penetrate the sensitive regions of a device, such as the reversed biased p-n junction. To be more specific, the energized particle ionizes the material atoms and generates electron-hole pairs, which are collected by the electric field in the p-n junction. This causes current and voltage perturbations in electronic devices, which propagate through the circuitry and hinder the system function, or even lead to system failures. As a result, it is both significant and necessary to develop innovative techniques to harden circuits against single events.

As a critical component in modern electronic systems, the bandgap reference circuit plays a key role by giving the stable and independent voltage reference in multiple circuit modules, such as DC/DC converters, low-dropout regulators (LDOs), analog-to-digital converters (ADCs), digital-to-analog converters (DACs), and comparators. It also serves as a reference signal in complex analog/mixed signal systems. For example, it can be monitored to give a power-on reset and power-good signal in complex systems. As a result, SET on bandgap reference dramatically affects the performance and function of the circuits and systems. Bandgap reference is reported to be increasingly sensitive to SET [3-4] in recent years. Even though there are some studies on radiation hardened PLLs [5-7] and amplifiers [8-10], these RHBD techniques are only limited to these specific circuits and little work is done to harden the bandgap reference circuits. As a result, it is both significant and necessary to develop RHBD bandgap reference voltage circuits.

In this paper, a RHBD structure specified to bandgap reference circuits is presented and analyzed. It isolates the core bandgap circuit from the output temporarily on the detection of SET at the sensitive nodes. When the SET event disappears, the core circuit will be coupled to the output again. In this way, the SET amplitude at the output of the circuit is reduced dramatically. This structure is integrated into a bandgap reference circuit implementing in IBM 130 nm

technology and tested with a pulsed laser with various laser energies. The test results show obvious suppression on the amplitude of the SET at the output. The paper is organized as follows: Section II proposed the concept and the simulation of a RHBD structure based on SET isolation technique while Section III described the implementation of the structure integrating into a typical bandgap reference circuit in bulk CMOS 130nm technology. The test facility and results are illustrated in Section IV following which is the analysis on the SET hardened bandgap reference circuit in Section V. Finally, the conclusions and future work are summarized in Section VI.

## 10.2 SET Isolation Structure

In analog/mixed signal circuits, there can be many potential sensitive nodes to the SET. For example, the structure on the left part of Fig. 10.1 is a current path. If the SET happens at the

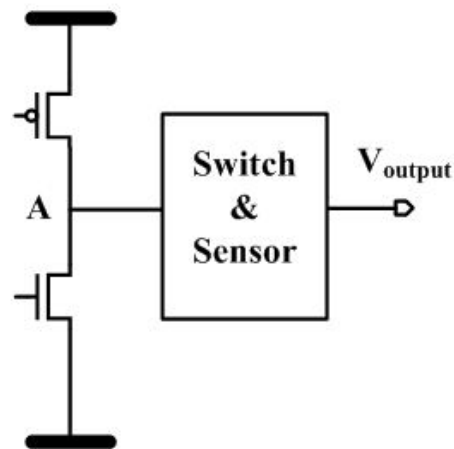


**Figure 10.1** Schematic for the RHBD structure.

node A, it will propagate to the output and affect the function of the subsequent circuits. Now a sensor and a switch can be added between the node and the output to isolate the output when SET happens. To be more specific, when there is a SET voltage glitch at the node, the sensor will sense this voltage variation and turn off the switch temporarily. As a result, the SET voltage at A fails to propagate to the subsequent circuitry.

One implementation for the sensor and switch is the inverter and the transistor transmission gate as shown in Fig. 10.2. In the case of a negative SET voltage glitch, an inverter and a PMOS transistor switch can be applied. The threshold of the inverter can be tuned to be a little lower than the expected voltage level of the node. So in normal working condition, the input of the inverter is considered to be logic high which results a logic low output. The inverter output is connected to the gate of the PMOS transistor. As a result, the PMOS transistor is turned on (deep triode region) due to the low input at its gate. Now, when a SET happens at A, the voltage drops

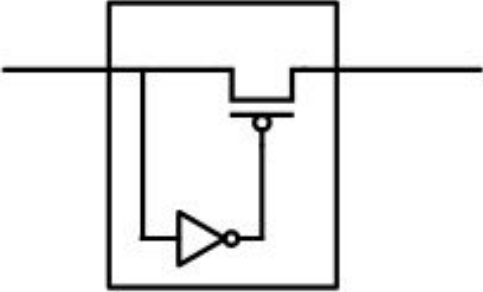


**Figure 10.2** The implementation of the Switch and Sensor.



at the inverter input. As a result, the inverter outputs a signal high to turn off the PMOS transistor, in which way, the output of the circuit is isolated with the SET propagation.

There are some considerations in designing this structure. First, the inverter delay should be minimized and the slope from high to low (or otherwise) should be sharp to increase the sensitivity of the sensor. In our design, IBM 130 nm process is used. Its minimal inverter delay is around 20 ps. And multiple inverters can be used to increase the slope of the transfer curve. According to the SPICE simulation, the slope of three-stage inverter is much sharper than that of one-stage while it is comparable to that of five-stage inverter. As a result, three-stage inverter is selected to implement the sensor. Second, the dimension of the switch transistor should also be minimized to reduce the possibility of being hit by particles. It can also make the transition faster.

After considering all aspects and properly selecting the devices, the simulation results for a

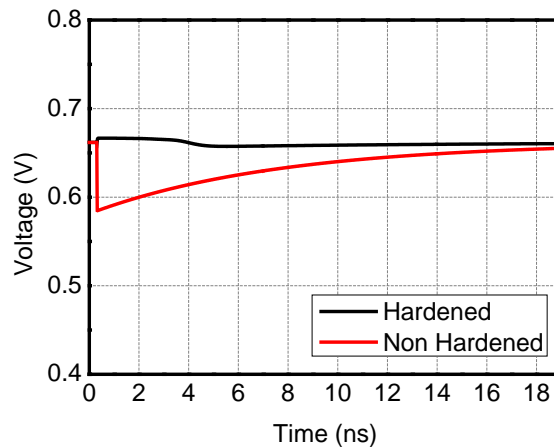


**Figure 10.3** Simulation result of the RHBD structure.

generic structure in Fig. 10.1 is shown in Fig. 10.3. Note that this simulation is presented to show the effect of the RHBD structure in terms of mitigate the SET amplitude. To be specific, the normal operation voltage at node A is 6.6 V. In the simulation, a double exponential current stimulus is used to characterize the effect of SET in node A. The peak current is set to be 500  $\mu\text{A}$  with a rising time and falling time of both 10 ps. And the pulse duration is set to be 1 fs. As we can see, the amplitude of the SET voltage is dramatically reduced. In this case, the SET amplitudes with and without the RHBD structure are 0.0048 mV and 0.077 mV, respectively. In other words, the SET amplitude at the output is decrease to around 6% of its original value.

### 10.3 Radiation Hardened Bandgap Reference

The SET isolation technique is further applied to a bandgap reference circuit shown in Fig. 10.4. The core circuit is a typical bandgap reference circuit. Q1, Q2, and R1 generate the PTAT current, which is injected into R2 by means of the current mirror composed of M1, M2, and M3.

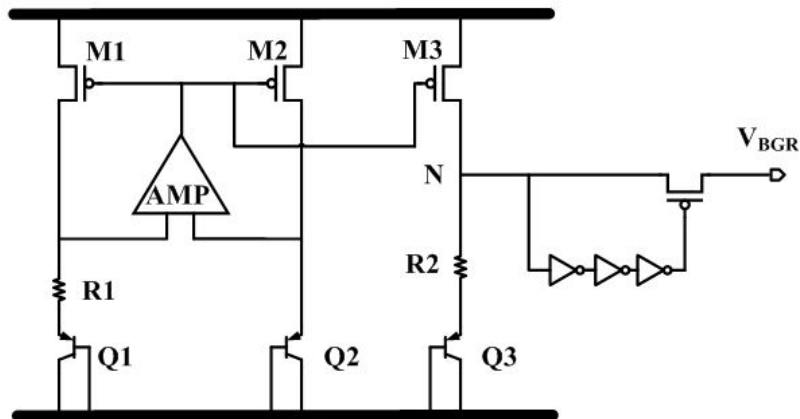


**Figure 10.4** Schematic of the RHBD BGR circuit.

The output of the BGR circuit is the voltage sum of R2 and  $V_{BE3}$ , which is expressed in (10.1)

$$V_{BGR} = V_{BE3} + \frac{R_2}{R_1}(V_{BE2} - V_{BE1}) \quad (10.1)$$

As is known, the base-emitter voltage  $V_{BE3}$  has a negative temperature coefficient (TC). Meanwhile, the voltage difference between  $V_{BE2}$  and  $V_{BE1}$  provides a positive TC. As a result, if the ratio of R1 and R2 is properly set, a temperature independent output voltage can be acquired (VBGR). One PMOS transistor switch is added to output N of the core BGR circuit. In a normal operation, the voltage at node N is a little higher than the pre-tuned inverter threshold. As a result, the output of the inverter chain is logic low and the PMOS switch is on. However, when SET results a negative glitch at node N, the sensor (three-stage inverter chain) will detect the voltage variation and cut off the PMOS switch connected to node N. In this way, the gate of M3 is floated temporarily and the SET effect is isolated with the output. And when the voltage at node N restores, the output of the three-stage inverter chain goes to logic low again to turn on the PMOS switch. The whole BGR circuit goes back to normal operation.

The chip under test is fabricated in IBM 130 nm technology, which is a mainstream process for analog/mix signal integrated circuit design currently. This technology features eight metal layers fabrication. The layout of the bandgap is specially designed so that the metal coverage on the sensitive areas is minimized. As a result, it is easier for the laser to hit the active areas. The nominal operation voltage for this bandgap is 2 V and the expected output voltage of the bandgap reference circuit is designed to be 1.21V.

## 10.4 Chip Test Results

### 10.4.1 Irradiation Facility

The irradiation facility used here is the pulsed laser system located in SSSC at University of Saskatchewan. It includes a Ti:Sapphire pulsed laser facility and a Laser Scanning Microscope (LSM). The schematic for the laser facility is illustrated in Fig. 10.5.

The pulsed laser system uses a continuous wave (CW) green diode-pumped solid-state (DPSS) laser as the pump laser, which provides 18W output at 532 nm. Its output goes into a regenerative amplifier (RegA) who uses Ti:Sapphire as its gain medium. The RegA can provide a repetition rate from 10 KHz to 300 KHz internally. To achieve an even lower repetition rate for the testing, an external signal generator is connected to its time controller. In fact, 1 KHz is used

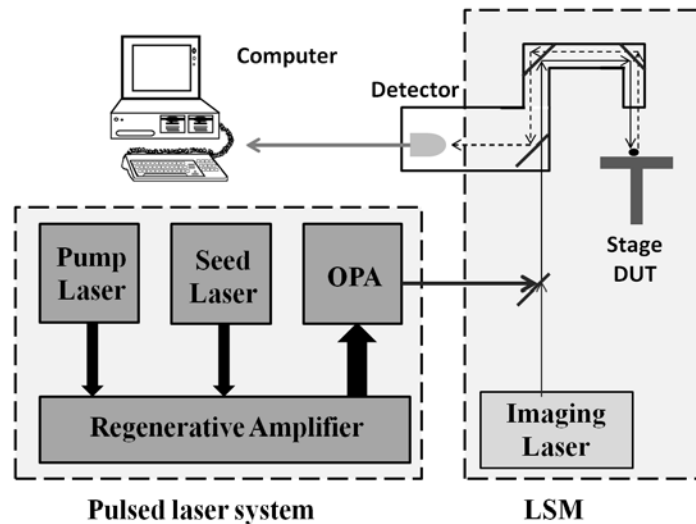


**Figure 10.5** Laser Facility Setup.

in our experiments. Note that the RegA is also seeded with a femtosecond pulsed laser. The pulse energy of the seed laser is amplified dramatically by the RegA. After that, it will be injected into an optical parametric amplifier (OPA) which extends the wavelength coverage. In our experiment, the 800 nm laser is adopted. The final output of the pulsed laser system is merged with imaging laser and sent to the optical path of the LSM as is shown in Fig. 10.5. The imaging laser is applied on the DUT and its reflection photons are collected by a detector and sent to the computer for image processing. The X-Y-Z directions are fully controlled from the computer end with a step size of 0.05  $\mu\text{m}$  for XY and 0.1  $\mu\text{m}$  for Z. During the scanning, the area is divided into 256 by 256 pixels with a dwell time of 5  $\mu\text{s}$  on each pixel. Thanks to the 50X objective, the minimum area can reach to 3.84  $\mu\text{m}$  by 3.84  $\mu\text{m}$ , which gives us decent accuracy in the experiments. An Agilent DSA90404A high speed oscilloscope with 4 GHz bandwidth is used to trigger the SET on the output of the BGR circuit.

#### ***10.4.2 Irradiation Process***

During the irradiation test, the laser beam is applied to scan each device of the BGR circuit with laser energy per pulse ranging from 0.2 nJ to 40 nJ. The voltage change of the output is monitored on the oscilloscope. Considering the relatively simple structure of the circuit, this testing procedure is feasible. Also, during our circuit designing, the exclusive layer was set on the circuit layout. This means no metal filling is allowed inside the area defined by it. In this way, all the devices of interest are exposed and ready to the laser irradiation. The minimum irradiation area for the laser system is 3.84  $\mu\text{m}$  by 3.84  $\mu\text{m}$ . This value is comparable with or smaller than the device dimensions. For example, the dimension for Q2 is 5  $\mu\text{m}$  by 10  $\mu\text{m}$ . This provides us with enough resolution to isolate the effect of each device.

### 10.4.3 Test Results

The output variations of the hardened and original BGR circuits are monitored and recorded during our test. A selection of test results with laser energy of 0.65 nJ, 4.5 nJ and 35.1 nJ is shown from Fig. 10.6 to Fig. 10.11.

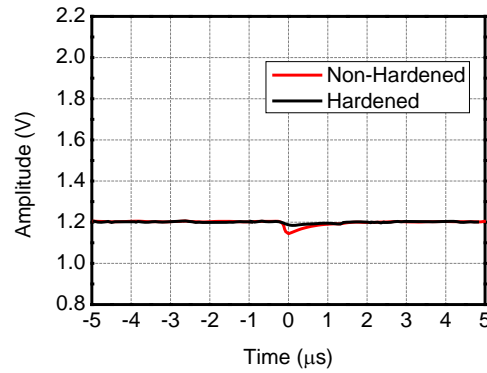


**Figure 10.6** Negative SET for laser energy 0.65 nJ.

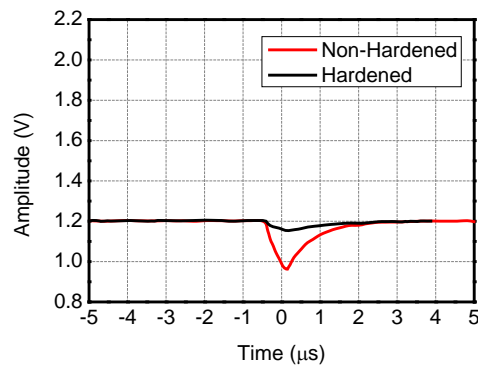


**Figure 10.7** Negative SET for laser energy 4.5 nJ.

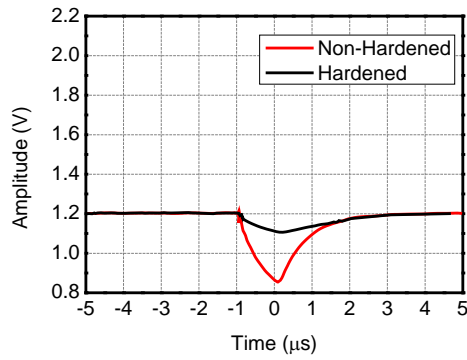


**Figure 10.8** Negative SET for laser energy 35 nJ.

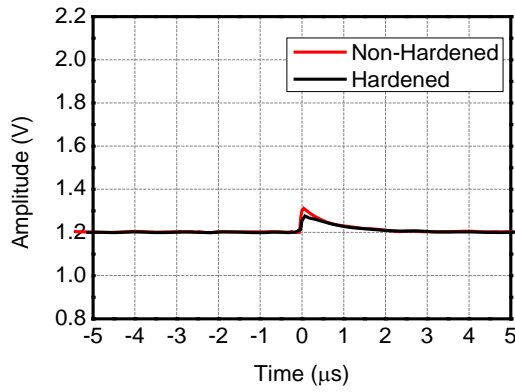


**Figure 10.9** Positive SET for laser energy 0.65 nJ.

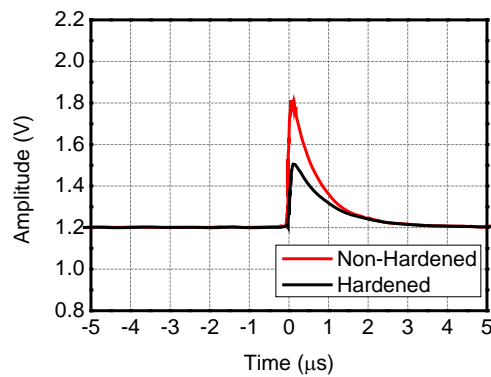


**Figure 10.10** Positive SET for laser energy 4.5 nJ.

As we can see from Fig. 10.6 to Fig. 10.8, which show negative SET glitches at the outputs,

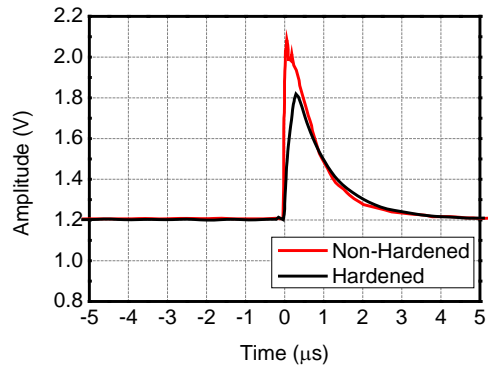


**Figure 10.11** Positive SET for laser energy 35 nJ.

the hardened structure suppresses the SET amplitude dramatically compared with its original counterpart. For the laser energy range we used, the hardened structure decreased the negative SET amplitude to 28%, 19%, and 27% of the original ones, respectively. The data are also summarized in Table 10.1.

Besides the negative SET, the positive SET is also observed, which is shown from Fig. 10.9 to Fig. 10.11. However, the mitigation effect is not as prominent as in the negative case. For the laser energy range we used, the hardened structure decreased the negative SET amplitude to 67%, 50%, and 69% of the original ones, respectively. The data are also summarized in Table 10.1.

One concern for the hardened structure is the SET sensitivity of the inverter chain and PMOS transistor switch. No glitch is observed at the BGR output when hitting the inverter chain. This is reasonable as the SET from inverter, if any, simply turn on and off the PMOS transistor and the will not affect the BGR output. On the contrary, when hitting the PMOS transistor, SET glitches are observed at the BGR output, which is shown in Fig. 10.12. However, the SET has



**Table 10.1 Experiment Data**

	Energy per pulse (nJ)	SET amplitude Nonhardened (mV)	SET amplitude hardened (mV)	SET amplitude decrease
Negative SET	0.65	5.5	1.5	28%
	4.5	23.7	4.6	19%
	35	34.6	9.3	27%
Positive SET	0.65	11.2	7.6	68%
	4.5	60.5	30.5	50%
	35	88.4	61.8	70%

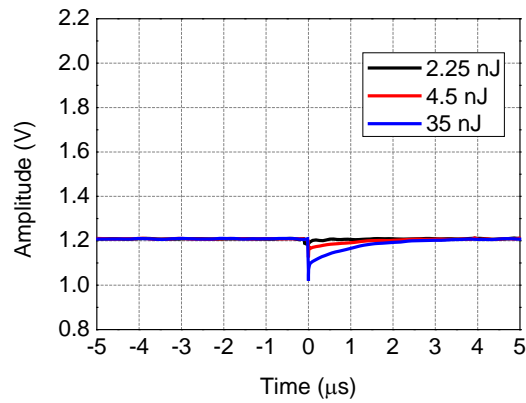


**Figure 10.12** SET glitches for hitting the PMOS switch.

smaller amplitude compared with SETs derived from inside the core circuit of the BGR circuits shown in Fig. 10.6 to Fig. 10.11. No measurable SET was observed until the laser energy

reached 2.25 nJ.

## **10.5 Discussions**

The aforementioned test results state themselves the outstanding mitigation effect of the hardened structure on negative SET glitches of BGR circuits in terms of voltage perturbation amplitude. However, there are some concerns to be discussed for the structure.

### ***10.5.1 Positive SET Mitigation***

As we can see from the data shown in Fig. 10.9 to Fig. 10.11 and Table I, the hardened structure seems to have limited effect on the mitigation of positive SET. However, this is only because the realization of the switch in Fig. 10.1 via a PMOS transistor. For example, this can be solved by simply changed the PMOS transistor to a NMOS and pre-tune the threshold of the inverter chain to be a little higher than the normal voltage of node A. In addition, the PMOS and NMOS switches can be combined to mitigate both positive and negative SET. The schematic is redrawn in Fig. 10.13. And the future work is to fabricate it and test its validity.

### ***10.5.2 The SET Sensitivity of the PMOS Switch***

Another concern for the hardened circuit is the SET sensitivity of the add-on devices, namely the inverter chain and the PMOS switch. The SET in the inverter chain will not affect the BGR output, which is proved both theoretically and practically in the experiment.

However, the PMOS switch exposed the BGR circuit to more SET probability. In other word, it tends to increase the cross-section of the BGR circuit. One way to minimize the SET effect of PMOS switch is to decrease the dimension of the PMOS transistor so that it is less likely to be hit in real life application. For example, the area of the PMOS transistor in our design

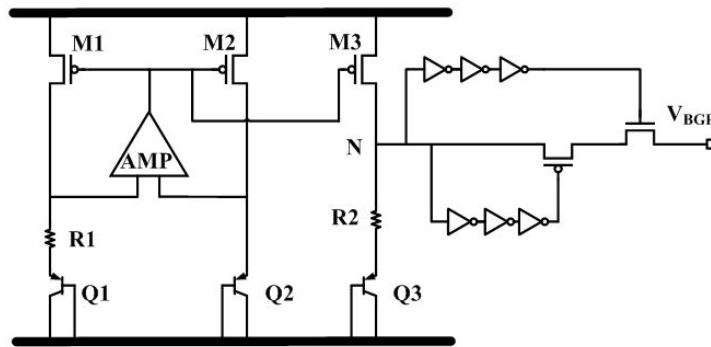


**Figure 10.13** Schematic of the improved RHBD BGR circuit.

is 160 nm by 120 nm while that of the total BGR circuit is 200  $\mu\text{m}$  by 100  $\mu\text{m}$ . In addition, the size of PMOS transistor switch can be decreased in the same pace with that of the technology shrinks. But it is a different case for the BGR circuit, which needs relatively large transistors to guarantee the function and performance as an analog structure. Another way is to minimize the SET amplitude and duration by using some SET mitigation techniques, such as guard ring. Finally, as far as we can see from our data in Fig. 10.12, for the same laser energy, the SET from the PMOS transistor is less in amplitude than the ones derived from the core BGR circuit.

### ***10.5.3 Power Dissipation of the Inverter Chain***

As we can see, the three inverters are not working totally in a rail-to-tail mode, especially for the first inverter. As a result, there can be a large power dissipation for the first inverter. However, this is a compromise between the SET hardening feature and the power dissipation. And we can seek other low power dissipation structures to realize this sensor, such as comparators. But the speed and area of the comparator need to be carefully selected.

#### **10.5.4 Capacitance**

Normally, an easy way to mitigate the SET is to use a big capacitor. However, it requires much larger areas than our SET hardened structure. Our SPICE simulation indicates that, the SET amplitude mitigation effect of our structure is better than a 2 pF capacitor which is much larger than our proposed structure.

### **10.6 Conclusions**

In this paper, an SET hardened BGR circuit taking the advantage of an SET isolation technique is proposed. The simulation showed excellent SET mitigation ability of the hardened circuit. Also, comprehensive tests were performed using the pulsed laser facility, which also proved its dramatic improvement in SET immunity. This design gives the engineers and researchers more choice in designing radiation hardened circuits.

However, some future work is required to improve the structure. A combination of PMOS and NMOS transistors can be used to mitigate both positive and negative SETs. Also, some layout SET mitigation techniques can be applied to the PMOS and NMOS switches so that decreased SET effects on them are expected.

### **Acknowledgements**

The authors would like to thank CMC for its support in the BGR chip fabrication. Also, we appreciate the effects from SSSC at University of Saskatchewan. Their hard work guarantees the smooth operation of the pulsed laser system used all through our experiments.

### **References**

[1] S. Buchner and D. McMorrow, "Single-event transients in bipolarlinear integrated circuits,"

- IEEE Trans. Nucl. Sci., vol. 53, pp. 3079–3102, Dec. 2006.
- [2] C. Poivey, J. Barth, J. McCabe, and K. Label, “A space weather event on the microwave anisotropy probe,” in Proc. RADECS Conf., Padova, Italy, Sep. 19–20, 2002, pp. 43–46.
- [3] A. Zanchi, S. Buchner, C. Hafer, S. Hisano, and D. B. Kerwin, " Investigation and mitigation of analog SET on a bandgap reference in triple-Well CMOS using pulsed laser techniques," IEEE Trans. Nucl. Sci., vol. 58, no. 6, pp. 2570-2577, Dec. 2011.
- [4] Y. Ren, L. Fan, L. Chen, S.-J. Wen, R. Wong, N. W. van Vonno, A. F. Witulski, and B. L. Bhuva, “Single-Event Effects Analysis of a Pulse Width Modulator IC in a DC/DC Converter,” Springer Journal of Electronic Testing, vol. 28, no. 6, pp. 877–883, Dec. 2012.
- [5] P. Maillard, W.T. Holman, T.D. Loveless, and L.W. Massengill, “A Radiation-Hardened Delay-Locked Loop (DLL) Utilizing A Differential Delay Line Topology," Radiation and Its Effects on Components and Systems (RADECS), Sept. 2011.
- [6] T.D. Loveless, L.W. Massengill, B.L. Bhuva, W.T. Holman, R.A. Reed, D. McMorrow, J.S. Melinger, and P. Jenkins, " A Single-Event-Hardened Phase-Locked Loop Fabricated in 130 nm CMOS," IEEE Trans. Nucl. Sci., vol. 54, no. 6, pp. 2012-2020, Dec. 2007.
- [7] B.G. Han, Z.J. Guo, X.H. Wang, L.S. Wu, and Y.B. Liu, "A radiation-hardened-by-design technique for suppressing SET in charge pump of PLL frequency synthesizer," SpringerScience China Technological Sciences, vol. 56, no. 2, pp. 286-292, Feb. 2013.
- [8] R.W. Blaine, N.M. Atkinson, J.S. Kauppila, T.D. Loveless, S.E. Armstrong, W.T. Holman, and L. W. Massengil, "Single-Event-Hardened CMOS Operational Amplifier Design," IEEE Trans. Nucl. Sci., vol. 59, no. 4, pp. 803-810, Jul. 2012.
- [9] S.E. Armstrong, B.D. Olson, W.T. Holman, J. Warner, D. McMorrow, and L. W. Massengill, " Demonstration of a Differential Layout Solution for Improved ASET Tolerance in CMOS AMS Circuits," IEEE Trans. Nucl. Sci., vol. 57, no. 6, pp. 3615-3619, Jul. 2010.
- [10] B. Narasimham, B.L. Bhuva, R.D. Schrimpf, L.W. Massengill, M.J. Gadlage, W.T. Homan, A.F. Witulski, W.H. Robinson, J.D. Black, J. M. Benedetto, and P.H. Eaton, "RHBD Bias Circuits Utilizing Sensitive Node Active (SNACC)," IEEE Trans. Nucl. Sci., vol. 58, no. 6, pp. 3060-3066, Dec. 2011.

- [11]R.W. Blaine, S.E. Armstrong, J.S. Kauppila, N.M. Atkinson, B.D. Olson, W.T. Holman, and L. W. Massengil, " Effects of guard bands and well contacts in mitigating long SETs in advanced CMOS processes," IEEE Trans. Nucl. Sci., vol. 55, no. 3, pp. 1708-1713, Jun. 2008.

## 11. SUMMARY AND CONTRIBUTIONS

### 11.1 Summary

This work investigates the SEE phenomenon using multiple evaluation techniques, such as proton, heavy ion, pulsed laser and X-ray, based on a commercial-off-the-shelf DC/DC PWM controller chip. The benefits and disadvantages of these testing methodologies are discussed. The correlations between them are also developed and explained. The optical-based methods are studied in more details, especially the pulsed laser technique. A comprehensive study is performed on applications of the pulsed laser technique on SEE testing in terms of experimental parameters, such as wavelength, repetition rate, and external temperatures. The most sensitive sub-circuit is found to be the bandgap reference circuit and a SET hardened structure is proposed and tested to mitigate the radiation effect. The main contributions of these works are listed as follows:

1. The SEE sensitivity of DC/DC PWM controller chip using pulsed laser technique
  - The SEE sensitivity of a commercial-off-the-shelf DC/DC PWM controller is presented based on the data from pulsed laser testing. The most sensitivity area is determined to be a bipolar transistor pair inside the bandgap reference sub-circuit. The sensitivity of other selected sub-circuits, such as power-on reset, comparator and current mirror, are also compared and analyzed. These conclusions give a clear idea of the most SEE sensitive devices in the DC/DC PWM system. This information can instruct the future DC/DC PWM design and test in the SEE field.

- The DC/DC PWM SEE sensitivity is also investigated with changed temperatures. It is found that temperature induced quiescent shift can affect the SEE sensitivity of a single device dramatically. Also, different circuit structures have different temperature response in terms of SEE sensitivity. These conclusions indicate that the simulation of quiescent point shift in sensitive nodes can predict the SEE sensitivity change with temperature shifting, which will facilitate the SEE testing procedure in some extent.
- The application of pulsed laser technique in SEE testing field is also investigated based on the DC/DC PWM chip. The conclusions show that one of its most beneficial features is well-controlled location information. In this way, the sensitive device can easily be pinpointed. The validity of the results is verified by device modeling and circuit simulations. The effects of different laser parameters, such as the wavelength and the repetition rate, are also studied. The conclusion indicates that relative low repetition rate should be adopted to simulate SEE using pulsed laser.

## 2. The correlations between pulsed laser, heavy ion and proton in SEE testing

- The correlation between pulsed laser and heavy ion data is developed using multiple wavelengths, namely 750nm, 800nm, 850nm, and 920nm. The equivalent LETs for these laser wavelengths are acquired. These conclusions will facilitate the data comparison between pulsed laser and heavy ion testing.
- The data correlation between heavy ion and high energy proton testing is also developed by means of a RPP model. The data show good consistency in terms of SEE cross section.



3. The application of pulsed X-ray technique in SEE study
  - The potential application of pulsed X-ray technique in SEE testing is discussed in this thesis. An obvious advantage is the smaller resolution step, which is required by modern sub-micro IC testing. The testing result is compared and verified with those of pulsed laser and heavy ion experiments.
4. The different SET sensitivity between BiCMOS and CMOS bipolar transistors
  - The different SET sensitivity between BiCMOS and CMOS bipolar transistors are compared and analysis. Its effect on the bandgap reference circuit is also presented and discussed. These conclusions give hints on the designing of SET hardened bandgap reference circuits.
5. The SET hardened bandgap reference circuit
  - An SET hardened BGR circuit taking the advantage of an SET isolation technique is proposed and tested. The simulation showed excellent SET mitigation ability of the hardened circuit. Also, comprehensive tests were performed using the pulsed laser facility, which also proved its dramatic improvement in SET immunity. This design gives the engineers and researchers more choice in designing radiation hardened circuits.

## **11.2 Contributions**

Generally speaking, this research contributes to the radiation effect community in two aspects, namely the testing methodology and the SET hardening circuit design. The profound and comprehensive investigation on each SET testing methods and their correlations facilitate the SET testing for researchers and engineers in this field. And the SET hardened circuitry proposed in this

research provides the researchers and engineers with more choices and hints on the radiation hardening design.

- .

## APPENDIX A

### LIST OF PUBLICATIONS

#### Journals:

1. **Y. Ren**, and L. Chen, "The Single Event Transient Study of a CMOS BGR Using Pulsed Laser Technique," *IEEE Transaction of Nuclear Science*, 2014. (Submitted)
2. **Y. Ren**, and L. Chen, "A Radiation Hardened Bandgap Reference Utilizing the Single Event Transient Isolation Technique," *IEEE Transaction of Nuclear Science*, 2014. (Submitted)
3. **Y. Ren**, and L. Chen, "SET Sensitivity Dependency of a DC/DC PWM on Laser Repetition Rate and Wavelength," *Springer Journal of Electronic Testing: Theory and Applications*, 2014. (Submitted)
4. **Y. Ren**, S.-T. Shi, L. Chen, R.-F. Feng, G. Guo, S.-J. Wen, R. Wong, N. W. van Vonno, and B. L. Bhuvu, "Single-Event Transient Measurement on a DC/DC PWM Controller Using Pulsed X-ray," *Journal of Microelectronics and Solid State Electronics*, vol. 3, no. 1A, pp. 30-35, 2014. (Published)
5. **Y. Ren**, and L. Chen, "The Effect of Temperature-Induced Quiescent Operating Point Shift on Single-Event Transient Sensitivity in Analog/Mixed-Signal Circuits," *Springer Journal of Electronic Testing: Theory and Applications*, vol. 30, no. 3, pp. 377-382, Jun., 2014. (Published)
6. **Y. Ren**, A.-L. He, S.-T. Shi, G. Guo, L. Chen, S.-J. Wen, R. Wong, N. W. van Vonno, and B. L. Bhuvu, "Single-Event Transient Measurements on a DC/DC Pulse Width Modulator Using Heavy Ion, Proton, and Pulsed Laser," *Springer Journal of Electronic Testing: Theory and Applications*, vol. 30, no. 1, pp. 149-154, Feb., 2013. (Published)
7. **Y. Ren**, S.-T. Shi, L. Chen, H.-B. Wang, L.-J. Gao, G. Guo, S.-J. Wen, R. Wong, and N. W. van Vonno, "Correlation of Heavy-Ion and Laser Testing on a DC/DC PWM Controller," *Springer Journal of Electronic Testing: Theory and Applications*, vol. 29, no. 4, pp. 609-616, Aug., 2013. (Published)
8. **Y. Ren**, L. Fan, L. Chen, S.-J. Wen, R. Wong, N. W. van Vonno, A. F. Witulski, and B. L. Bhuvu, "Single-Event Effects Analysis of a Pulse Width Modulator IC in a DC/DC Converter," *Springer Journal of Electronic Testing: Theory and Applications*, vol. 28, no. 6, pp. 877-883, Dec., 2012. (Published)
9. Z. Zhang, **Y. Ren**, L. Chen, N. J. Gaspard, A. F. Witulski, T. W. Holman, B. L. Bhuvu, S.-J. Wen, and R. Sammynaiken, "A Bulk Built-In Voltage Sensor to Detect Physical Location of Single-Event Transients," *Springer Journal of Electronic Testing: Theory and Applications*, vol. 29, no. 2, pp. 249-253, April, 2013. (Published)
10. S.-T. Guo, J.-X. Li, P. Gui, **Y. Ren**, L. Chen, and B. L. Bhuvu, "Single-Event Transient Effect on a Self-Biased Ring-Oscillator PLL and an LC PLL Fabricated in SOS Technology," *IEEE Trans. Nucl. Sci.*, vol. 60, no. 6, pp. 4668-4672, Dec. 2013. (Published)

## Conferences:

11. **Y. Ren**, S.-T. Shi, L. Chen, R.-F. Feng, G. Guo, S.-J. Wen, R. Wong, N. W. van Vonno, and B. L. Bhuvu, "Single-Event Transient Measurement on a DC/DC PWM Controller Using Pulsed X-ray," IEEE International Reliability Physics Symposium (IRPS), April, 2013.
12. **Y. Ren**, A.-L. He, S.-T. Shi, G. Guo, L. Chen, S.-J. Wen, R. Wong, N. W. van Vonno, and B. L. Bhuvu, "Heavy-Ion and Proton Sensitivity Measurements of a Commercial DCDC Pulse Width Modulator," Radiation Effects on Components and Systems (RADECS), Sep. 2012.
13. **Y. Ren**, H.-B. Wang, L. Chen, S.-T. Shi, L.-J. Gao, G. Guo, S.-J. Wen, R. Wong, N. W. van Vonno, B. L. Bhuvu, and T. Sammynaiken, "Correlation of Heavy Ion and Laser Testing on a DC/DC PWM Controller," IEEE Nuclear and Space Radiation Effects Conference (NSREC), Jul. 2012.
14. **Y. Ren**, L. Chen, S.-J. Wen, R. Wong, N. W. van Vonno, A. F. Witulski, and B. L. Bhuvu, "Single Event Effects Analysis of a Pulse Width Modulator IC in a DC/DC Converter," IEEE Nuclear and Space Radiation Effects Conference (NSREC), Jul. 2011.
15. **Y. Ren**, L. Chen, S.-J. Wen, R. Wong, N. W. van Vonno, A. F. Witulski, and B. L. Bhuvu, "Pulsed laser investigation in a DC-DC Controller," IEEE Conf. Electron Devices and Solid-State Circuits (EDSSC), Nov. 2011.